

4.0 Identification of Bridges Prone to Deterioration (Task 3)

4.1 Introduction

The objective of Task 3 was to identify bridges that are vulnerable to end distress. Bridge management in Michigan is performed using a relational database integrated under a software program called "Pontis." Pontis data that has been collected by MDOT bridge inspectors was analyzed along with the data collected from the research team's field investigation. A cursory inspection of recent I-girders as well as a visit to the precast plant showed that the girder ends are often cracked. The primary objective of the Pontis data analysis is to evaluate the impact of early age cracking on girders durability. The methodology and results of the analysis are described in this chapter.

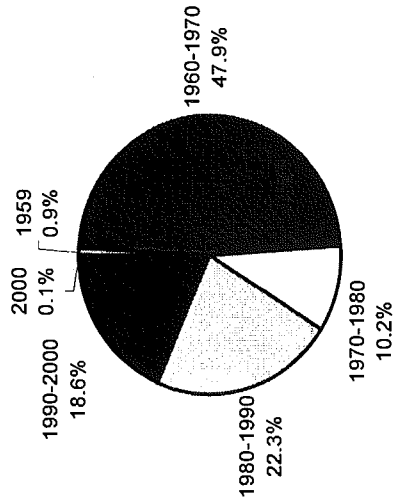
4.2 Pontis Data Analysis

Pontis data as of May 2001 indicates that there are 5902 bridges under MDOT's responsibility. Out of this total, there is in excess of 2600 prestressed concrete bridges with the design types of I-beam, box beam, or spread box beam. Further analysis of Pontis data indicates that there are about 750 prestressed concrete I-beam bridges under MDOT's responsibility. Further investigation of the Pontis data showed that there are approximately 50 duplicate entries of the prestressed concrete I-beam bridges. In this report the research team ignored the duplicates and used the sample space as 750. Figure 4-1 shows the fleet parameters of prestressed concrete I-beam bridges.

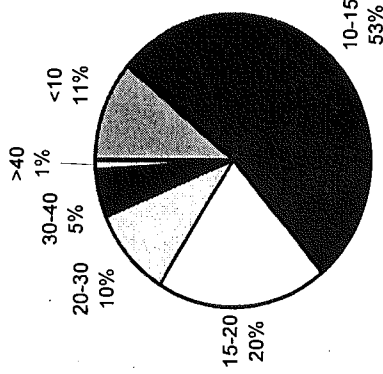
The Michigan Design Manual, Bridge Design Section 7.02.03 discusses beam material selection. This manual provides a guide for beam material selection. Prestressed concrete box beams can be used up to a span of 140-feet. AASHTO type prestressed concrete I-beams can be used up to a span of 105 feet, and Michigan 1800 I-beams up to a span of 150 feet. It is stated that concrete beams are preferable in freeway bridges subjected to severe exposure conditions.

The changes to the prestressed concrete bridge stock were investigated by querying the reconstructed bridges in Pontis. Table 4-1 summarizes the results. Also, Figure 4-2 shows the percentages of where the prestressed concrete I-beam bridges are located by region, and county. County numbers shown in Figure 4-2 are correlated to County names in Table 4-2.

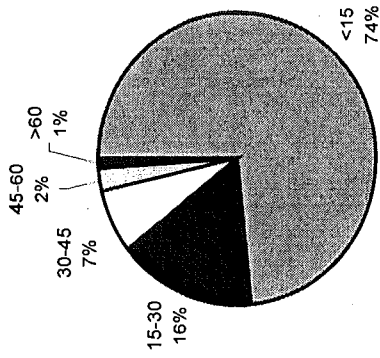
Year Built



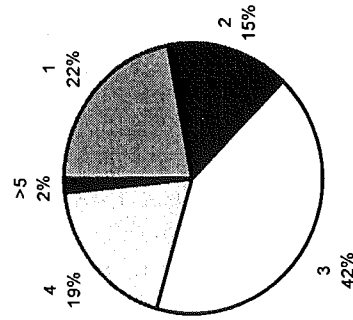
Deck Width (meters)



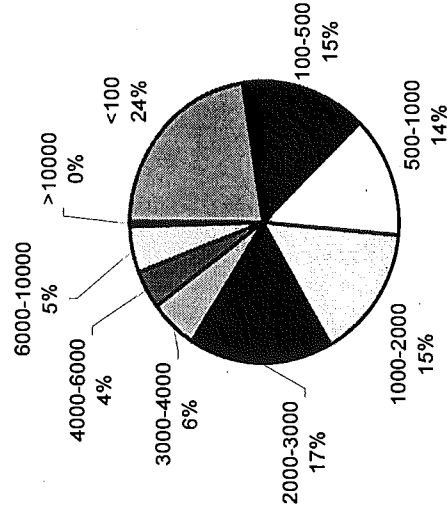
Skew Angles (degrees)



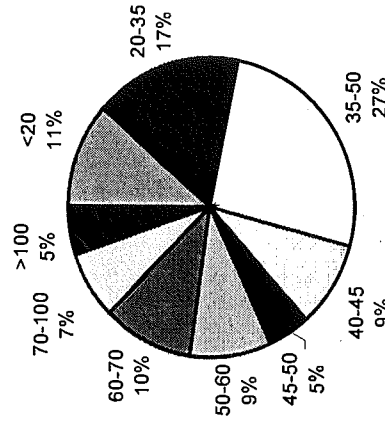
Number of Spans



ADTT



Length (meters)



ADTT: Average Daily Truck Traffic

Figure 4-1. Fleet Parameters of Prestressed Concrete I-Beam Bridges

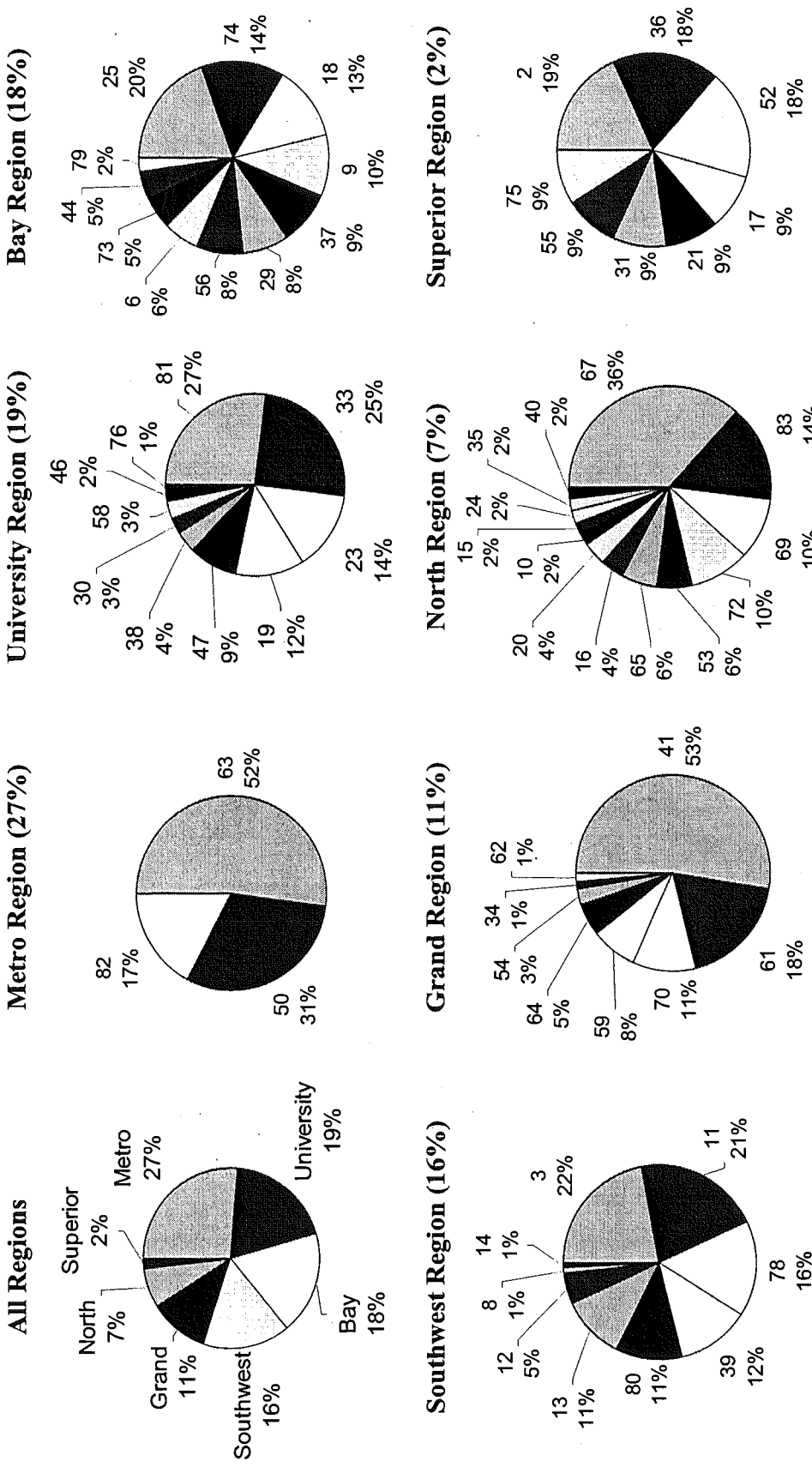


Figure 4-2. Fleet Location by Region of Prestressed Concrete I-girder Bridges

Table 4-1. Material Selection in Reconstructed Bridges

Years	Total Replaced	PC I-Beam	Box Beam	Spread Box Beam
1960-70	69	2	2	-
1970-80	127	4	9	-
1980-90	161	18	6	-
1990-00	261	51	24	18

Table 4-2. County Numbers as given by MDOT

#	Counties	Region	#	Counties	Region
1	ALCONA	NOR	43	LAKE	NOR
2	ALGER	SUP	44	LAPEER	BAY
3	ALLEGAN	SWR	45	LEELANAU	NOR
4	ALPENA	NOR	46	LENEWEE	UNIV
5	ANTRIM	NOR	47	LIVINGSTON	UNIV
6	ARENAC	BAY	48	LUCE	SUP
7	BARAGA	SUP	49	MACKINAC	SUP
8	BARRY	SWR	50	MACOMB	METRO
9	BAY	BAY	51	MANISTEE	NOR
10	BENZIE	NOR	52	MARQUETTE	SUP
11	BERRIEN	SWR	53	MASON	NOR
12	BRANCH	SWR	54	MECOSTA	GR
13	CALHOUN	SWR	55	MENOMINEE	SUP
14	CASS	SWR	56	MIDLAND	BAY
15	CHARLEVOIX	NOR	57	MISSAUKEE	NOR
16	CHEBOYGAN	NOR	58	MONROE	UNIV
17	CHIPPEWA	SUP	59	MONTCALM	GR
18	CLARE	BAY	60	MONTMORENCY	NOR
19	CLINTON	UNIV	61	MUSKEGON	GR
20	CRAWFORD	NOR	62	NEWAYGO	GR
21	DELTA	SUP	63	OAKLAND	METRO
22	DICKINSON	SUP	64	OCEANA	GR
23	EATON	UNIV	65	OGEMAW	NOR
24	EMMET	NOR	66	ONTONAGON	SUP
25	GENESEE	BAY	67	OCEOLA	NOR
26	GLADWIN	BAY	68	OSCODA	NOR
27	GOGEBIC	SUP	69	OTSEGO	NOR
28	GD. TRAVERSE	NOR	70	OTTAWA	GR
29	GRATIOT	BAY	71	PRESQUE ISLE	NOR
30	HILLSDALE	UNIV	72	ROSCOMMON	NOR
31	HOUGHTON	SUP	73	SAGINAW	BAY
32	HURON	BAY	74	SANILAC	BAY
33	INGHAM	UNIV	75	SCHOOLCRAFT	SUP
34	IONIA	GR	76	SHIAWASSEE	UNIV
35	IOSCO	NOR	77	ST. CLAIR	METRO
36	IRON	SUP	78	ST. JOSEPH	SWR
37	ISABELLA	BAY	79	TUSCOLA	BAY
38	JACKSON	UNIV	80	VAN BUREN	SWR
39	KALAMAZOO	SWR	81	WASHTENAW	UNIV
40	KALKASKA	NOR	82	WAYNE	METRO
41	KENT	GR	83	WEXFORD	NOR
42	KEWEENAW	SUP			

According to MDOT terminology a bridge is termed reconstructed even when the project activity is limited to deck replacement, consequently in Table 4-1 'Total Replaced' also includes deck replacement projects. In other words, the difference between the numbers of "Total Replaced" and total of prestressed concrete beams does not necessarily indicate the use of steel girders. Simple analysis of the data in the table shows that during the last decade an average of ten bridges per year are being replaced using prestressed concrete girders (PC I-Beam, Box Beam, or Spread Box Beam). These reconstructed prestressed concrete bridges are predominantly being rebuilt using prestressed concrete I-beams (51 of 93).

The Pontis data was further analyzed specifically for evaluating the condition of I-beams. Inspection reports prepared by an MDOT inspector are documented in Pontis. A total of 499 reports were analyzed by reviewing each record and counting the occurrences of the following specific terms: cracking (denoted by C), corrosion or rust (R), delamination (D) and spalling (S). Data processing revealed that the delamination term is redundant because this phenomenon is always accompanied with spalling. Therefore, the analysis was focused on inspector reports containing the terms of rusting and spalling. In order to see the influence of cracking on the beams, the data was analyzed with respect to numbers of bridges with beams with cracks and without cracks.

The total number of 499 records was obtained from Pontis for prestressed concrete I-beam bridges with available inspection reports. The histogram of these bridges built between 1960 and 2000 is shown in Figure 4-3. Out of this total of 499 bridges, 55 records contained duplicate Bridge ID numbers but different inspection comments.

The histogram of cracked and uncracked prestressed concrete I-beams showing rust are shown in Figure 4-4. Using all 499 inspector comment records, the number of bridges with notes indicating cracked prestressed concrete I-beams was counted as 263, leaving 236 records for the bridges with no mention of beam cracking. Further review of inspector comments showed that 109 bridge beams include "cracks and rusting or corrosion," whereas 40 comments were found for the beams that only indicate "corrosion or rusting" but with no mention of cracking. When both "rusting or corrosion" and "spalling" are searched in the inspector comments, the numbers reported with cracked beams was 87, and 23 for the beams with no mention of cracks.

The influence of cracking on prestressed concrete I-beam durability is depicted in Figure 4-4. Taking beam corrosion as the primary parameter, the ratio of bridges with prestressed concrete I-beams showing signs of corrosion to the total number of cracked and uncracked beams document the importance of cracking in beam durability. The ratio of the number of bridges with observed signs of corrosion to the total number bridges with cracked beams is 0.41 whereas this ratio decreases to 0.17 for the bridges with beams where inspectors did not indicate any cracks.

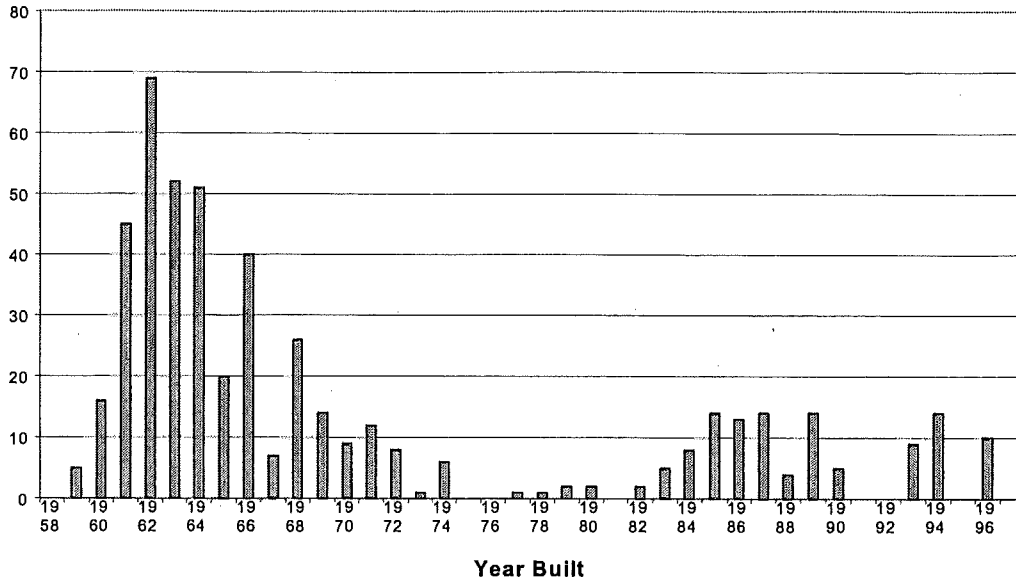


Figure 4-3. Prestressed Concrete I-Beam Bridges Constructed Since 1960

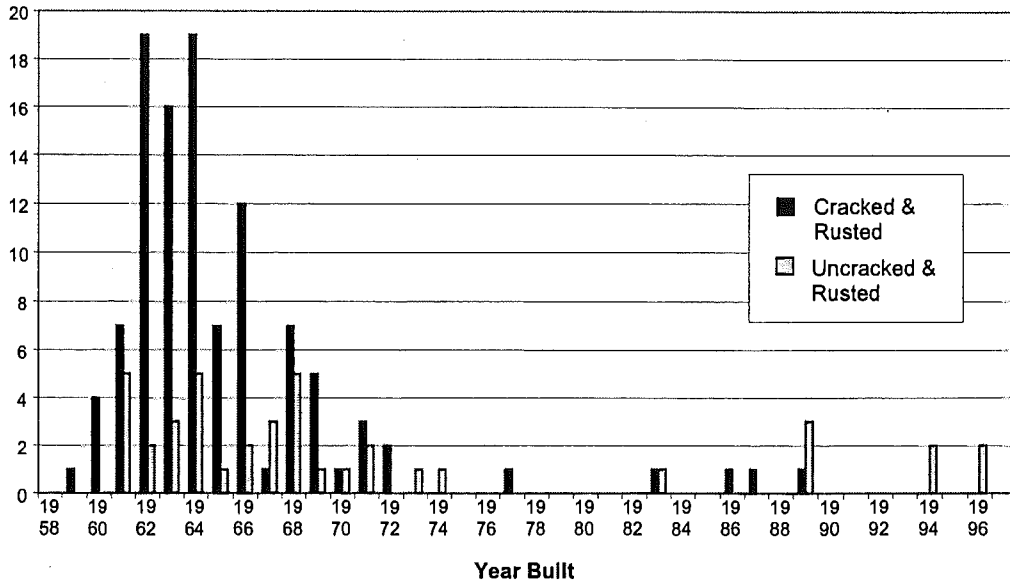


Figure 4-4. Corrosion Comparison in Cracked and Uncracked Prestressed Concrete I-Beam Bridges showing rust

4.3 Field Inspection Data Analysis

The field investigation data was collected on template forms. The template includes the bridge ID on the top left of the sheet and the beam layout on the top right of the sheet. The inspector designated the specific beam being inspected on the beam layout and completed the condition information on the beams and diaphragms.

During field visits, all faces of the beam-ends were inspected and signs of distress/deterioration were entered onto the form. Cracks were drawn to a rough approximation with respect to their length, location, and orientation. For each crack the length was measured and the width was estimated sometimes using crack gages. Corrosion, delamination, spall, water stain, efflorescence, and exposed rebar were carefully sketched onto the form to show approximate areas and locations. Figure 4-6 is an example of one of the field investigation forms with data sketched from the field. The data presented on all the field investigation forms is qualitative information, therefore a database was created to transform that data into quantitative information so it could be analyzed. The beam condition data was entered into a custom made Microsoft Access database that was described in Section 3.8.1.

As seen in Figure 4-6 there are six faces to a beam-end and the seventh face is the bearing. There are a total of 5364 faces in the database for the 20 bridges that were investigated. On those faces there are 5041 cracks for which four items of data was entered (width, length, location, and orientation). Additionally, the corrosion, delamination, and/or spall evidence on each face was entered. Sometimes for a face “notes” were entered describing the moisture stains, exposed rebar, efflorescence, and any other indicators of distress.

The Pontis analysis conducted on the “Inspector Notes” documented the influence of early age cracks on prestressed concrete I-beam end durability. For this purpose, the hypothesis developed for the analysis of inspection data was related to the influence of cracking. The hypothesis of beam end deterioration for prestressed concrete I-beams is that cracks in the early part of a bridge’s life results to more rapid progression of rebar and tendon corrosion. To verify this hypothesis a statistical analysis was conducted on the field inspection data.

First, 12 queries were performed to yield all the primary faces of interest. The inspection data is organized for each face of the girder-end. These faces are the north and south elevation, or east and west elevation (dependent upon orientation of the bridge), bottom, and side faces of all 20 bridges with a total of 3000 faces. The remaining 2364 faces are the two diaphragm faces and bearing. The results from the 12 queries are given in Table 4-3. (In all of the following tables of this section “Corr” is an abbreviation of corrosion and “Del” is an abbreviation of delamination.)

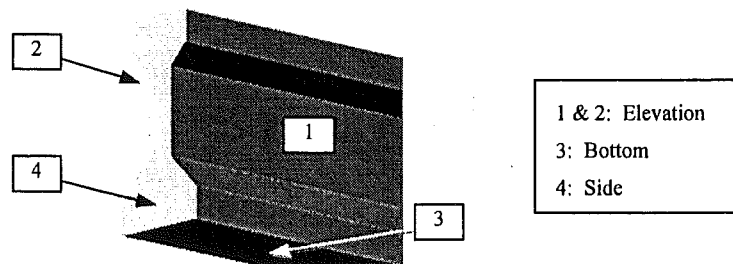


Figure 4-5: Primary Faces of Girder-end

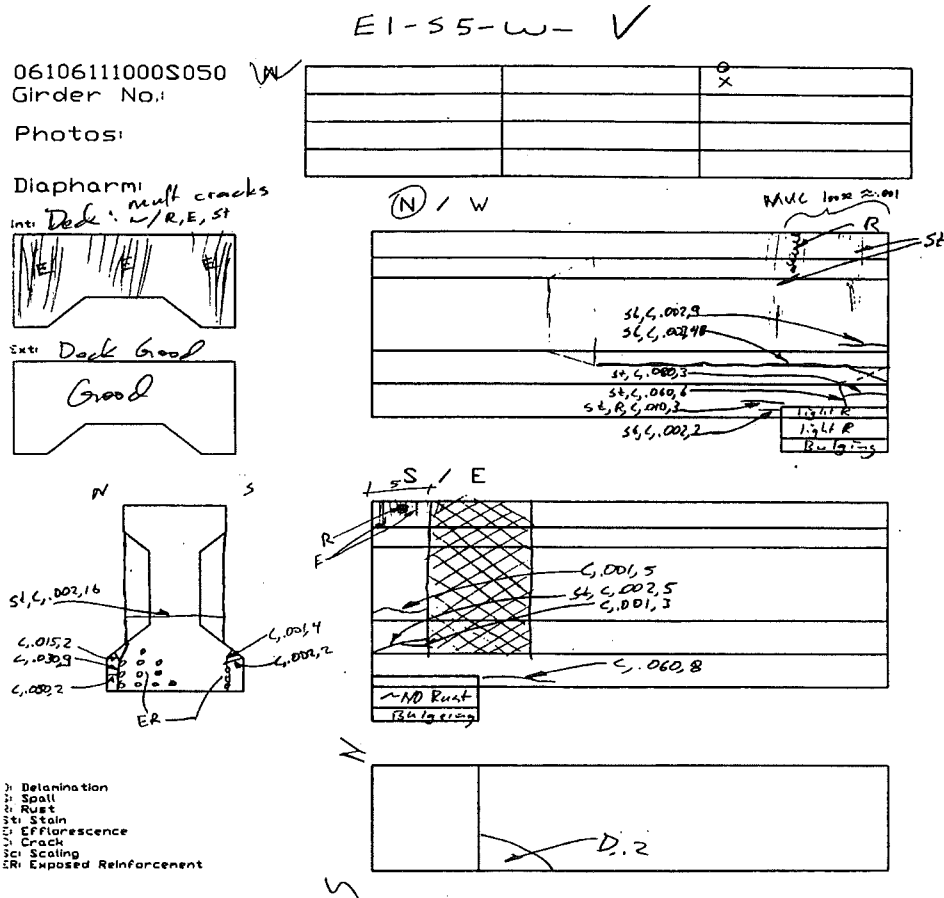


Figure 4-6. Example of Field Investigation Template Form

The girder-end condition database contains information on cracked, corroded, delaminated, and spalled states. The information is recorded for each one of the four girder-end faces. The direct query using a specific condition state provided the data given in Table 4-3. The data in Table 4-3 was further processed to obtain the bridge and girder-end specific data as tabulated in Table 4-4 as frequencies and Table 4-5 as percentages. The data in Table 4-5 is represented in Figure 4-7 temporally by year built in terms of distress frequencies. The deterioration against bridge age is observed in Figure 4-7. The relation between cracking and deterioration cannot be observed because of linked samples of uncracked girders.

Table 4-3. Queries from Condition Database of Faces Inspected

	Total Faces	Cracked Faces	Crack & Corr Faces	Corr Faces
Total	3000	1515	704	888
Delamination	990	602	350	420
Spall	674	477	328	405
Spall & Del	399	293	200	237

Table 4-4. Summary of Result from Condition Database with respect to Each Bridge and Beam-ends

Bridge ID	County	Region	Year Built	No. of Spans	No. of Girders	Total No. of Beam-ends Inspected	Beam-ends w/ No Cracks & No Corr	Beam-ends w/ Cracks	Beam-ends w/ Cracks & Corr	Beam-ends w/ Del	Beam-ends w/ Spall	Sum
29011 S03	Gratiot	Bay	1961	3	27	54	0	0	15	21	18	54
06111 S04	Arenac	Bay	1968	3	18	35	0	9	9	6	11	35
06111 S05	Arenac	Bay	1968	3	15	30	0	2	10	9	9	30
06111 S06	Arenac	Bay	1968	3	15	30	0	1	10	8	11	30
06111 S11	Arenac	Bay	1968	6	54	62	0	12	3	6	41	62
25042 S12-8	Genesee	Bay	1969	4	16	28	1	1	5	4	17	28
25042 S12-3	Genesee	Bay	1969	4	22	44	0	0	4	5	35	44
25042 S12-4	Genesee	Bay	1969	4	22	43	0	0	3	5	35	43
25042 S12-7	Genesee	Bay	1969	4	16	32	0	0	4	5	23	32
25132 S34	Genesee	Bay	1971	4	24	48	0	10	10	17	11	48
41025 S07	Kent	Grand	1961	4	24	47	0	2	10	16	19	47
41027 S06	Kent	Grand	1963	3	36	71	0	12	11	12	36	71
41029 S16-3	Kent	Grand	1964	3	24	46	0	1	8	6	31	46
41029 S16-4	Kent	Grand	1964	3	24	48	0	7	9	15	17	48
41029 S23	Kent	Grand	1972	3	24	48	0	28	3	5	12	48
67016 S09	Oceola	North	1984	1	6	11	0	2	2	6	1	11
67016 S10	Oceola	North	1984	1	7	14	0	9	2	1	2	14
53034 S05	Mason	North	1986	4	24	27	0	5	14	6	2	27
83033 S06	Wexford	North	1997	1	8	16	0	15	1	0	0	16
83033 S05	Wexford	North	1998	2	8	16	2	13	1	0	0	16
Total					414	750	3	129	134	153	331	750

Table 4-5. Percentages of Summary of Result from Condition Database with respect to Each Bridge and Beam-end

Bridge ID	County	Region	Year Built	No. of Spans	No. of Girders	Total No. of Beam-ends Inspected	Beam-ends w/ No Cracks & No Corr (%)	Beam-ends w/ Cracks (%)	Beam-ends w/ Cracks & Corr (%)	Beam-ends w/ Del (%)	Beam-ends w/ Spall (%)	Sum (%)
29011 S03	Graftiot	Bay	1961	3	27	54	0	0	28	39	33	100
06111 S04	Arenac	Bay	1968	3	18	35	0	4	21	34	40	100
06111 S05	Arenac	Bay	1968	3	15	30	0	17	16	17	51	100
06111 S06	Arenac	Bay	1968	3	15	30	0	2	17	13	67	100
06111 S11	Arenac	Bay	1968	6	54	62	0	15	19	31	35	100
25042 S12-8	Genesee	Bay	1969	4	16	28	0	26	26	17	31	100
25042 S12-3	Genesee	Bay	1969	4	22	44	0	7	33	30	30	100
25042 S12-4	Genesee	Bay	1969	4	22	43	0	3	33	27	37	100
25042 S12-7	Genesee	Bay	1969	4	16	32	0	19	5	10	66	100
25132 S34	Genesee	Bay	1971	4	24	48	4	4	18	14	61	100
41025 S07	Kent	Grand	1961	4	24	47	0	0	9	11	80	100
41027 S06	Kent	Grand	1963	3	36	71	0	0	7	12	81	100
41029 S16-3	Kent	Grand	1964	3	24	46	0	0	13	16	72	100
41029 S16-4	Kent	Grand	1964	3	24	48	0	21	21	35	23	100
41029 S23	Kent	Grand	1972	3	24	48	0	58	6	10	25	100
67016 S09	Oceola	North	1984	1	6	11	0	18	18	55	9	100
67016 S10	Oceola	North	1984	1	7	14	0	64	14	7	14	100
53034 S05	Mason	North	1986	4	24	27	0	19	52	22	7	100
83033 S06	Wexford	North	1997	1	8	16	0	94	6	0	0	100
83033 S05	Wexford	North	1998	2	8	16	13	81	6	0	0	100
Total					414	750	0	17	18	20	44	100

An observation from the pontis data analysis and the research team's field data is the count of delaminated beam-ends. The research team's approach of checking delaminations at the beam-ends and diaphragms is by sounding across the entire surface area. The data in Table 4-6 came from 20 bridges inspected by the research team. The column titled "Inspector's Comment on Delaminated Stringers" came from the comments regarding stringers from the Safety Inspection Reports completed for those bridges by MDOT bridge inspectors as seen in Figure 4-8. If the inspector's comments included delaminations on any stringer, then "Yes" is entered into that cell. The column titled "Research Team's Comments on Delaminated Stringers" is based on the research team's inspection forms indicating delaminations on any stringer. For the 20 bridges investigated in this research, the stringers comments field in the MDOT Inspection Reports indicating delaminations show only 3 bridges versus 17 bridges determined by the research team. With all fairness the amount of man-hours it took the research team to complete an inspection was well above the inspector could afford to spend. In any case, these data indicate that delaminations are difficult to check during inspection.

Table 4-6. Findings on Evidence of PCI Girder-end Delaminations

Pontis Bridge ID	County	Region	Year Built	Inspector's Comment on Delaminated Stringers	Research Team's Comments on Delaminated Stringers
29011 S03	Arenac	Bay	1968	No	Yes
06111 S04	Arenac	Bay	1968	No	Yes
06111 S05	Arenac	Bay	1968	Yes	Yes
06111 S06	Arenac	Bay	1968	No	Yes
06111 S11	Genesee	Bay	1969	Yes	Yes
25042 S12-8	Genesee	Bay	1969	No	Yes
25042 S12-3	Genesee	Bay	1969	No	Yes
25042 S12-4	Genesee	Bay	1960	No	Yes
25042 S12-7	Genesee	Bay	1971	No	Yes
25132 S34	Gratiot	Bay	1961	No	Yes
41025 S07	Kent	Grand	1961	Yes	Yes
41027 S06	Kent	Grand	1963	No	Yes
41029 S16-3	Kent	Grand	1964	No	Yes
41029 S16-4	Kent	Grand	1964	No	Yes
41029 S23	Kent	Grand	1972	No	Yes
67016 S09	Mason	North	1986	No	Yes
67016 S10	Oceola	North	1984	No	Yes
53034 S05	Oceola	North	1984	No	No
83033 S06	Wexford	North	1998	No	No
83033 S05	Wexford	North	1997	No	No

Pontis Bridge ID 251250420009127	Struc Num 2545	Location SWILTS OFF INT	Agency / Consultant SPICER	Inspection Date 10/20/2000	Insp Key 2/DK
Facility RAMP E	Brg Length-Width 640 82	Scour (113) N	Inspector Name WAZ, ARB	Insp Freq 24	UW Meth-Lnth 0 0
Feature I-75	SAFETY, APPRAISAL, AND GENERAL NOTES				

Brg Rail (38A)	Rail Tr (38B)	Appr (36C)	Rail Term (38D)	Watr Adéq (71)	Appr Align (72)	Temp Supp	Hi Ld Hit	General Notes
1	1	1	1	N	8	<input type="checkbox"/>	<input type="checkbox"/>	

NBI INSPECTION		
1. Surface	3	Several transv crks in dk surf and 7-10 SY of scattered asphalt patched spalls in S2. Scattered small open spalls. (98)Patched areas continue to spall. More than 25 % of the dk map crkd or delam.
2. Expansion Jts	3	Leaking. (98)Over all piers. P1-conc patch full width, p2-torn, p3-sunk & spalled full length. (00)-Compression seals sunk, missing, or torn.
3. Joints	3	(00)-Compression seals sunk, missing, or torn.
4. Railings	5	Conc para w/ 1 alum tube 2'-3' high. A few posts have shallow leaching rusty incip spalls and open spalls. (00)-Thrie bm retrofit. Curb edges spalled slightly & rusting in spots.
5. Approach Pavt	7	(00)-Concrete approaches appear sound, 1 sqft patched spall @ NE quad.
6. Deck	4	Some horizontal cracks in curb fascias. (98)Few leaching crks. (98) 10-25% of the deck has map cracks or is delaminated.
7. Stringer (Superst) (NBI Item 59)	4	(98)-Sp4 bay 1 diaph 8' crk. P3-bm2-(2) 1/4in vert crks on bm ends. (00)-Half of the bm ends have cracks, spalls, & active corr.

8. Paint	N	
9. Paint at Jts	N	
10. Bearings	6	(00)-Elastomeric pads at piers and steel bearing pads at abutments.
11. Abutments	7	A few vert crks in abut walls. Concrete ap
12. Piers	7	Concrete piers and caps appear sound.
13. Channel	N	
14. Culvert	N	

This is where the Research Team found the comments for the column titled "Inspector's Comment on Delaminated Stringers"

CREW RECOMMENDATIONS		
	Priority	Comments
Deck Patch	H	(00)-Continue patching dk potholes.
Appr Pavt	-	
Jt Repair	-	
Rail Repr	-	
Detailed Inspect	M	(00)-Consider inspecting bm ends.
Zone Pt	-	
Subst Repr	-	
Slope Repr	-	
Brush Cut	-	
Other	H	(00)-Measure and post underclearance.

CONTRACT RECOMMENDATIONS		
	Priority	Comments
Bridge Repl	-	-1
Super Repl	-	
Deck Repl	M	(00)-Consider replacement of dk when funds become available.
Deck Ovfy	-	-1
Widening	-	-1
Full Paint	-	-1
Zone Paint	-	-1
Pin/Hanger	-	
Substr Repr	-	
Other	-	

Figure 4-8. Example of a MDOT Safety Bridge Inspection Report

4.4 Indicators of Beam-End Vulnerability

Upon completing the inspection of 20 bridges it appeared clear that the vulnerable areas of a prestressed concrete bridge are: (1) beam-ends on piers, (2) beam-ends on abutments and (3) beam under-side near bearing pad/sole plate. These areas will be the first to exhibit the early signs of beam-end deterioration. Thus the inspection of these particular areas is recommended for vulnerability assessment as a part of maintenance inspection.

Specifically it is recommended that at the time of the inspection:

(1) The inspection of beam-ends on piers should focus on a 5.0-6.5 ft portion of the beam-end along the web and flange of the beam. Any cracks (especially hairline cracks in excess of 0.001 inch) and wet stains need to be documented. Such fine cracks should be visible using a water spray within arms length of inspection. Also, any moisture stain/leakage on the pier caps under the beam-ends should be noted. Special effort is required for the inspection of the beam-end back face at the piers. To be able to inspect the beam-end back face, one needs to get in between diaphragms and use a flashlight.

(2) The inspection of beam-ends at the abutments should focus on a 5.0-6.5 ft portion of that beam-end which extends from the edge of the abutment. The presence of hairline cracks and minor water stains is especially useful for vulnerability assessment. It is a concern sometimes the beam-end back face is encased in a diaphragm and cannot be inspected.

(3) The condition of elastomeric bearing pad, bearing plate, and sole plate should be noted. The elastomeric pad condition may be of corners curling, crack, delaminated. Bearing plate and sole plate may have corrosion.

Inspection shows the following in the proposed vulnerability assessment procedure the beam can be considered "not vulnerable" (see Photo 4-1).

- No cracks or hairline cracks (≤ 0.001 inch) at the girder end,
- Joint intact (not leaking),
- Sole plate clean free of rust,
- Functional elastomeric bearing pad,
- Beam faces and pier caps are dry.

It is the opinion of the research team that the possibility of water infiltration and freeze thaw mechanism has a small chance of affecting the intended design of the air entrainment system. Therefore, the criterion of less than 0.001 inch for "not vulnerable" is considered as a small value.

The following conditions should be considered as the first signs of beam-end problem:

- Moderate cracks (0.002-0.01 inch) at the girder end,
- Corroding sole plate,
- Moisture staining or leaking joint,
- Non-functional elastomeric bearing pad,
- Beam faces and pier caps show moisture staining.

If the inspection indicates any one of the above conditions, the beam is considered as “vulnerable” to end deterioration (see Photo 4-2).

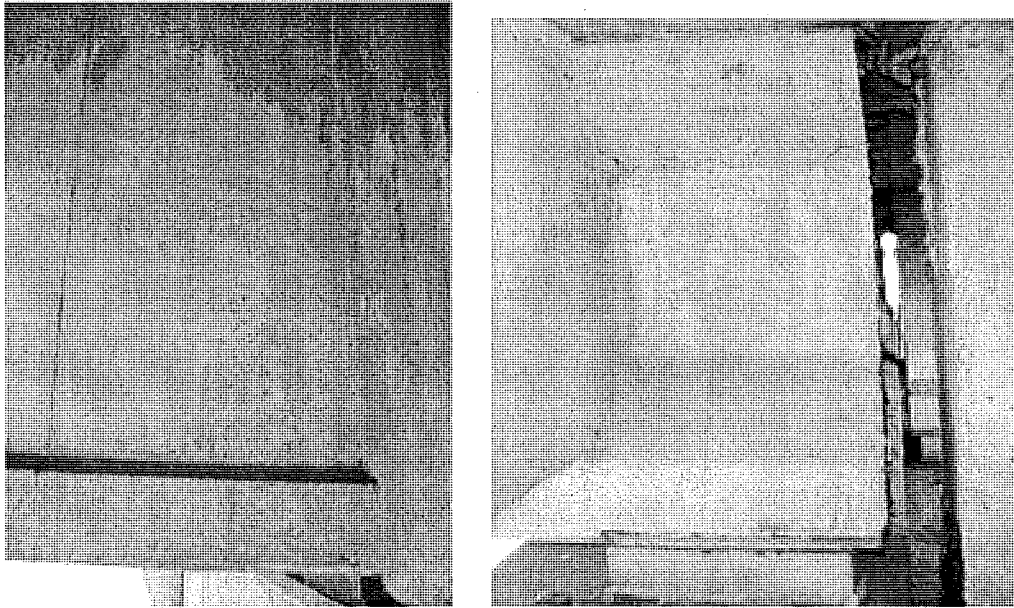


Photo 4-1. “Not vulnerable” Prestressed Concrete I-Beam

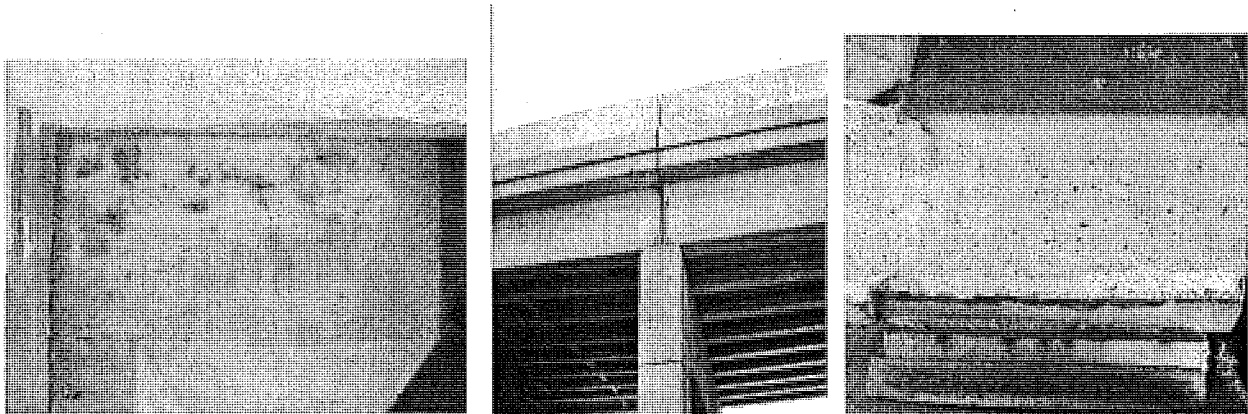


Photo 4-2. (Left and Middle) Wet stain at beam-end (Right) Sole plate corrosion

Additionally, if two or more of the conditions below are observed during inspection, the beam is considered as “highly vulnerable” to end deterioration (see Photo 4-3).

- Major cracks (> 0.01 inch) at the girder end,
- Leaking joint,
- Corroding sole plate, bearing plate
- Non-functional elastomeric bearing pad,
- Beam faces and pier caps are moist.

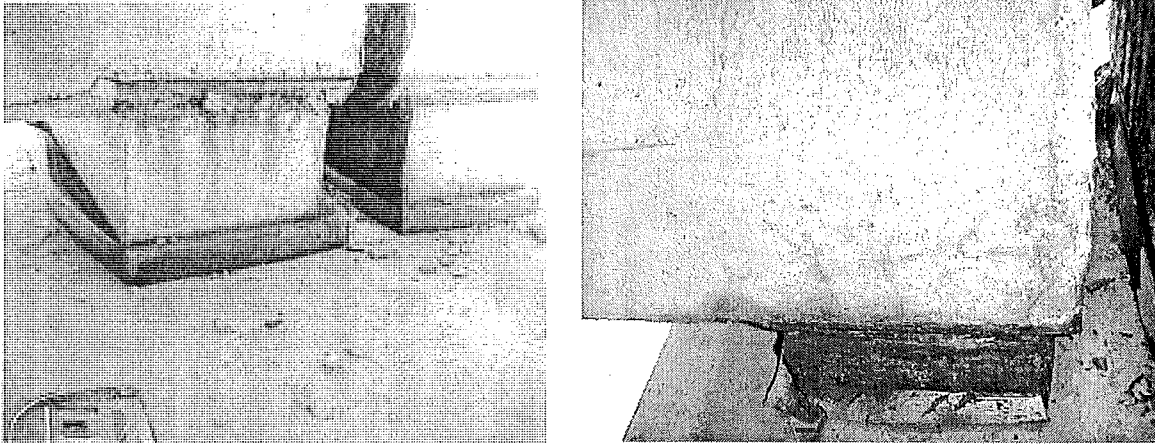


Photo 4-3. (Left) Sole plate corrosion and bulging at the sides of bearing pad, (Right) Sole plate corrosion and splitting, tearing and bulging at bearing pad

4.5 Summary

In this chapter, the prestressed concrete I-beam vulnerability to deterioration is defined based on the distress observed at the girder ends. A reason aggravating the beam-end distress is the expansion joint and/or the drainage system failure. As a result, the surface water together with dissolved deicing salts drain over the girder ends. With sufficient time deicing salts reach and initiate corrosion of the reinforcement and the tendons.

After performing the inspection and reviewing the inspection data consisting of 750 beam-ends and an equal number of bearings and sole plates, a pattern of deterioration was identified and a vulnerability assessment measure was proposed. The vulnerability assessment measure is based on the state of girder-end cracking in excess of 0.001 inches, expansion joint condition, functionality of the bearing pads and the state of corrosion of the sole-plate and bearing plate. The vulnerability can directly be assessed from the biennial visual inspection reports.

Five of the bridges inspected were of more recent vintage incorporating the continuous joint detail cast monolithically with the diaphragm and deck. The behavior of newer bridges is significantly different due to the lack of water infiltration (no leaky joint) and lack of subsequent restraint at the pier and abutment reduce sole plate corrosion.

The field survey of twenty prestressed concrete I-beam bridges included detailed visual inspection of the overall I-beam structure condition, including end deterioration for each I-beam. Beam-ends aging from two to ten years old were in very good condition, while older structures exhibited a greater amount of deterioration. Joint details in this bridge group vary with age and are likely the source of deterioration (high volumes of de-icing salts through leaky joints cause end deterioration of the I-beams). There is a need to include end condition assessment in the inspection procedure. This will allow for inspectors to rate the condition and properly assign a protective strategy prior to severe deterioration.

5.0 Multi-State Survey (Task 4)

5.1 Introduction

Having already obtained some Michigan data on the inspection, preventive maintenance and repair of prestressed concrete I-beams with the literature review and field inspections, it was imperative to know whether other states may be experiencing beam-end durability problems. To understand potential problems in other states, the research team developed, issued, and reviewed the feedback from a technical survey. With well-structured questions and an adequate response, a survey can be an effective tool for quickly interviewing a wide range or set group of respondents. The use of surveys is not a new concept in research. The durability and deterioration of prestressed concrete bridges has been investigated using surveys of state transportation departments in at least three past projects (Moore et al, 1970; Shanafelt and Horn, 1980; Rolander et al, 2001).

5.2 Objectives and Approach

Objectives of the survey included determining practices that are used for inspecting and repairing prestressed concrete I-beam ends, and identifying reports relating to the evaluation or repair of prestressed concrete I-beam ends. Specifically, five objectives were identified when preparing questions for the survey and they included:

1. Obtain a nationwide response rate of 20%; 100% from WI, IN, OH, MN, and IL.
2. Identify contacts for specialized areas of bridge engineering.
3. Locate potential sources of overall bridge condition and detailed beam end survey data.
4. Determine what practices are being used for evaluating and repairing prestressed concrete I-beam ends.
5. Identify reports relating to the evaluation or repair of prestressed concrete I-beam ends.

A section in the survey was also included for additional comments where recipients could clarify their overall opinions or comments relating to prestressed concrete I-beam evaluation and repair.

The survey was constructed to obtain as much information as possible from the respondents with as little effort on their part as possible. However, because of the unique information to be

gathered from each respondent, some questions request document information and most questions provide space for a contact name and telephone number. Where possible, the questions were structured with established answers (yes/no, or multiple choice). A copy of the survey and an accompanying cover letter is included in Appendix G-1: Survey Sent to State Departments of Transportation and Appendix G-2: Cover Letter for Multi-State Survey Instrument.

Several options were available for distributing and receiving survey responses. These formats consisted of:

1. Hardcopy (with U.S. Mail or fax return)
2. Response inside of e-mail text
3. Response inside of an e-mail attachment
4. On-line at the project or other website

Mr. Roger Till of MDOT Construction and Technology Division suggested that based on his experience, more responses would be generated if the survey was structured in a hardcopy or e-mail text format. To better satisfy the survey objectives, reference to completion and return of the survey on hardcopy or through the e-mail text was included in the survey cover letter.

The survey was distributed via email to the state bridge engineer, at each state's department of transportation, on June 27, 2001 by Mr. Till. The survey was accompanied by a cover letter, which is included in Appendix G-2: Cover Letter for Multi-state Survey Instrument. Email addresses for these engineers are contained in the MDOT list-serve database. Surveys were collected by Mr. Till and forwarded to Dr. Tess Ahlborn at Michigan Tech in order to centralize, review, and sort the survey data. Responses to MDOT were received between June and August 2001. The survey responses are tabulated in Appendix H and results discussed below.

5.3 Findings

Objectives for the multi-state technical survey were partially to fully met. A survey return-rate of 40 percent was achieved with 20 states responding. Responding states were located across the country and are shown as darkened states in Figure 5-1.

Two of Michigan's five neighboring states responded to the survey by the requested date and follow-up with non-responding states generated one additional survey response. One survey respondent indicated that the state did not have a prestressed concrete I-beam end deterioration problem and did not include a completed survey. This state was eliminated for the purposes of discussing the remainder of the results, leaving a base of 19 respondents.

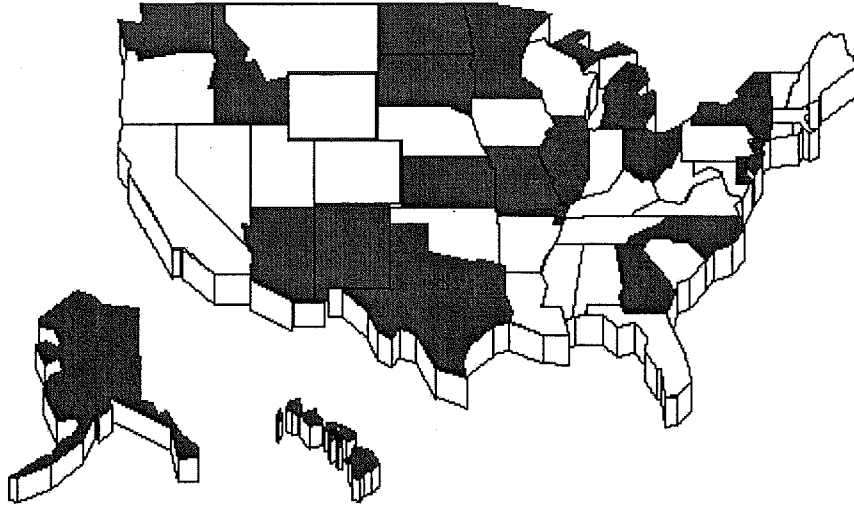


Figure 5-1. States Responding to the E-mail Survey

5.3.1 Inspection-Bridge Management Practices

Over 70 percent of the respondents indicated that they use some unique internal software for management of their state's bridge structural / safety data. All respondents indicated they do not gather specific inspection data on prestressed concrete beam end conditions. In regard to bridge inspection, all respondents indicated that the *FHWA Bridge Inspector's Training Manual / 90* (Hartle et al, 1990) is being used by their agency. The *AASHTO Manual for Condition Evaluation of Bridges* (AASHTO, 2000) was reported as being used by 74 percent of those responding. Nearly half (9 of 19) of those responding indicated that they also used some type of separate state-created document for inspecting bridges.

Illinois indicated having an inspection or assessment guideline, Illinois System Structure Information and Procedure Manual, (ISSIPM) which specifically addressed prestressed concrete I-beams. However, subsequent conversations with the Illinois Bridge Investigations and Repair Plans Unit Chief, Mr. Carl Puzey, indicated that the ISSIPM is only the Illinois version of how ratings for the NBIS should be taken (Puzey, 2001). The ISSIPM is largely based on the FHWA Recording and Coding Guide, according to Mr. Puzey (Puzey, 2001). Specific data on beam end conditions is not recorded and the ISSIPM is not intended to have the inspector pay closer attention to any one (bridge) item, according to Mr. Puzey.

Texas and Washington responded that non-destructive testing equipment (impact echo, detachable mechanical strain gauge, and fiber optic camera) was being used for inspection and assessment of their prestressed concrete I-beams. Follow-up with Mr. Randy Cox, Texas Department of Transportation Field Operations Section Director, indicated that bridge inspectors are not using impact echo and DEMEC gauges as part of routine bridge inspections (Cox, 2001). According to Mr. Cox, these tools are being used in special circumstances to investigate alkali-silica reaction (ASR) and delayed ettringite formation (DEF) deterioration of about 40 prestressed concrete I-beam bridges in Texas. Further, according to Mr. Cox, the DEMEC gauges are used to measure crack widths rather than strain in the members.

The remaining states indicated that their review of prestressed I-beams is limited to visual inspection and hammer sounding techniques.

5.3.2 Preventive Maintenance Practices

It was unclear from the survey responses if any states are using existing documentation (reports, etc.) to aid in the preventive maintenance of prestressed concrete I-beams.

Illinois was the only responding state that indicated they had documented prestressed concrete I-beam end preventive maintenance projects in their state. 3M's Zinc-Hydrogel Anode 4727 was applied to beam-ends as a preventive maintenance measure according to Illinois' survey response. Follow-up with Mr. Mark Gawedzinski of the Illinois Department of Transportation generated an IDOT report on Illinois' experience with the anode (Gawedzinski, 2001). According to this report, select I-beam ends of four structures were chosen for anode application in Illinois (IDOT, 2001). Both fascia and interior beams were selected (IDOT, 2001). The anodes were evaluated over a period of approximately three years for conformance with National Association of Corrosion Engineers (NACE) Standard 290-90 "Standard Recommended Practice for Cathodic Protection of Reinforcing Steel in Atmospherically Exposed Concrete Structures" (IDOT, 2001).

Although the 3M Zinc-Hydrogel Anode 4727 showed initial promise by conforming to the NACE Standard performance requirements, subsequent review of the anodes in 2000 revealed anode separation from the substrate and degradation of the hydrogel adhesive (IDOT, 2001). In addition, test procedures that were used to determine conformance to the Standard were suspected of not being representative of actual conditions. Consequently, Illinois rejected the 3M Zinc-Hydrogel Anode 4727 as a cathodic protection system.

On Texas' prestressed concrete I-beams affected by ASR and DEF, distresses are both local and widespread (Cox, 2001). Mr. Cox stated that some distresses are occurring at beam-ends where there are open joints (and water infiltration). Conversations with Mr. Cox, TxDOT, revealed that TxDOT applied a silane / paint treatment roughly 8 years ago to some prestressed concrete I-beams to try to mitigate ASR and DEF damage. Although no report was available on the study, Mr. Cox indicated that some additional distress has occurred to beam-ends since the treatment was first applied. Future distress of ASR and DEF damaged prestressed concrete I-beam bridges in Texas is anticipated to be so severe in the future that full replacement will be required, per Mr. Cox. Texas Special Specification 4421, Penetrating Concrete Surface Treatment, was cited by Mr. Cox as a specification that may be used in the preventive maintenance of prestressed concrete I-beams.

5.3.3 Repair Practices

While most states have not repaired prestressed I-beams for end deterioration, roughly 50 percent of the respondents indicated that their state's DOT specifications would be used in the rehabilitation of prestressed concrete I-beam ends. With the exception of Michigan, all states were contacted that indicated the potential use of their state's DOT specifications in beam repair. The reason for the follow-up was to obtain specific applicable section numbers that would govern the work. Hawaii and New Jersey engineers replied to the follow-up by indicating that, in contrast to their earlier response, a DOT specification did not exist that would govern prestressed concrete I-beam end repair. Both states indicated either a special provision or new specification section would need to be prepared to perform the work. Additional information was also obtained from three other states that indicated DOT specifications were available (Texas, New Mexico, and Illinois).

Texas Standard Specification Item 429, Concrete Structure Repair governs the repair of spalled and chipped areas of concrete structures. Epoxy mortar, portland cement concrete, and pneumatically placed concrete materials are permissible concrete repair materials in Texas per Item 429. Item 429 also includes recommended concrete removal, repair preparation, repair anchorage, and repair curing. Texas Special Specification 4421, Repair of Impact Damaged Prestressed Concrete Beams, was also cited by Mr. Cox as a potential document of interest to this project.

Mr. Puzey, IDOT, indicated that their Guide Bridge Special Provisions on Formed Concrete Repair, High Performance Shotcrete, and Polymer Modified Portland Cement Mortar could be followed for prestressed concrete I-beam end repairs in Illinois (Puzey, 2001). He indicated that Illinois had not found much success with epoxy mortars in repair. Other specifications are generated on a project specific basis.

Texas was the only state that cited the use of the *ACI Concrete Repair Manual* and *ICRI Repair Guidelines* for repairs. One initiative of the government funded SHRP was to develop concrete assessment and rehabilitation technologies (TTI, 1998). Although not mentioned in the survey, SHRP documents were not indicated as being used by any states.

Missouri was the only responding state that indicated using FRP repairs for the repair of damaged beams, however the respondent indicated that these repairs were not applied to beam ends.

Michigan has developed an overcasting repair procedure for prestressed concrete I-beams with end distress (Needham, 1999). Prior to encasing the beam end, the Michigan procedure specifies removal of deteriorated web and flange concrete. The overcast section on the beam end is also integrated with a new diaphragm. Repair concrete for this design is MDOT Grade D polymer (latex) modified concrete. MDOT plans were prepared detailing an end repair method for prestressed concrete I-beams with and without end blocks. This repair technique was executed in 1999 in Lower Michigan (Needham, 2000). Although numerous problems were encountered in the field repairs, they appeared to be attributed to contractor/engineer miscommunication and not necessarily the design details. According to MDOT, the cost of repairing prestressed concrete I-beam ends using this procedure was found to be 35 to 69 percent of full-replacement cost.

5.4 Summary

The survey was successful in showing that only a few states have addressed prestressed concrete I-beam end deterioration from an inspection, preventive maintenance, or repair point of view.

All states responding to the survey indicated that *FHWA Manual 90* was used as a guideline for the inspection of their bridges. Most states also use the *AASHTO Manual for Condition Evaluation of Bridges (2000)*. No states appear to be using non-destructive testing, other than acoustic emission testing, as part of routine bridge inspections, nor is any state paying particular attention to prestressed concrete I-beam ends during their inspections.

Preventive maintenance techniques that are currently in use include passive cathodic protection and sealers. According to the survey, Michigan is the only state that has attempted beam-end repair. Half of the responding states indicated that if beam-end repair was needed, that their state's standard specifications would govern the work.

6.0 Survey of Inspection Techniques (Task 5)

6.1 Introduction

The primary goal of this task was to develop an inspection procedure for early identification of prestressed concrete I-beam ends prone to deterioration. Due to field constraints it is desirable to limit the inspection techniques to visual (at an arms length). The techniques presented here are based on the literature review and the field inspection conducted during this project. The research team inspected 20 bridges and performed casual drive by inspections of numerous other prestressed concrete I-beam bridges. Afterwards the expectations from the inspection procedure were defined as to identify the symptoms related to: 1) material distress, 2) structural behavior, loading distress and 3) distress resulting from deferred maintenance. In some cases the symptoms related to the distress may overlap.

In reviewing the observations and data obtained during the inspections there are three inspection items of importance that directly impact I-beam end deterioration. These items are:

1. Presence of beam end cracking,
2. Bearing condition and their influence on beam end restraints, and
3. Drainage and expansion joint condition.

The presence of beam end cracks was observed as early as during production. Additional causes of beam end cracking may be due to loading and end restraints. Beam end restraints are controlled by the bearings, diaphragms and the deck if cast continuously. The effects of the restraints to beam behavior is investigated and described in Chapter 10.

Aside from the maintenance and structural behavior related distress, the material related distress is observed as cracking around the beam-end forming at the time of production. It is the research team's opinion that these cracks contribute significantly to premature end deterioration. Field inspection data showed that these cracks are widened with moisture ingress and freezing action. Later the ingress of chlorides further widens cracks during the shear reinforcement and tendon corrosion process. The initial crack widths are often around 0.001 inch and detection during inspection is difficult. (The cracking was observed using a water spray bottle and a magnifying crack gage). However, identification of cracks during early ages and including those beams in a preventive maintenance program with an appropriate sealant will prolong beam life.

Another inspection item identified during the field inspection was the sole plate and bearing plate assembly. Sole plate corrosion causes cracking of the beam near the base of the bottom flange. This cracking is perhaps initiated by the corrosion progressing to the sole plate anchors. Also,

this cracking propagates parallel to the bottom flange as corrosion progresses. Corrosion to the sole plate should be prevented either during design by the use of a non-corrosive plate or by maintenance. For existing bridges, maintenance solutions to the sole plate corrosion issue need identification. Sole plate corrosion is different from bearing plate corrosion by the fact that the sole plate is directly in contact with the beam and generates stresses in concrete unlike bearing plate corrosion which only effects the integrity of the bearing plate and elastomeric bearing pad.

6.2 Common States of I-Beam End Deterioration

This section reviews the current standards for the condition assessment of prestressed concrete beams and proposes condition states specifically for beam end deterioration.

6.2.1 Standards for Condition Assessment in Michigan

There are two current standards in Michigan for assessing the amount of deterioration to prestressed concrete I-beams. First, certified bridge inspectors for the State of Michigan are trained to assigned condition state numbers to each component of the bridge such as the deck, stringers, piers, and abutments, according to the Federal Highway Administration guidelines listed in the *FHWA Bridge Inspector's Manual / 90* (1991, revised 1995). These eleven condition states are given in Table 6-1.

Table 6-1. Federal Highway Administration condition ratings

Rating	Description
N	NOT APPLICABLE
9	EXCELLENT CONDITION
8	VERY GOOD CONDITON – no problems noted
7	GOOD CONDITION – some minor problems
6	SATISFACTORY CONDITION – structural elements show some minor deterioration.
5	FAIR CONDITION – all primary structural elements are sound but may have minor section loss, cracking, spalling, or scour.
4	POOR CONDITION – advanced section loss, deterioration, spalling, or scour.
3	SERIOUS CONDITION – loss of section, deterioration, spalling, or scour have seriously affected primary structural components. Local failures are possible. Fatigue cracks in steel or shear cracks in concrete may be present.
2	CRITICAL CONDITION – advanced deterioration of primary structural elements. Fatigue cracks in steel or shear cracks in concrete may be present or scour may have removed substructure support. Unless closely monitored it may be necessary to close the bridge until corrective action is taken.
1	“IMMINENT” FAILURE CONDITION – major deterioration or section loss present in critical structural components, or obvious vertical or horizontal movement affecting structure stability. Bridge is closed to traffic but corrective action may put bridge back in light service.
0	FAILED CONDITION – out of service; beyond corrective action

Certified bridge inspectors also assign a Pontis Condition State using the Pontis Bridge Inspection Manual (MDOT Lansing Maintenance Division, 1999). The manual illustrates four condition states for prestressed concrete I-beams; see Figure 6-1.

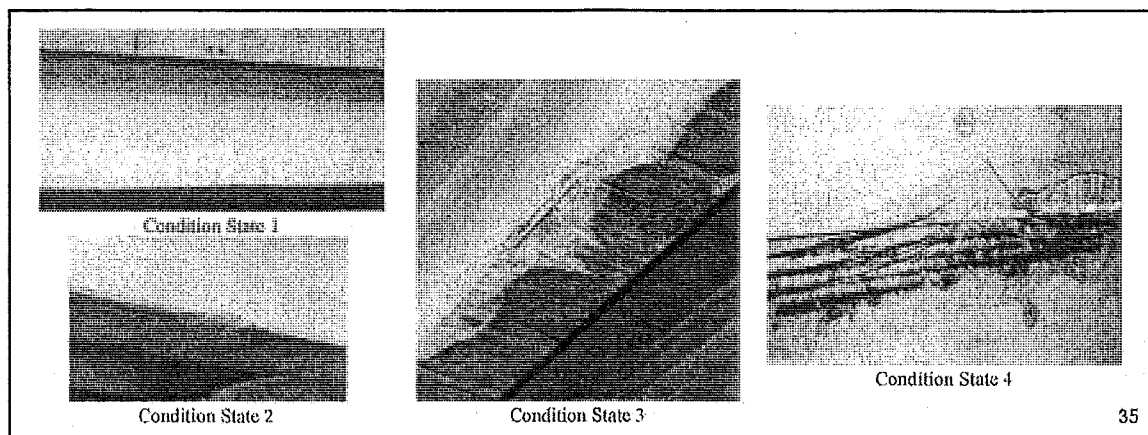


Figure 6-1. Pontis Bridge Inspection Condition State

While both inspection documents noted above are well known and highly used, neither is specifically written for inspection of prestressed concrete I-beam end deterioration.

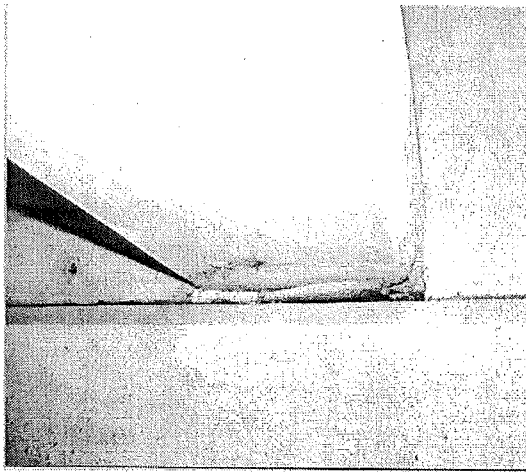
6.2.2 Condition States

An accurate condition assessment of prestressed concrete beam-end deterioration is necessary to determine that level of distress and an appropriate preventative maintenance or repair technique. Condition states for a prestressed concrete I-beam should describe the level of distress at the beam-end that progresses with time. The following information has been assembled to assist an inspection crew with accurately assessing the condition of a beam-end. Twelve condition states have been developed (Table 6-2) utilizing the inspection data compiled during a field investigation of twenty prestressed concrete bridges in Michigan ranging in age from 2 to 40 years old (see Chapter 3). These condition states are only applicable to the beam-end and are meant to refine the FHWA Condition Ratings 9-4 and Pontis Condition States 1-3 reviewed above. In Table 6-2, hairline, moderate, and major crack widths are the same ranges as described in section 3.8.1-Condition Database.

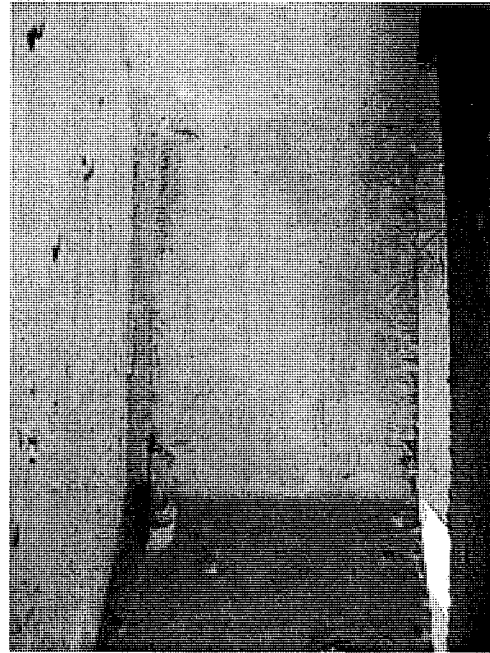
Table 6-2. Condition States of Prestressed Concrete I-Beam Ends

Rating	Condition State
1	No cracks observed, no staining
2	Efflorescence, water-stains, and/or corrosion
3	Hairline Cracks. They can be horizontal, vertical, and/or diagonal
4	Map Cracks
5	Hairline Cracks with efflorescence, water-stains, and/or corrosion with a horizontal crack propagating from the sole plate
6	Cracked and Deformed Neoprene Pad, probably non-functional
7	Moderate Cracks
8	Moderate Cracks with efflorescence, water-stains, and/or corrosion
9	Major Cracks with efflorescence, water-stains, and/or corrosion
10	Delamination with Moderate and/or Major Cracks
11	Spall, Delamination, Corrosion, and Cracks
12	Spall, Exposed Reinforcement, and Corrosion

All photographs taken during the field inspection were grouped into respective condition states folders based on the distress demonstrated in the photo and the information obtain from the inspection form. The most distressed beam-end condition that was seen in the photo and on the inspection form defines the condition state for that beam-end. For example, if a photo of a beam-end only showed moderate cracks, and the inspection form also noted an area of delaminated concrete then the inspection form data will define the condition state and the assigned rating would be 10 and not 7. Two examples of every condition state are given in Photo 6-1 through Photo 6-12; photo name and bridge inventory number are also provided for each photo. The photo file convention is described in section 8.3.2.1-Bridge Inspection Photo Database. Photos are also tabulated to assist the inspector in defining condition states (Table 6-3).

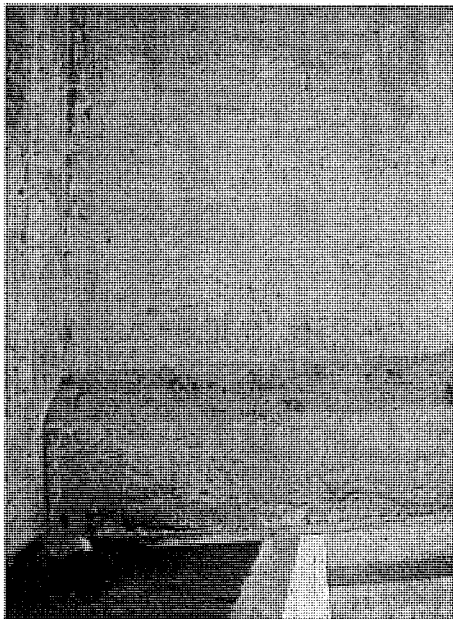


(a)

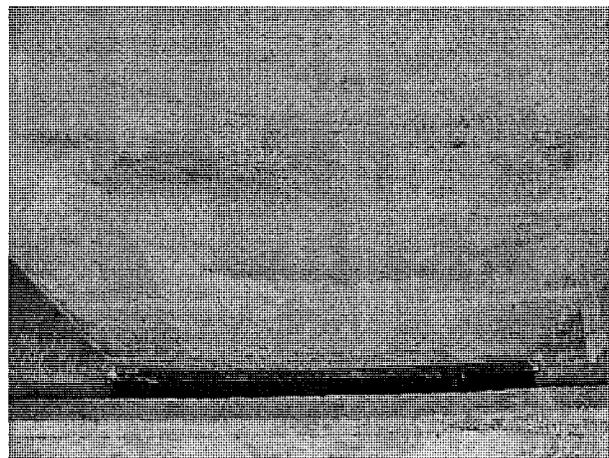


(b)

Photo 6-1. Condition State 1—No cracks observed, no staining (a) E1-S4-E-U from 25132 S34 and (b) S1-E2-N-E.2 from 06111 S04

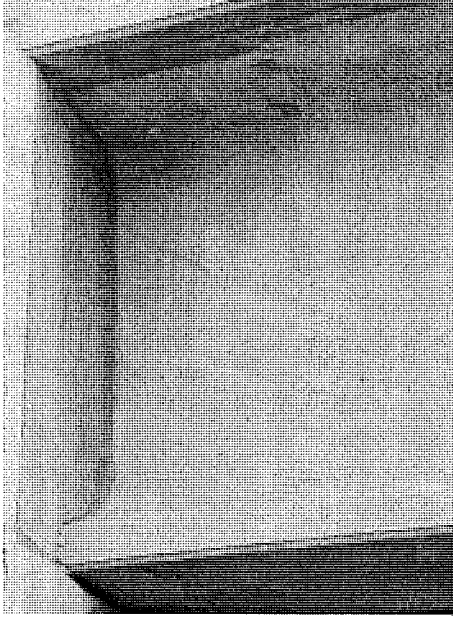


(a)

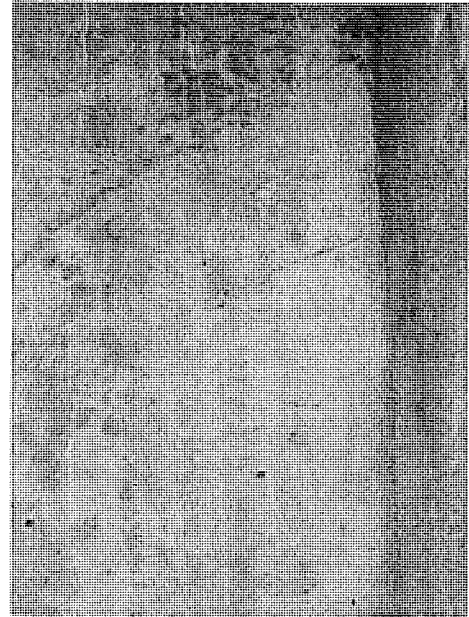


(b)

Photo 6-2. Condition State 2—Efflorescence, water-stains, and/or corrosion (a) E4-S5-W-B from 53034 S05 and (b) S1-E2-N-U from 67016 S09

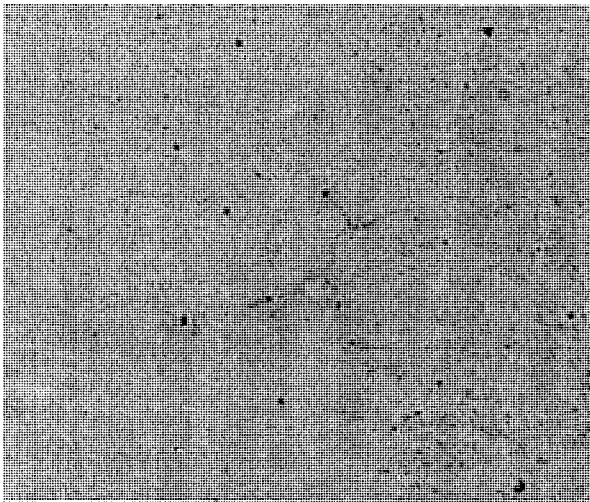


(a)

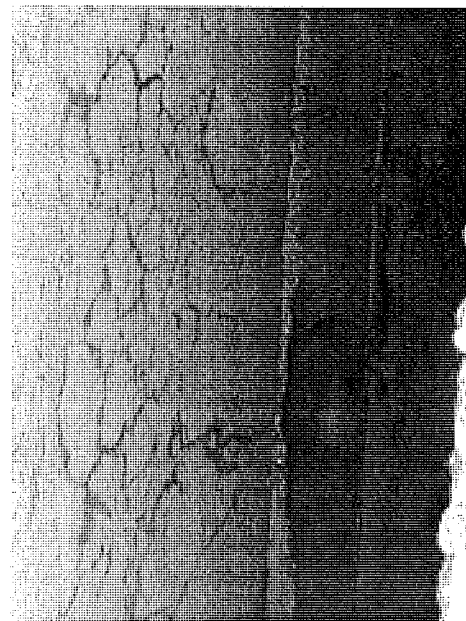


(b)

Photo 6-3. Condition State 3—Hairline Cracks. They can be horizontal, vertical, and/or diagonal (a) E1-S1-W-S.3 from 83033 S06 and (b) E1-S8-W-N.2 from 83033 S06

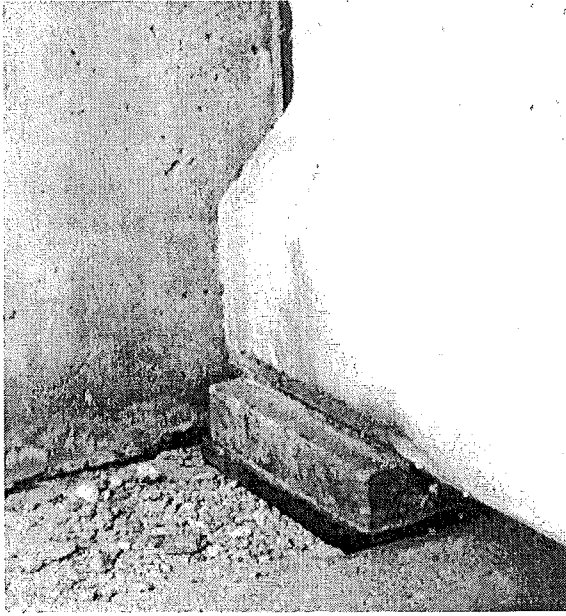


(a)

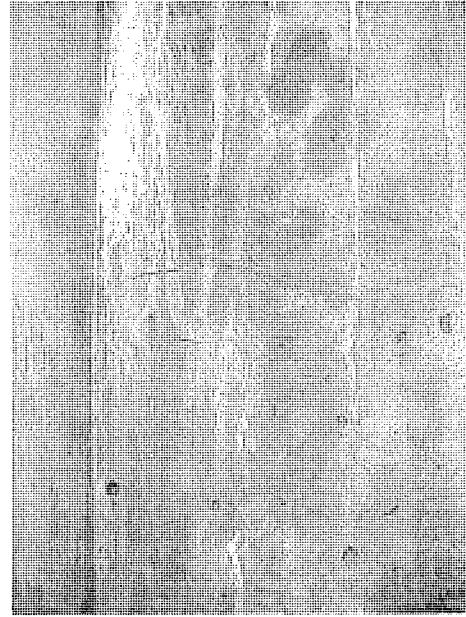


(b)

Photo 6-4. Condition State 4—Map Cracks (a) E2-S3-E-S from 25132 S34 and (b) E4-S1-E-R from 53034 S05

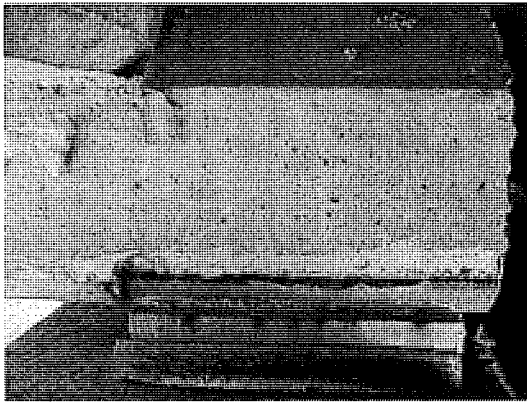


(a)

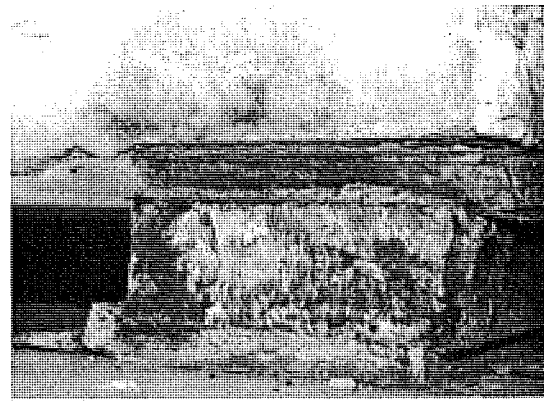


(b)

Photo 6-5. Condition State 5—Hairline Cracks with efflorescence, water-stains, and/or corrosion with a horizontal crack propagating from the sole plate (a) S3-E9-N-E.1 from 29011 S03 and (b) E1-S8-W-S.1 from 83033 S06

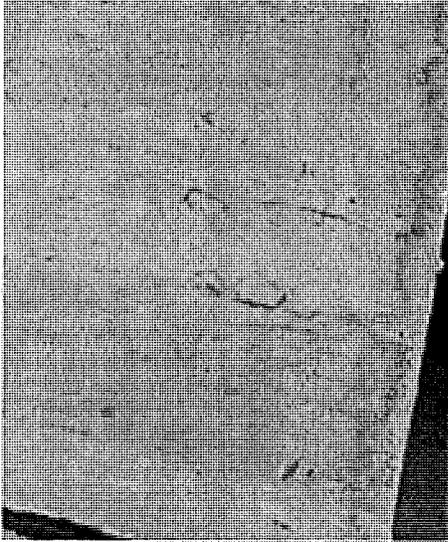


(a)

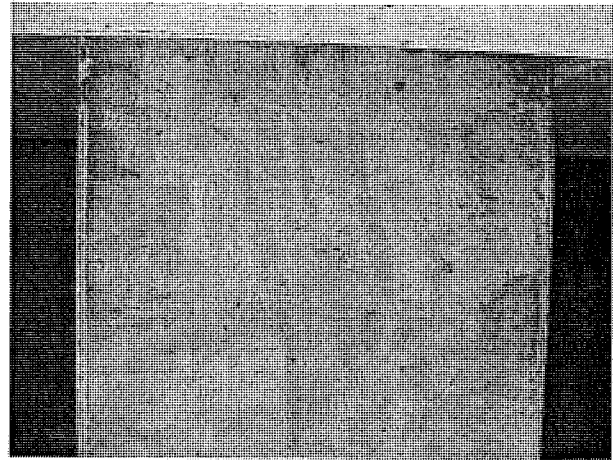


(b)

Photo 6-6. Condition State 6—Cracked and Deformed Neoprene Pad, probably non-functional (a) S1-E2-N-B from 06111 S04 and (b) E1-S2-W-N from 41029 S16-3

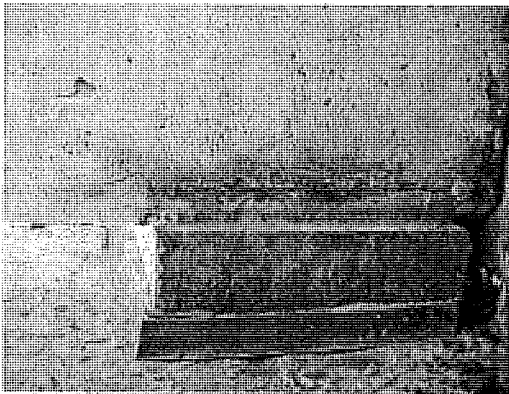


(a)



(b)

Photo 6-7. Condition State 7—Moderate Cracks (a) E4-S1-E-S from 53034 S05 and (b) S1-E3-N-U from 67016 S09

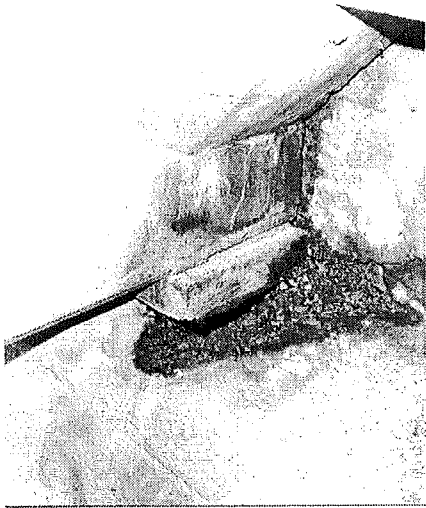


(a)



(b)

Photo 6-8. Condition State 8—Moderate Cracks with efflorescence, water-stains, and/or corrosion (a) E2-S3-E-B from 25132 S34 and (b) E2-S8-E-S.2 from 41029 S16-4



(a)

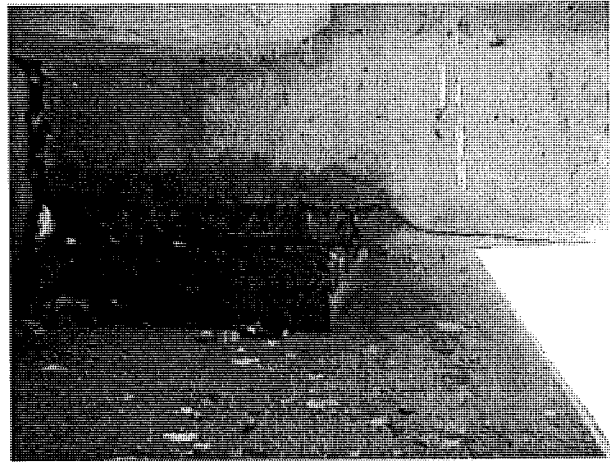


(b)

Photo 6-9. Condition State 9—Major Cracks with efflorescence, water-stains, and/or corrosion (a) S3-E9-N-W.2 from 29011 S03 and (b) S2-E9-N-W from 29011 S03

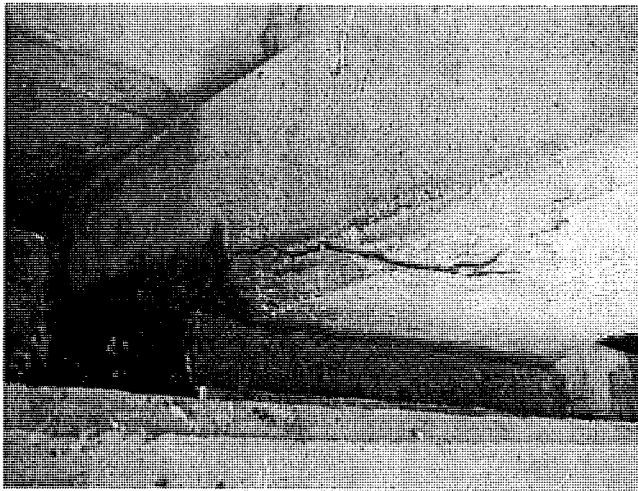


(a)



(b)

Photo 6-10. Condition State 10—Delamination with Moderate and/or Major Cracks (a) E2-S5-E-S.1 from 25132 S34 and (b) S2-E8-N-W from 29011 S03



(a)

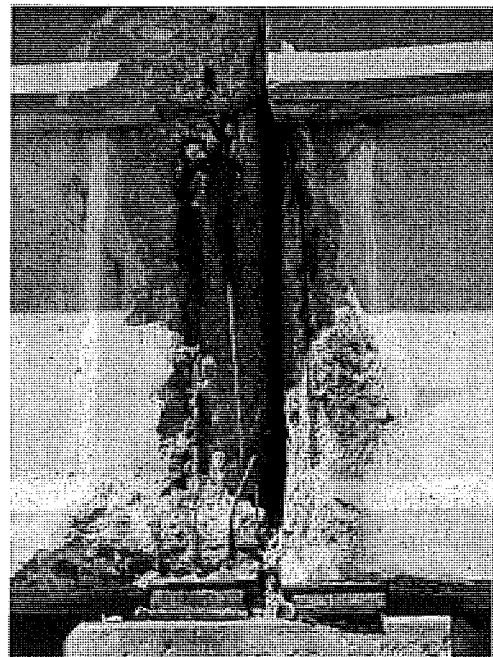


(b)

Photo 6-11. Condition State 11—Spall, Delamination, Corrosion, and Cracks (a) S2-E7-N-U from 29011 S03 and (b) E2-S8-E-N.6 from 41029 S16-4



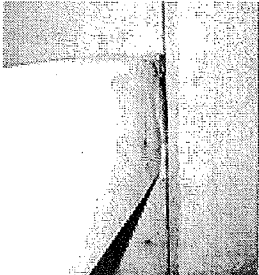
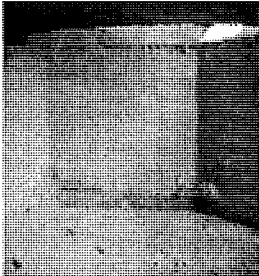
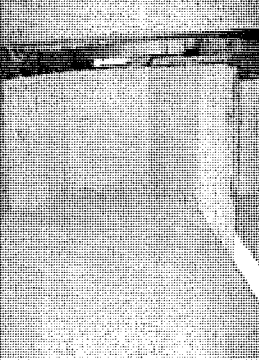
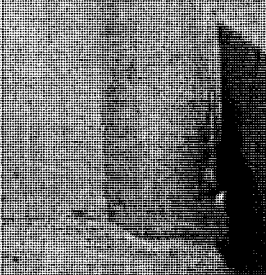
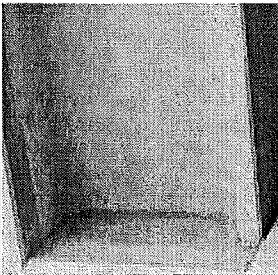
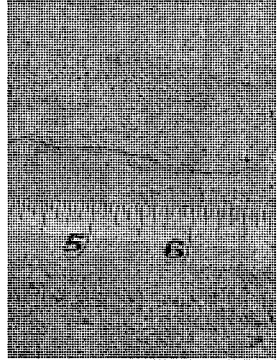
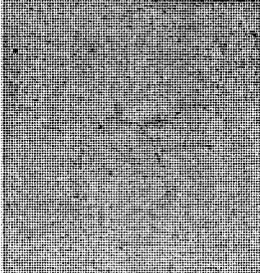
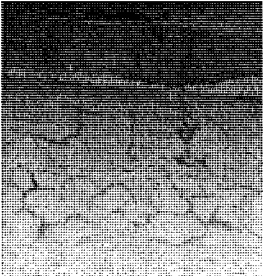
(a)

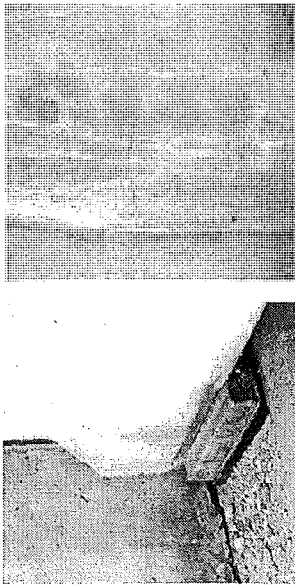
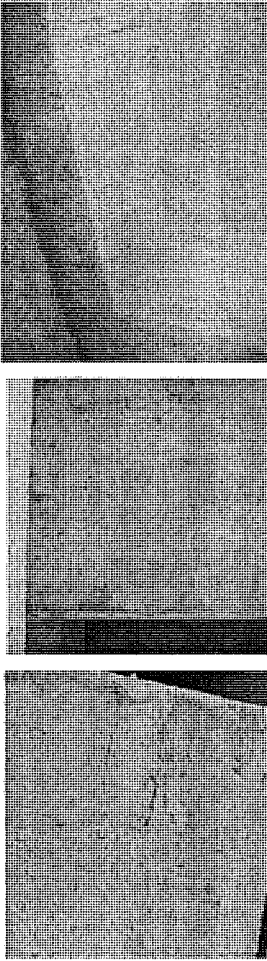
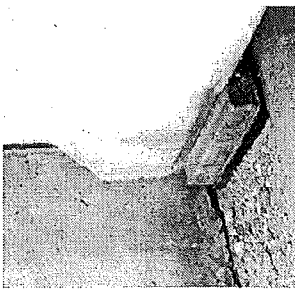
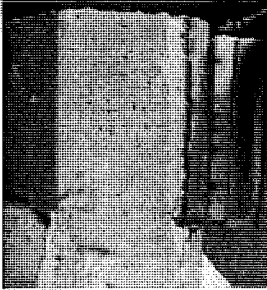
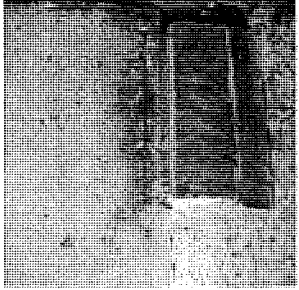


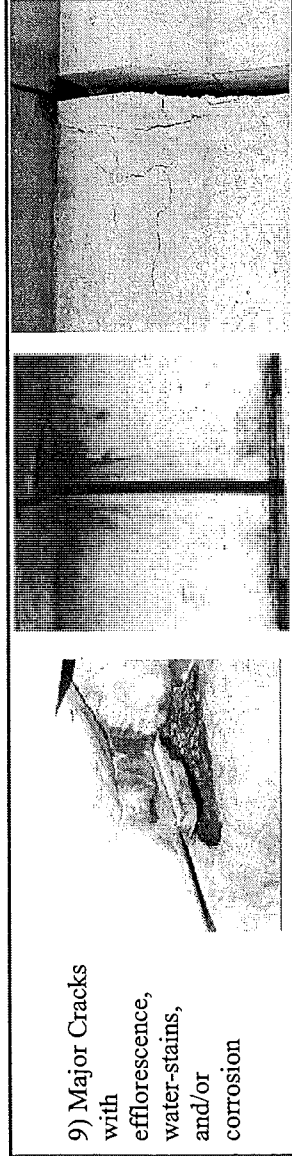
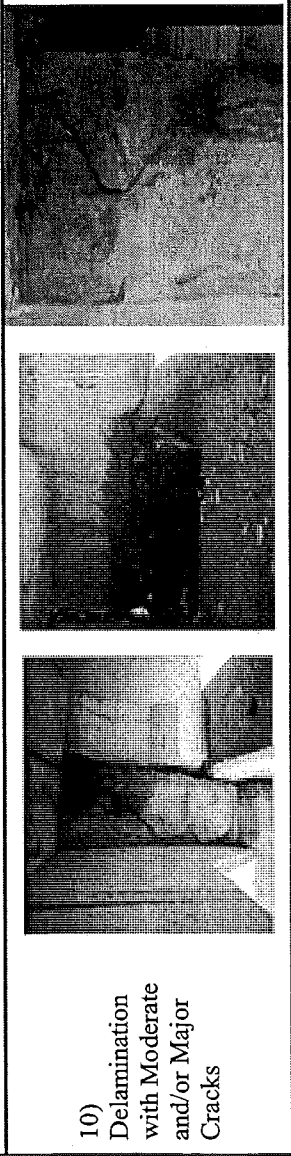
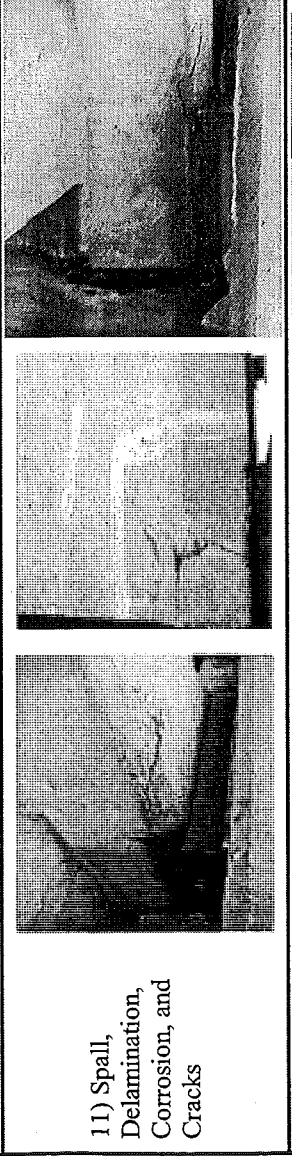
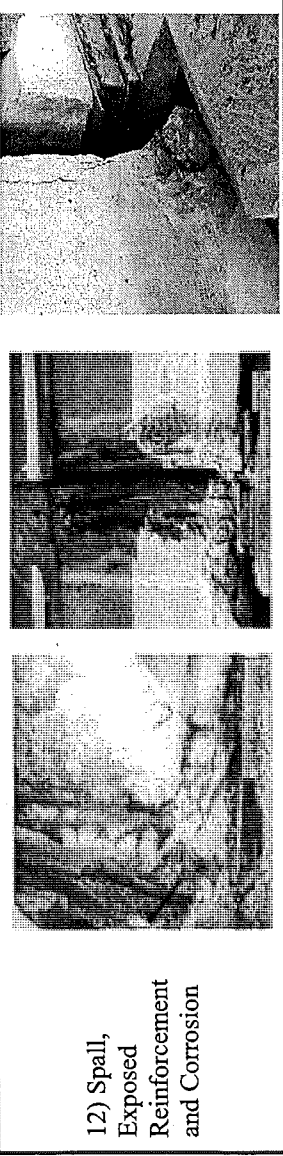
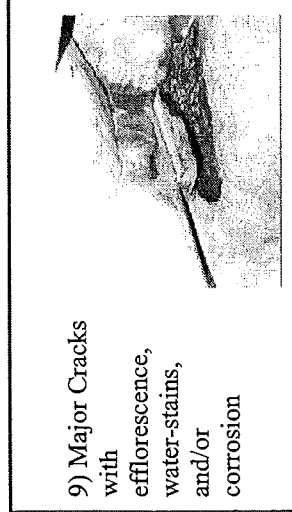
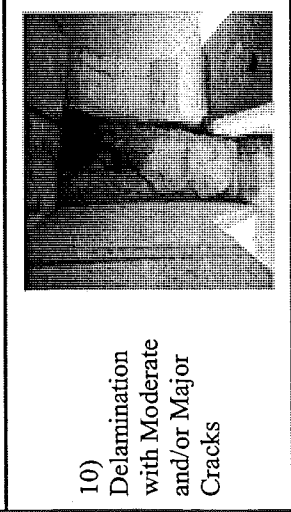
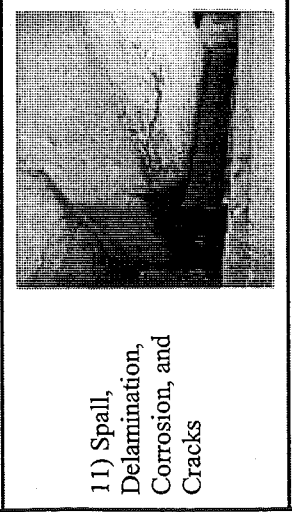
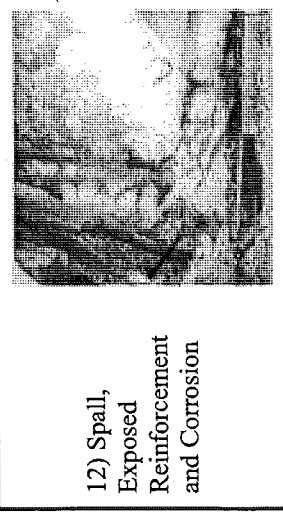
(b)

Photo 6-12. Condition State 12— Spall, Exposed Reinforcement, and Corrosion (a) E3-S1-E-N.2 from 41029 S16-4 and (b) E2-S1-W-S.3 from 41029 S16-4

Table 6-3. Condition States Photographs

Condition State	Photos Demonstrating the Condition States		
1) No cracks observed, no staining			
2) Efflorescence, water-stains, and/or corrosion			
3) Hairline Cracks. They can be horizontal, vertical, and/or diagonal			
4) Map Cracks			

<p>5) Hairline Cracks with efflorescence, water-stains, and/or corrosion with a horizontal crack propagating from the sole plate</p> 		<p>6) Cracked and Deformed Neoprene Pad, probably non-functional</p> 	<p>7) Moderate Cracks</p> 
<p>8) Moderate Cracks with efflorescence, water-stains, and/or corrosion</p> 			

<p>9) Major Cracks with efflorescence, water-stains, and/or corrosion</p> 			
			
<p>10) Delamination with Moderate and/or Major Cracks</p>			

6.3 Summary

Accurate condition assessment of prestressed concrete I-beam ends is essential for the decision related to providing adequate preventative maintenance and repairs. Table 6-2 and Table 6-3 will assist the inspectors with accurate assessment. Later in Chapter 12, Table 6-3 is further linked to suggestions for preventative maintenance and repair.

7.0 Preventive Maintenance Techniques for End Deterioration (Task 6)

7.1 Introduction

This study identified four major families of preventive maintenance approaches that can be applied to beam-ends. These techniques were:

- Structure Modifications,
- Surface Insulating Methods,
- Electrical Control Methods, and
- Environment Modifying Methods.

These families of techniques were discussed in detail in Section 2.4.2 and are also presented in Appendix J. Advantages and disadvantages were also discussed in Section 2.4.2. As shown in Appendix J, several techniques are available for use. However, the research team found that silanes, siloxanes, and sacrificial anode cathodic protection are currently being used by other states for preventive maintenance purposes.

7.2 Analysis Tools

The research team has identified and developed analysis tools that can be used by MDOT to classify the severity of end-distress and determine which techniques may be most effective in preventing corrosion-induced deterioration of beam-ends. These tools are discussed in the following sections and apply to both preventive maintenance and repair type work.

7.2.1 Distress Severity Classification

To arrive at or decide upon an appropriate preventive maintenance or repair approach, say during a bridge scoping or as a prelude to a structural analysis, information on the condition of a deteriorated beam-end would need to be obtained. To this end, several different observations or tests can be performed to assess the condition of a beam-end. The research team has identified tests applicable to corrosion-induced deterioration that could be performed by MDOT to assist in classifying the severity of end distress. These tests are listed in Table 7-1. Engineering

judgment was largely used to establish severity levels based on a test result. However some references provided insight in setting each level. These references are included in Table 7-1.

Table 7-1. Testing Procedures and Distress Severity Criteria for Prestressed Concrete I-Beam End Deterioration

Test	Testing Performed In	End Distress Severity (references)			Notes
		Low	Moderate	High	
Air Content	Lab	≥ 6.0% (Kosmatka et al, 2002; ACI, 1999; ACI, 1992)	< 6.0%	< 6.0%	Deicer environment. Assuming a nominal maximum aggregate size of 3/4-inch (severe exposure)
		≥ 5.0% (ACI, 1992; AASHTO, 1996)	< 5.0%	< 5.0%	Non-deicer environment (moderate exposure)
Carbonation	Field / Lab	< 1-inch	≥ 1-inch and < 1.5-inches	≥ 1.5-inches	All conditions
Chloride Ion Content	Field / Lab	< 0.06% by wt. cement, water soluble (ACI, 1992; ACI, 1999)	≥ 0.06% and < 0.12% by wt. cement	≥ 0.12% by wt. cement	For all conditions, as measured at reinforcement.
Concrete Cover	Field	≥ 2-inches (ACI, 1999)	< 2-inches and ≥ 1-inch	< 1-inch	Deicer environment, tension less than $6(f'_{ci})^{0.5}$ (ACI, 1999)
		≥ 1.5-inches (ACI, 1999)	< 1.5-inches and ≥ 1-inch	< 1-inch	Non-deicer environment
Concrete Loss (Delamination and Spalling)	Field	No Concrete Loss	< 10% of end or any one side surface area	> 10% of end or any one side surface area	All conditions
Corrosion Potential	Field	more + than -200mV (ASTM, 1991)	more - than -350mV (ASTM, 1991)	more - than -350mV (ASTM, 1991)	All conditions
Corrosion Current Density	Field	≤ 0.2-mA/sf (Clear, 1989)	> 0.2-mA/sf and ≤ 1-mA/sf	> 1-mA/sf	All conditions
Crack Size (non-delamination)	Field	≤ 4-mils (Moore et al, 1970)	> 4-mils and ≤ 7-mils	> 7-mils	Deicer environment.
		≤ 7-mils (PCI, 1999)	> 7-mils and ≤ 10-mils	> 10-mils	Non-deicer environment.
Crack Type	Field	Non-structural	Non-structural	Structural	All conditions
Crack Length	Field	No criteria established			
Crack Direction	Field	No criteria established			
Staining	Field	No Evidence	Any Evidence	Any Evidence	All conditions

Test	Testing Performed In	End Distress Severity (references)			Notes
		Low	Moderate	High	
Water / Cement Ratio	Lab	≤ 0.40 (Kosmatka et al, 2002; ACI, 1999)	> 0.40 and ≤ 0.45	> 0.45	Deicer environment
		≤ 0.50 (Kosmatka et al, 2002; ACI, 1999)	> 0.50	> 0.5	Non-deicer environment Note: Criteria assumes air-entrained concrete

Some tests listed in Table 7-1 cannot be performed rapidly in the field or by inexperienced staff. These tests are generally more costly to perform and inherently less preferable to less intensive or advanced procedures. In addition, some tests hold more worth in assessing the condition of a beam-end compared to other tests. For example, the amount of concrete loss is, even to the casual observer, more influential in determining the condition of a beam-end than say air content. To effectively use Table 7-1, MDOT would need to first identify which tests or observations to perform and second, assign weighted importance to the tests themselves. Lastly, a procedure would need to be developed to sum the results of all tests performed to determine the distress severity. Recommendations for accomplishing the effective use of Table 7-1 are included in Section 14.4 of this report.

7.2.2 Distress Cause and Recommended Follow-up Techniques

Determining the level of distress severity is one step towards selecting a preventive maintenance or repair technique to use on a beam-end. In order for a preventive maintenance or repair technique to be effective, the cause of the distress must be known and technique selected to properly address the cause. Table 7-2 presents several cause-evidence relationships that field personnel can use to identify the cause of beam-end distress. It should be noted that although beam-end distress in Michigan I-beam bridges appears to be corrosion induced deterioration, other forms of deterioration might surface in the future. Therefore, several cause-evidence relationships are listed.

A natural progression of Table 7-2 is to identify preventive maintenance or repair techniques that can be used for a particular cause-evidence (effect) relationship. At a basic level, a subjective approach can be used to say that one technique for one or multiple distress severities (e.g., use passive cathodic protection for low and moderate severity beam-end distress). It is imperative to understand that while each cause of distress can be linked to a preventative maintenance or repair technique, every case must be considered on an individual basis. For example, for a case where the primary cause of distress is leaking expansion joints the immediate solution appears to be repairing the joint. However, corrosion must be halted so that continued degradation does not occur. Depending on the level of distress, chloride ion extraction may be necessary in conjunction with cathodic protection and additional sealers. MDOT can use and extend this approach to future work as another means of obtaining desirable results.

Table 7-2 attempts to list preventative maintenance (PM) and repair techniques for low, moderate and high severity levels of distress. For distresses directly linked to corrosion-induced deterioration, methods from Appendix J have been subjectively assigned to varying distress levels. For non-corrosion induced distress, such as thermal-induced movements, no techniques

have been listed at this time. Rather a note has been added stating “Identify and Subjectively Assign Techniques” and should be addressed through future work.

Table 7-2. Cause-Evidence Relationships for Beam-End Distress

Primary Cause of Distress	Secondary Cause of Distress	Beam-End Evidence	PM / Repair Technique		
			Low Severity Distress	Moderate Severity Distress	High Severity Distress
Leaking expansion joints	Chloride-induced corrosion	<ul style="list-style-type: none"> Failed joint (look between diaphragm pairs). Fine debris (sand, cigarette butts) will be present on the top of the pier (investigators observations). Top or sides of pier may show deterioration. Elevated levels of chloride ion may be present with corrosive staining. Spalled, cracked, or delaminated concrete may be present (investigators observations). Vertical cracks may be present. 	see App. J 1.0 2.0	1.0 3.0 4.0 5.0	1.0 4.0 5.0
Wet or moist service environment	Frozen, corroded bearings	<ul style="list-style-type: none"> Localized spalling at the bearings with little to no signs of reinforcement corrosion Steel bearing plates would show complete corrosion 	Identify and Subjectively Assign Techniques		
	Freeze-thaw deterioration	<ul style="list-style-type: none"> Surface scale, cracking, or crumbling of the beam end will be evident. Of these distresses, scaling will likely give the greatest indication that the distress is freeze-thaw related. Low air content of concrete. 			

Primary Cause of Distress	Secondary Cause of Distress	Beam-End Evidence	PM / Repair Technique		
			Low Severity Distress	Moderate Severity Distress	High Severity Distress
Acidic service environment	Carbonation-induced corrosion	<ul style="list-style-type: none"> • High w/c. • Older structures may be affected to a greater degree. • Distress may extend to the entire member. • Some source of moisture would need to be present; a high humidity environment may be sufficient. • Vertical cracks may be present. 	see App. J 2.0 4.0	4.0	4.0 5.0
Inadequate concrete cover	Carbonation-induced corrosion	<ul style="list-style-type: none"> • Cover to reinforcement may be less than indicated on the design drawings or less than current design requirements. • High w/c. • Older structures may be affected to a greater degree. • Distress may extend to the entire member. • Some source of moisture would need to be present; a high humidity environment may be sufficient. • Vertical cracks may be present. 	see App. J 1.0 2.0	1.0 2.0 5.0	1.0 5.0
	Chloride-induced corrosion	<ul style="list-style-type: none"> • Cover to reinforcement may be less than indicated on the design drawings or less than current design requirements. • Elevated levels of chloride ion will be present with corrosive staining, spalled, cracked, or delaminated concrete. • Vertical cracks may be present. 	see App. J 1.0	1.0 3.0 4.0 5.0	1.0 3.0 4.0 5.0
Thermal-induced movements	None identified	<ul style="list-style-type: none"> • Twisting or other distortion of the member, possibly in the weak axis. 	Identify and Subjectively Assign Techniques		
Diaphragm bonding	None identified	<ul style="list-style-type: none"> • Horizontal cracking may be present. 			

Primary Cause of Distress	Secondary Cause of Distress	Beam-End Evidence	PM / Repair Technique		
			Low Severity Distress	Moderate Severity Distress	High Severity Distress
Overloading or impact of the element	None identified	<ul style="list-style-type: none"> Diagonal cracking may be present. 	Identify and Subjectively Assign Techniques		
Improper cutting of prestressing strands	None identified	<ul style="list-style-type: none"> Horizontal, diagonal, or frown cracking may be present. 			
Location of un-bonded strands	None identified	<ul style="list-style-type: none"> Longitudinal flange cracking may be present. 			
Insufficient reinforcement	None identified	<ul style="list-style-type: none"> Diagonal or map cracking may be present. 			

*PM is an Abbreviation for Preventative Maintenance

7.2.3 Performance Matrix

If it is desired to use preventive maintenance to prolong beam life, a performance matrix may aid in selecting the most effective approach between multiple suitable approaches. For this study, an example matrix was developed specifically for distresses attributed to corrosion-induced deterioration from leaking transverse deck joints. Similar tables may be developed for other cause-effect scenarios, however this relationship appears to govern a majority of the time.

In order to develop a performance matrix, technical requirements for the preventive maintenance approach need to be identified. For this study, technical requirements were selected as those having the greatest impact on prestressed concrete I-beams in Michigan. MDOT will ultimately need to identify which technical requirements are most important, however, as a starting point, MDOT may want to consider the:

- Effectiveness to control reinforcement corrosion.
- Durability of the technique.
- Infrastructure requirements of the technique.
- Service life of the technique.

In Table 7-3, each preventive maintenance approach is evaluated for meeting the technical requirements. The research team attempted to identify a consistent procedure that could be used to assign a score to a technical requirement. At a basic level, a technical requirement score could be determined by review of independent or vendor provided literature, and conclusions can be made for products either meeting, not meeting, or inconclusively meeting the technical requirements.

Table 7-3. Example Performance Matrix for Preventive Maintenance Techniques

Approach All approaches are not listed.	Technical Requirement	Effectiveness	Durability	Infrastructure	Service Life	Total Score (60 max)
	Weighted Importance	10	7	8	5	
	Impact Definition	0 = Not effective 1 = Inconclusive 2 = Effective	0 = Not durable 1 = Inconclusive 2 = Durable	0 = Required 1 = Inconclusive 2 = Not required	0 = < 4 years 1 = Inconclusive 2 = ≥ 4 years	
Transverse Deck Joint Maintenance	Weighted Score (weighted importance x impact definition)	20	7	16	10	53
Sacrificial Anode Cathodic Protection, SACP		10	7	16	5	38
Penetrating Sealers		0	7	16	5	28
Surface Sealers		0	7	16	5	28
Surface Coatings		10	14	16	10	40
Surface Applied Corrosion Inhibitors		10	7	16	5	38
Crack Treatment for Beams		10 ^a	7	16	5	38
Impressed Current Cathodic Protection		20	0	0	10	30

^aNo data available, therefore an inconclusive impact definition was assigned

Table 7-3 is an example of what a completed performance matrix may look like. In Table 7-3, the importance of each requirement was viewed relative to one another and assigned weights using a point scale of 1 to 10. A high score in the matrix does not necessarily mean a technique is appropriate for a certain level of distress, but does establish preference among the available options. MDOT can refine this matrix or develop new matrices based on specific input from their personnel. Additionally, ideas for future development of this performance matrix are given in Chapter 14 – Recommendations for Future Work.

7.3 Summary

Four families of preventative maintenance techniques were identified and can be applied for beam-end deterioration. Several test procedures are identified for inspectors and field personnel to assist in categorizing the level of distress (low, moderate, high). While determining the level of distress is important in selecting a preventative maintenance technique, the cause of distress must be known (usually through beam-end evidence) so that technique can properly address the cause. Therefore, several cause-evidence relationships were identified, including those forms of deterioration beyond corrosion-induced deterioration. Each distress cause and its beam-end evidence has been linked to several preventative maintenance and repair techniques for varying levels of distress. It is important to understand that while each distress cause can be linked to a preventative maintenance technique, every case must be considered on an individual basis.

8.0 Project Website (Task 7)

8.1 Introduction

The Center for Structural Durability's website provides information on completed and current projects activities. The project website is regularly being updated and modified as new and old projects are started and completed. The website is located at Wayne State University in accordance with Task 7 description. Figure 8-1 shows the Homepage of the project website. The current website address is:

<http://webpages.eng.wayne.edu/durabilitycenter>

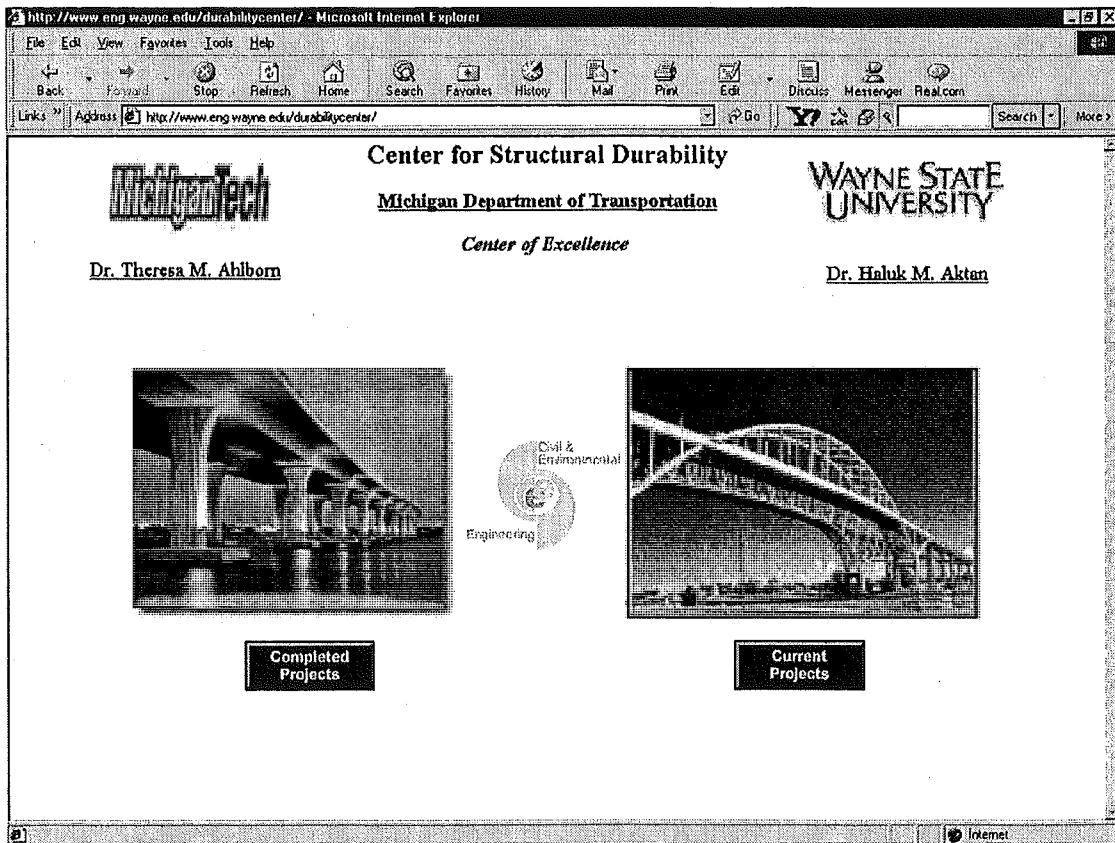


Figure 8-1. Durability Center's Homepage

8.2 Site Map

The site map provides a visual overview of how the web pages are connected through hyperlinks. Figure 8-2 depicts the main pages of the Center for Durability's website.

- A. Homepage of Center for Durability
- B. List of Completed Projects
- C. Project Homepage of Evaluation of Concrete Permeability by Ultrasonic Techniques
- D. List of Current Projects
- E. Project Homepage of Causes & Cures of PC I-Beam End Deterioration
- F. Project Homepage of Criteria and Benefits of Penetrating Sealants for Bridge Decks

As projects are completed, they will move to the List of Completed Projects.

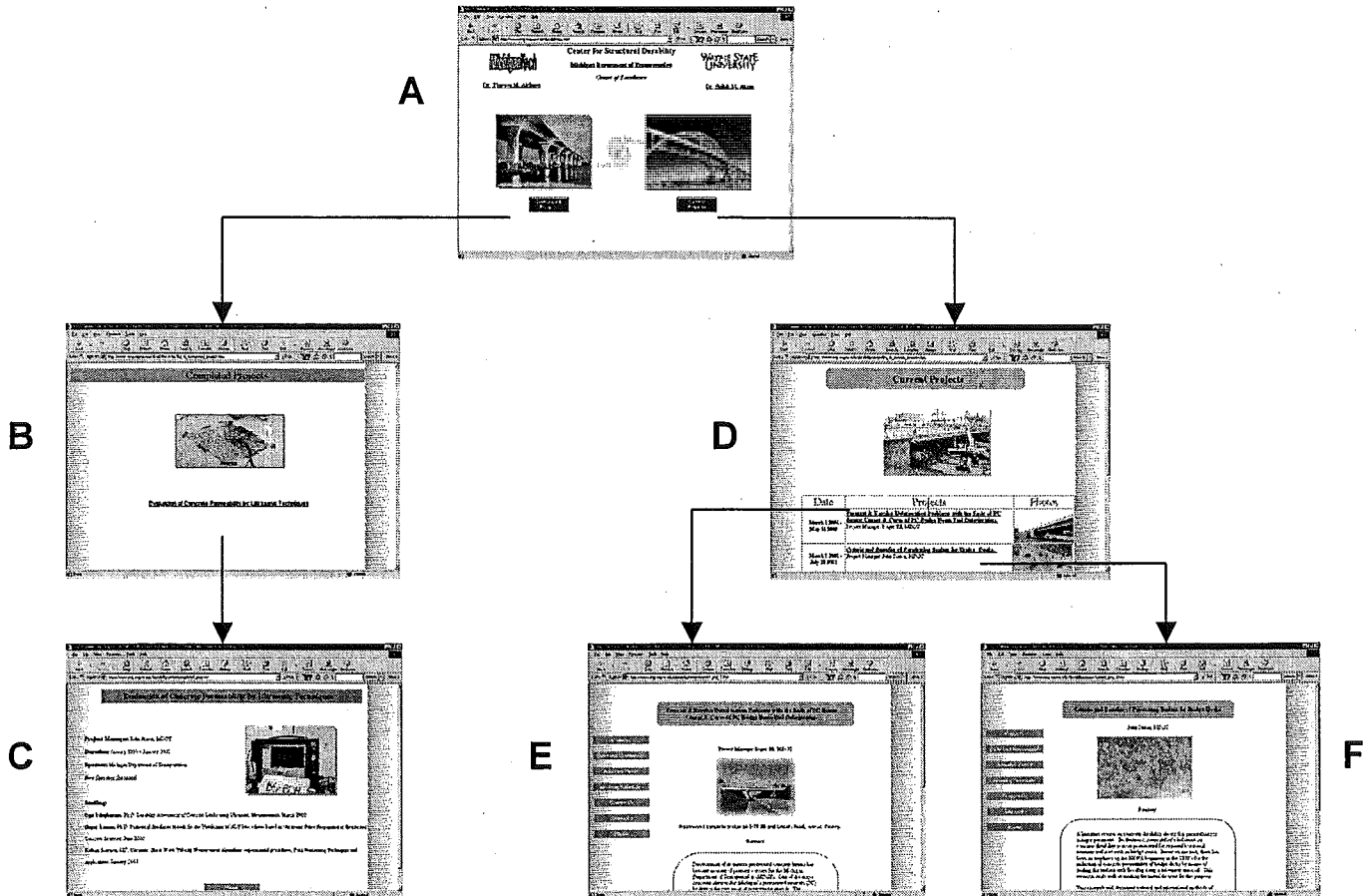


Figure 8-2. General Site Map of Durability Center Website

8.3 Project Homepage of Causes & Cures for Prestressed Concrete I-Beam End Deterioration

The project home page is an active site. The web site contains two areas: one area is limited to the project group, and the other area is open for public access. The ID's and Passwords were transmitted to the project participants during July 2001. The public part of the website contains overview information on the ongoing status of the Causes & Cures for Prestressed Concrete I-Beam End project.

8.3.1 Password Protected Portion

The password-protected portion of the website is for use by the project staff as a communication medium. Two features are currently implemented. One feature is for compiling all the references reviewed to date, including abstracts. This feature allows coordination of the literature review between Michigan Tech and Wayne State. Its primary purpose is to avoid duplication of work by the project participants located at the two institutions. An additional purpose is to provide information to the research advisory panel in terms of the extent of work being performed.

The second feature of the password-protected portion is for report preparation. This feature of the site allows the research team to develop report outlines and enter report text. This site will also give information to the research advisory panel about the development of the reports.

8.3.2 Public Access Portion

This portion of the site contains general information regarding the project. Data and Documents, Advisory Panel, Meeting Schedule, Contact Us, and Site Links are the buttons that a user can choose to access information. The Data and Documents link contains data, abstracts, papers, and reports completed to date. The Advisory Panel link contains a list of the research advisory panel members with email addresses and some telephone numbers. The Meeting Schedule link contains the schedule of meeting, meeting minutes, and handouts. The Contact Us button contains email addresses and telephone numbers of the people responsible for this project. The Site Links button contains links to the two universities' civil engineering homepages and links to other organizations. The bridge inspection picture database (which is part of Data and Documents) will be discussed in the following subsection.

8.3.2.1 Bridge Inspection Photo Database

During the field investigation, digital pictures and photographs were taken of a fraction of the beam-ends and of the overall structure as the research team completed their field investigation forms. Pictures of the beam-ends were taken when the research team members saw repetitive deterioration features such as mapping cracks or horizontal hairline cracks at the web. The pictures of the research team's field investigation are displayed on the Center of Durability's website (<http://www.eng.wayne.edu/durabilitycenter>). Access the site by "Current Projects," they by "Causes & Cures for Prestressed Concrete I-Beam End Deterioration," next by "Data and Documents," then the hyperlink Bridge Inspection Picture Database. These actions will display the image depicted in Figure 8-3. Once this page is reached access to the bridge file is by the bridge's ID number.

Bridge ID - Microsoft Internet Explorer

File Edit View Favorites Tools Help

Back Forward Stop Refresh Home Search Favorites History Mail Print Edit Discuss

Address <http://www.eng.wayne.edu/durabilitycenter/Tables/20of%2020%20bridges%201.0.htm> Go Link >>

Bridge ID	County	Region	Year Built	No. of Spans	No. of Girders	Deck Width (ft)	Length (ft)	Facility Carried	Feature Intersected
29129011000S030	Greilot	Bay	1961	3	27	47	114	US-27 NB	US-27BR(POLK RD)
06106111000S040	Arenac	Bay	1968	3	18	43	112	I-75 NB	M-61
06106111000S050	Arenac	Bay	1968	3	15	32	156	LINCOLN ROAD	I-75 SB
06106111000S060	Arenac	Bay	1968	3	15	32	156	LINCOLN ROAD	I-75 NB
06106111000S110	Arenac	Bay	1968	6	54	49	381	M-33	I-75
25125042000S128	Genesee	Bay	1969	4	18	27	210	I-69 RAMP F	I-75
25125042000S129	Genesee	Bay	1969	4	22	43	210	I-69 EB	I-75
25125042000S124	Genesee	Bay	1969	4	22	43	210	I-69 WB	I-75
25125042000S127	Genesee	Bay	1969	4	16	27	210	I-69 RAMP E	I-75
25125132000S340	Genesee	Bay	1971	4	24	52	167	I-475 SB	CLIO RD
41141025000S070	Kent	Grand	1961	4	24	33	211	KNAPP STREET	I-96
41141027000S060	Kent	Grand	1963	3	36	69	139	US-131 NB	6TH AVE
41141029000S163	Kent	Grand	1964	3	24	46	126	I-196, M-21 EB	LANE AVE
41141029000S164	Kent	Grand	1964	3	24	46	126	I-196, M-21 WB	LANE AVE
41141029000S230	Kent	Grand	1972	3	24	50	117	I-196 WB	36TH ST
67167016000S090	Oceola	North	1984	1	6	47	111	US-131 N B	US-10
67167016000S100	Oceola	North	1984	1	7	53	108	US-131 S B	US-10
53153034000S050	Mason	North	1986	4	24	41	306	CHAUVEZ RD	US-31
93183033000S060	Wexford	North	1997	1	8	47	146	NO. 36 ROAD	US-131
83183033000S050	Wexford	North	1998	2	8	47	244	WHALEY ROAD	US-131 RELOC.

<http://www.eng.wayne.edu/durabilitycenter/Tables/25125132000S340.htm> Internet

Figure 8-3. Table of 20 Inspected Bridges, which is located on the Website

For example access by bridge ID “25125132000S340” will display Figure 8-4. This is a schematic representation of this bridge’s primary elements to show the location of the pictures. The name of each picture will access display that particular picture. For example the name E2-S5-E-S.1 will access Photo 8-1. The name of the picture also denotes the location of that picture. The picture file convention was developed to give each picture a name that relates the contents of the picture to a position on the bridge (see Figure 8-5). A complete explanation of the picture file convention is provided in this sub-section.

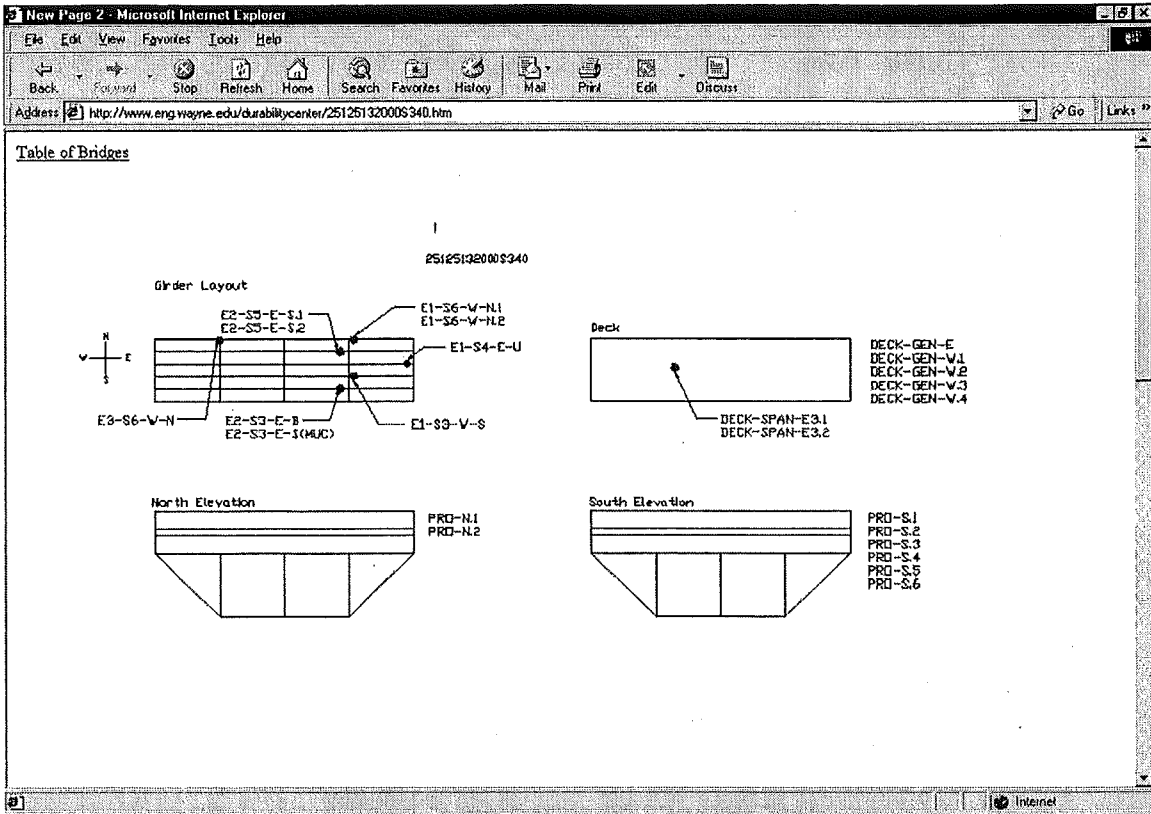


Figure 8-4. Schematic Representation of Bridge 25125132000 S340



Photo 8-1. E2-S5-E-S.1 from 25125132000 S340

- Girder Photo: (span; S#, E#)-(girder; S#, E#)-(end; N,S,E,W)-(face; N,S,E,W,R,U,B,X,I). # in set
- Profile Photo: PRO-(face of bridge shown; N,S,E,W). # in set
- Abutment Photo: ABUT-(end; N,S,E,W)-(face N,S,E,W)-(nearest girder; S#, E#, GEN). # in set
- Pier Photo: PIER-(pier; S#, E#)-(column; S#, E#, GEN)-(face; N,S,E,W). # in set
- Deck Photo: DECK-(type; GEN, APP, JOINT, SPAN, UNDER)-(if GEN then looking direction; N,S,E,W / if APP then approach; N,S,E,W / if JOINT or SPAN then ; S#, E# / if UNDER then SPAN; S#, E#). # in set

Figure 8-5. Photo File Convention

- **Girders Photos** are named using the same convention used in designating the Girder Numbers in the database. The girder photo file name includes a span, a beam in the span, a beam-end, a face of the beam-end, and a photo index number in that set. The first letter in the notation describes which direction to index the spans from (either S-south or E-east), and the number that follows is the span index. Next is a letter denoting which direction to start counting from for the beams (either S-south or E-east), and the number that follows is the beam index. The following letter determines the end of the beam of interest on (either {N-north or S-south} or {E-east or W-west}). The last letter designates one of the seven faces (either {N-north and S-south} or {E-east and W-west}, U-underneath, R-rear end, B-bearing, I-interior diaphragm, X-exterior diaphragm). The last number in the convention gives the photo index in that set. An example of a girder photo file for a bridge orientation of north to south with three spans and seven girders in a span is S2-E5-N-W.2. Such an example defines the second span from the south, fifth beam from the east, north end, west face, and second photo in this set.
- **Profile Photos** convention all begin with the designation PRO followed by a letter that denotes the face of the bridge shown in the photo (either {N-north or S-south} or {E-east or W-west}). The last number in the convention gives the photo index in that set. An example of a profile photo file is PRO-N.3. Such an example defines the north face profile of a bridge and the third photo in that set.
- **Abutment Photos** convention all begin with the designation ABUT followed by a letter that denotes one of the two abutments of the bridge that is shown in the photo (either {N-north or S-south} or {E-east or W-west}). The following letter in the photo file gives the primary face of the abutment shown in the photo (either N-north, E-east, S-south, W-west). The third letter denotes which direction to index the nearest girder shown in the photo—or, if it is a general view, then GEN is used (either S-south or E-east)—and the number that follows is the girder index. The last number in the convention gives the photo index in that set. An example of an abutment photo

file is ABUT-W-N-S8.2. Such an example reads abutment photo, west abutment of bridge, north face, nearest girder is eighth from the south, and second photo in this set.

- **Pier Photos** convention all begins with the designation PIER. The first letter in the notation explains which direction to index the piers from (either S-south or E-east), and the number that follows is the pier index. Next, is a letter denoting which direction to index the columns, and if it is a general view then GEN is used (either S-south or E-east), and the number that follows is the column index. The last letter designates the face shown in the photo (either {N-north or S-south} or {E-east or W-west}). The last number in the convention gives the photo index in that set. An example of a pier photo file is PIER-S2-GEN-N.2. Therefore this example of a pier photo file reads the second pier from the south, general view of all columns, north face, and second photo in this set.
- **Deck Photos** convention all begins with the designation DECK. Then the following group of letters in the notation denotes the type of the deck photo general view, approach, joint, span, or underneath the deck (either GEN, APP, JOINT, SPAN, UNDER). If the type is GEN then the following letter will represent the looking direction in the photo (either N, S, E,W). If the type is APP then the following letter will represent an approach (either N, S, E,W). If the type is JOINT or SPAN then following letter will represent which direction to index the joints or spans respectively (either S-south or E-east), and the number that follows is the joint or span index respectively. The last number in the convention gives the photo index in that set. An example of a deck photo file is DECK-JOINT-E3.1. Therefore this example of a deck photo file reads deck photo, joint of bridge, third joint from the east, and first photo in this set.

8.4 Summary

Overall, the Center for Structural Durability's website is a useful tool that provides easy to access information to the research advisory panel and the research team. The site map shows an overview of how to navigate to a project homepage. The password and public access portions of the project homepage supply a balance of protected and accessible information. The bridge inspection photo database displays a set of organized web-based images of bridge photographs, and shows potential for further growth in digital organization of bridge management.

9.0 Repair Techniques for Beam-End Deterioration (Task 9)

9.1 Introduction

This study identified four major families of repair approaches that can be applied to deteriorated prestressed concrete I-beam ends. These techniques are:

- Structure Modifications,
- Surface Insulating Methods,
- Electrical Control Methods, and
- Environment Modifying Methods.

These techniques are discussed in detail in Section 2.4.2 of this report and are combined with preventative-maintenance techniques. The discussion also includes the advantages and disadvantages of each group. A corresponding detailed list of preventative maintenance and repair techniques is included in Appendix J. This study found that very few individual techniques have been attempted in the concrete-repair field on general concrete structures as well as by state transportation departments on deteriorated prestressed concrete I-beam ends. Repair alternatives that have been implemented on prestressed concrete beam-ends include partial depth repair, the MDOT “chip and overcast procedure” (MDOT R-1373, 1999) and complete beam replacement. Results from all but the latest techniques, for which long-term performance data is not available, generally suggest that no repair or preventive-maintenance strategy (excluding beam replacement) can restore the member to an original level of service.

9.2 Analysis Tools

For this study, the research team searched for ways to move from identifying the extent of beam-end deterioration to selecting an appropriate preventive-maintenance or repair technique. These efforts were discussed in 7.2 *Analysis Tools* for both preventive-maintenance and repair techniques. In summary three analysis tools have been developed and were included:

- Table 7-1. Testing Procedures and Distress Severity Criteria for Prestressed Concrete I-Beam End Deterioration (This table listed several tests applicable to corrosion-induced deterioration that could be performed by MDOT to assist in classifying the severity of end distress.)
- Table 7-2. Cause-Evidence Relationships for Beam-End Distress (This list suggested preventative-maintenance and repair techniques for low-, moderate- and high-severity levels of distress for various causes of distress.)
- Table 7-3. Example Performance Matrix for Preventive Maintenance Techniques (This matrix was initialized to aid in the selection of an appropriate preventative-maintenance technique. A similar concept can be used for selection of appropriate repair techniques. Ideas for future refinement of this matrix are given in Chapter 14 – Future Life-Cycle-Cost-Benefit Optimization Studies.)

Accurate assessment of I-beam end conditions is necessary for providing adequate preventative maintenance and repairs. Condition states developed from field inspections (Table 6-2) and photo collection (Table 6-3) will assist inspectors with accurate assessment. Chapter 12 links these condition states to preventative-maintenance and repair techniques.

9.3 Basics of Beam Repair

Repair of a deteriorated beam-end can range from a simple solution to a complex long-term process. It is imperative to understand that, while the simple solution may be to employ a one-fix-cures-all approach, every case must be considered on an individual basis. For example, a carbonation test (from Table 7-1) may show a moderate level of deterioration at the reinforcement level. However, the moderate level is only at that isolated location or locations where sampling has been conducted. The true extent of deterioration may turn out to be different as the concrete-removal process takes place. A few basic issues related to beam-end repair are listed here for consideration.

1. The 1996 MDOT *Specifications for Construction, Section 712, Bridge Rehabilitation – Concrete* provides information regarding the removal of concrete and patching. However, no attention is given for prestressed concrete I-beam repairs, and little direction is given for vertical repair work.
2. The MDOT *Special Provision – Vertical and Overhead Structure Repairs* should consider two additional acceptance criteria: maximum crack-width criterion of 6 mils and a bond-tensile-strength criterion other than simple delaminations (see Chapter 11).
3. All concrete-removal processes in the beam-end region should list provisions for temporary shoring of the beams. The true depth of deterioration often cannot be known until the removal process progresses. Safety of the structure and personnel dictates that temporary shoring be provided for all repair procedures where concrete removal is needed.
4. Corroded steel must be cleaned during any repair process. To reduce or eliminate further corrosion, a non-corrosive environment must be provided and/or a sacrificial anode system should be incorporated. Placing sacrificial anodes around the patch perimeter can reduce the “ring” effect, an area of accelerated deterioration due to chloride imbalance.

5. All unsound or contaminated concrete must be removed to effectively halt further deterioration. Placing patches over material such as chloride-contaminated concrete will accelerate deterioration near the patch, rendering the patch ineffective. In addition, patching over unsound concrete will not be effective in holding the unsound concrete in place for long-term conditions.

9.4 Summary

As in Chapter 7, we have identified several families of repair techniques that can be applied for beam-end deterioration. Testing procedures and distress-severity criteria applicable to corrosion-induced deterioration are appropriate for classification of beam-end distress as noted throughout this document. A list of repair techniques has been developed for low-, moderate-, and high-distress severity. And a concept of a performance matrix was developed to assist in selecting the most effective technique for a given situation. In addition, suggestions for beam-end repair and clarifications to MDOT standard practices have been documented for consideration.

10.0 Analytical Modeling of a PC I-Beam Bridge (Task 10)

10.1 Introduction

Inspection and evaluation of the conditions of the inspected bridges revealed the possibility of design and manufacture related factors aggregated to the aggressive environmental effects causing the end deterioration in PC I-beams (see Chapter 3 for the inspection results). In order to investigate the stress states near the beam-ends, analytical studies are performed under the load effects during manufacture, construction, and operation. The analyses are completed in two main phases. First, the finite element modeling of a PC I-beam is performed to identify the effects of prestressing loads and the design changes in tendon geometry and arrangement. Second, the behavior of a PC I-beam bridge is modeled and analyzed under dead and live loads and environmental conditions to evaluate the diaphragm impact on beam-ends and load distribution in the bridge.

The essential parts and goals of the analyses included:

1. Assessing the prestressing force effects on the stresses at PC I-beam ends.
2. Evaluating the effects of bearing condition on the life span of the beams.
3. Evaluating the load paths on a PC I-beam with non-functional bearing pad near beam-ends under dead and live loads.
4. Assessing the structural behavior of a PC I-beam bridge.
5. Evaluating the effect of the diaphragms material and geometry on the structural behavior of bridges.
6. Attaining a better geometry and a type of diaphragm that will enable the inspectors to examine the conditions of the beam-ends efficiently.

10.2 Programs Utilized

10.2.1 HyperMesh

HyperMesh is used as pre and post processor in structural modeling. It also includes a linear and non-linear finite element analysis program, which was not utilized in this research. The pre- and post-processor helps to generate the finite element models for simulation and analysis (HyperMesh 2.0 Documentation, 1995). HyperMesh pre-processor provides extensive finite

element analysis assistance for generating models and advanced post-processing capabilities for in-depth visualization of simulations.

10.2.1.1 *Pre-processing*

One of the main advantages in using HyperMesh, as a pre-processor, is its ability to create compatible input files for the structural analysis programs. Its library is large enough to generate input files, including model data to be analyzed, for many other programs such as ABAQUS, Ansys, Ls-Dyna3d, Madymo, Nastran, and Radioss.

The pre-processing consists of the following steps (HyperMesh 4.0 Documentation, 2000):

1. The geometry of the structural element is generated by creating the geometric properties and the form of the structure.
2. Based on the geometry of the structure, finite element discretization is performed.
3. The completed finite element representation of the geometry is checked for continuity and element quality by using fundamental relations of structural analysis.
4. Boundary conditions such as loads and constraints are described.
5. Material properties and other properties are defined.
6. The finite element description of the model is exported in the format suitable for the analysis code.

10.2.1.2 *Post-processing*

In post-processing, the analysis results are interpreted by completing the following tasks (HyperMesh 4.0 Documentation, 2000):

1. Translating the results from the ABAQUS's output format into HyperMesh's own format.
2. Reviewing and animating the model with deformed shapes.
3. Reviewing color contours of the element and nodal data (stress, strain, or displacement) displayed on the finite element model.
4. Generating plots and stress contours for reporting and documenting the analyses results.

10.2.2 ABAQUS

ABAQUS is an engineering simulation program. It is based on the finite element method and designed specifically for advanced analysis applications. The program capabilities are described by its element library, material models, and analysis procedures. The program is developed with a very extensive library of elements that can be used for modeling different structures virtually and geometrically. The material library includes many engineering materials, such as metals, rubber, polymers, composites, reinforced concrete, crushable and resilient foams, and geotechnical materials (ABAQUS / Standard Version 5.8 Manual, 1998). The material response for each of these models may be highly nonlinear. General elastic, elastic-plastic, and elastic-viscoplastic behaviors are provided. Both isotropic and anisotropic behavior can be modeled. User-defined materials can also be created with a subroutine interface.

ABAQUS provides various time- and frequency-domain analysis procedures. These procedures are divided into two groups:

General Analyses: In this case the response may be linear or nonlinear.

- Static stress/displacement analysis
- Viscoelastic / viscoplastic response
- Transient dynamic stress/displacement analysis
- Transient or steady state heat-transfer analysis
- Transient or steady state mass-diffusion analysis
- Steady-state transport analysis
- Coupled problems
- Thermo-mechanical (sequentially or fully coupled)
- Thermo-electrical
- Pore fluid flow-mechanical
- Stress-mass diffusion (sequentially coupled)
- Piezoelectric (linear only)
- Acoustic-mechanical (linear only)

Linear Perturbation Analyses: In this case linear response is computed about a general, possibly nonlinear, base state.

- Static stress/displacement analysis
- Linear static stress/displacement analysis
- Eigenvalue buckling-load prediction
- Dynamic stress/displacement analysis
- Determination of natural modes and frequencies
- Transient response via modal superposition
- Steady-state response resulting from harmonic loading
- Response spectrum analysis
- Dynamic response resulting from random loading

10.3 Overview of Analytical Modeling

Finite element (FE) analysis method is a useful tool to determine the behavior of structures. It is the highly improved form of structural analyses commonly used for research and development purposes. In FE analysis, a structure is divided into finite elements, and their behaviors are investigated. In this way the mechanisms within the structure, the load response of each finite element, and behavior of the entire structure are studied.

Bridge inspection results on beam-ends conditions and a visit to the PC plant revealed the possibility that some of the beam-end cracking is formed at the plant. Inspection data showed that cracks are common in almost all PC I-beams near the bottom flange and web-transition zone and at the mid-web. Literature also indicated that there are various mechanisms causing beam-end cracking. Some of these mechanisms are initiated as soon as the girders are cast and the tendons are released (Buckner, 1995; Russell and Burns, 1996; Kannel et al, 1997; Russell and Burns, 1997; Leonhardt, 1964, Sozen, 1965 and 1967). The cracking during fabrication leads to further and rapid deterioration of the girders. The initial cracking, therefore, should be reduced

in order to extend service life of PC I-girders. In order to develop reliable remedies for the structures in distress and to provide necessary precautions for new girder and bridge designs, analytical modeling is a useful tool for generating the realistic stress state for comparisons to nominal stresses assumed in design. Detailed inspection of PC I-beam bridges also revealed that non-functional elastomeric bearing pads and rigid concrete diaphragms might also contribute to girder-end distress. Finite element analysis method is applied to investigate the causes for initial cracking, the impact of non-functional bearings, structural behavior in a bridge, and diaphragm impact on the girder-ends.

The main goals of the analyses are summarized as below:

1. Assessing the shear and flexural stresses near I beam-ends due to prestressing force transfer length, strand debonding, and strand draping.
2. Quantifying the cracking potential near the beam-ends.
3. Evaluating the load paths near beam-ends under dead and live loads.
4. Evaluating the influence of bearing conditions on the beam-end stresses.
5. Investigating the full bridge behavior under live and dead loads.
 - a. Diaphragm restraining effects on girder-ends.
 - b. Effects of various diaphragm types on girder-end stresses.
 - c. Temperature effects on a bridge, considering functional and non-functional elastomeric bearing pads.

The beam cross-section and tendon geometry affect the structural behavior and performance. Single girder analyses are grouped according to the cross-section and tendon geometry, design of the beam, bond properties of the concrete, and loading cases to identify the significance of each parameter independently. The first parameter is the cross-section and tendon geometry of AASHTO I-beams. Therefore, the girders with the following tendon geometries are studied to document the geometry effects.

1. Beams with Straight Tendons
2. Beams with Draped Tendons
3. Beams with Bond-Breakers (Sheathed Tendons)

The concrete quality may vary due to several reasons such as admixtures, placing, and curing procedures and conditions that, in turn, affect the quality of bond between the tendon and the concrete. Therefore, as another parameter, the concrete quality effect is studied to evaluate its impact on the stress pattern and transfer length near the beam-end. Three bond qualities are assumed; good bond quality (high estimate), average bond quality (best estimate), and poor bond quality (low estimate).

The finite element analyses are further expanded by evaluating the stresses and deformations generated in three stages of a PC I-beam during its lifespan, the manufacture, the construction, and the service. Loading conditions are based on these stages. Accordingly, the following loading cases are considered in the model.

1. Prestressing Load
2. Dead Load
3. Live Load

The dead and live load analyses are performed to verify the effect of the non-functional bearing on the beam-end stresses and on the load path from deck to the supports.

Additionally, the structural behavior of the full bridge and restraining effects of the diaphragms are analyzed in a PC I-beam bridge model. The model is developed from the structural components. In the analyses, the significance of the concrete diaphragms, their geometry effects are assessed and compared to steel bracings as a potential replacement to concrete diaphragms. The thermal effects on the girder-ends and load distribution induced by temperature deviations are also investigated.

Analytical modeling steps are summarized in Figure 10-1.

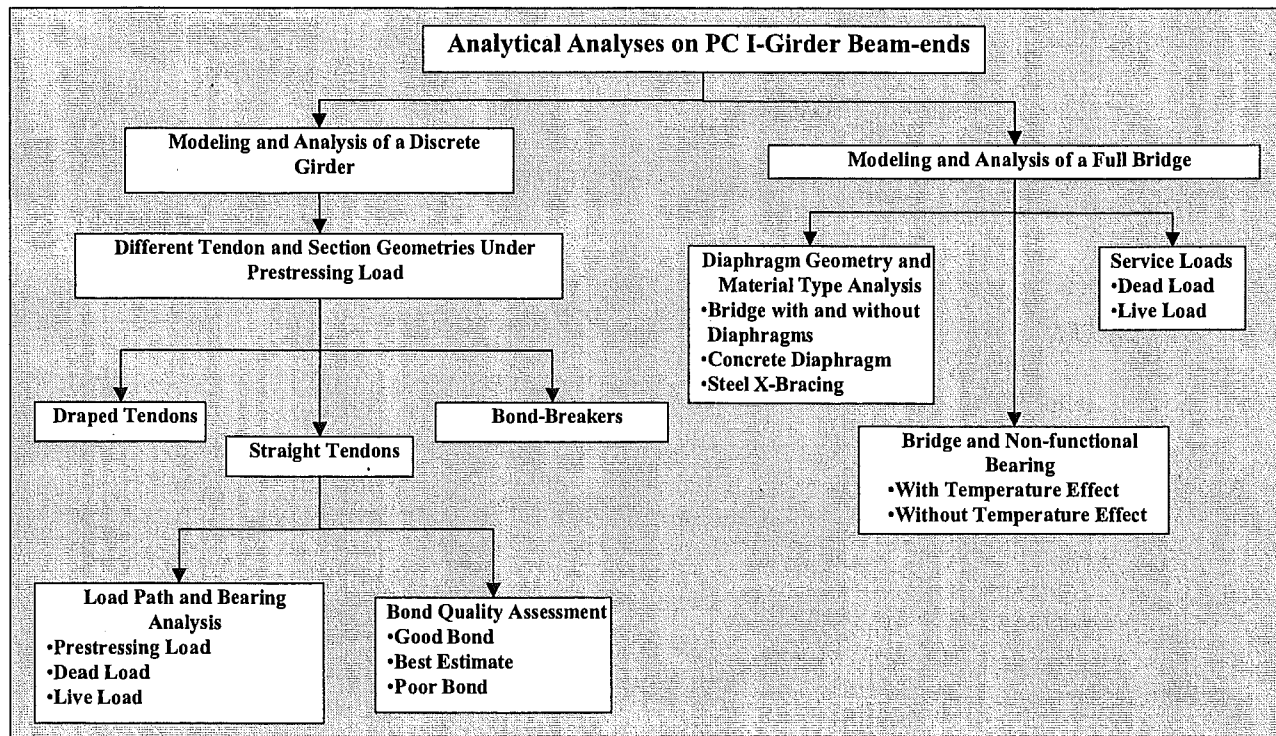


Figure 10-1. Steps of Analytical Modeling

10.4 Cracking Potential of a Prestressed Concrete I-Beam

Previous research and field inspection results has identified the presence of cracks near the beam-ends as one of the significant parameters in the girder service life. Prestressing tendons corroding due to the presence of oxygen and the infiltration of moisture through cracks is the most common distress mechanism seen near the I-beam ends. Field studies showed that PC I-beam end cracks form as early as in the precast plant as shown in Figure 10-2-a and -b. The cracked girders exposed to aggressive environmental conditions deteriorate rapidly. The moisture ingress increases in a cracked girder, and freezing action widens the cracks as seen Figure 10-2-c and -d. The moisture carries aggressive agents, which further aggravate the deterioration and feed back moisture ingression. Aggressive agent exposure generates

delamination, Figure 10-2-e, and spall of concrete cover, Figure 10-2-f, reducing the durability of the girder by a significant amount. Consequently, cracking prevention or reduction during manufacture, construction, and operation is the proper way to increase the durability and the lifetime of the PC I-beams.

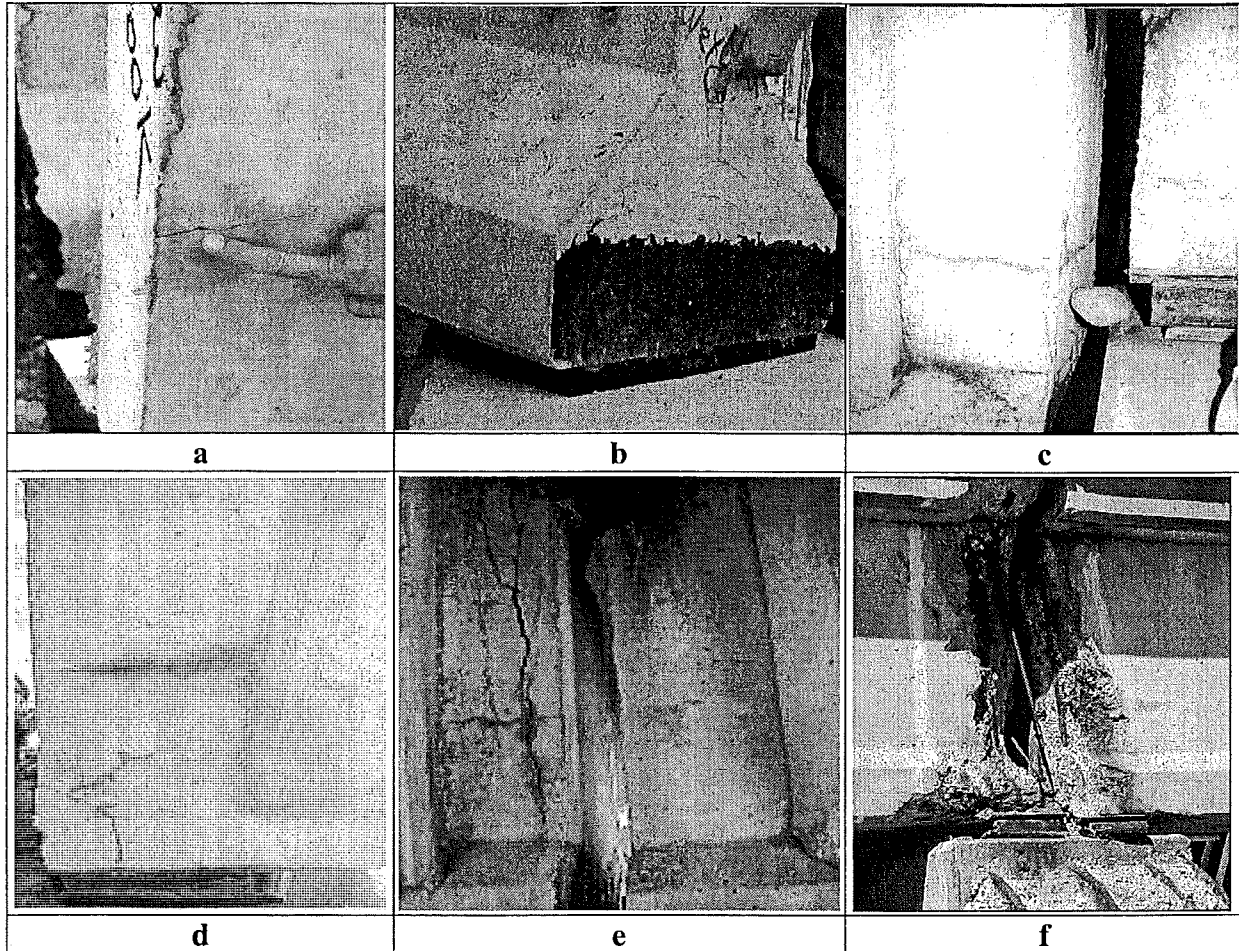


Figure 10-2. (a) Cracking at the Web Zone at the Precast Plant; (b) Cracking within the Proximity of Bottom Flange of a Girder in a Bridge under Construction; (c) Cracking Observed on the Web and Around the Bottom Flange of Girders in-Service; (d) Moisture Presence Around Cracking on the Web; (e) Delamination and Spalling on a Girder; (f) Spalling of Cover Concrete and Exposed Rebar

Detailed structural analyses of the PC I-beams are necessary to clearly verify and identify the cracking mechanisms, their causes, and the significance of the load stages and the environmental factors. Finite element analyses are performed to identify the cracking potential and vulnerability of girders to cracking. By using the results of the finite element analysis, better reinforcement details for beam-ends can be developed for crack width and length minimization. Finite element models are generated utilizing the existing geometrical, environmental, and load conditions to simulate the real structural behavior as much as the theoretical assumptions allow. In modeling the girder for FE analysis, certain assumptions are necessary. Some of these assumptions are behavioral and others are for incorporating some mechanisms into FE model of the girder.

Behavioral assumptions are as follows:

1. Statical analysis is performed, excluding the dynamic effects.
2. Small deformations are considered; therefore, second order effects are not incorporated.
3. Materials, steel for the tendons and concrete for the girder, are assumed to remain in their elastic state.
4. Prestressing losses due to creep and shrinkage is ignored in evaluating early age load effects.
5. Symmetrical tendon-cutting pattern is assumed. Thus, moments generated by unbalanced tendon forces are not included.
6. To identify only the early age effects that occur during manufacturing on a PC I-beam, the initial prestressing forces before concrete shrinkage losses are not applied. Only losses due to elastic shortening of the beam are included.
7. Shrinkage effects of the deck on the girder are not incorporated. Deck is only regarded as dead load.
8. The boundary conditions at the both ends are assumed free.

The FE modeling related assumptions are as follows:

1. The deformations are calculated only at the nodes. The variations between the nodes are assumed linear.
2. The bond properties between the tendons and concrete are modeled using the flexible springs as connection elements.
3. The tendons are attached to the concrete only at the nodes through flexible springs.
4. Tendons are assumed to have only axial stiffness and modeled as linear truss elements with no change in cross-sectional geometry under prestressing forces.

The finite element analyses are performed on models based on three types of I-beams taken from existing bridges in Michigan, considering girder tendon and section geometries as main parameters. AASHTO I-beam types, Michigan 1800, and Wisconsin-70 (WI-70) are used in Michigan. Their use according to years is summarized in Table 10-1; AASHTO I-IV were first utilized in 1958, then in 1977 WI 70-inch, and in 1997 MI 1800 were introduced.

Table 10-1. PC I-Beam Types Used in Michigan According to Years and Maximum Span Lengths

Beam Types	AASHTO I-IV	AASHTO I-IV	AASHTO I-IV	AASHTO I-IV	WI 70	AASHTO I-IV	AASHTO I-IV MI 1800
Years	1958	1959	1964	1975	1977	1989	1997
Span Length (ft)	80	100	90	100	90-150	100	90-150

The first analysis model describes an AASHTO girder with straight tendons as shown in Figure 10-3.

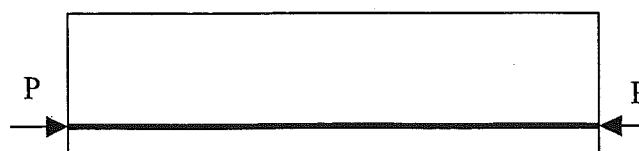


Figure 10-3. PC Girder with Straight Tendons

The second model is a Wisconsin type girder with bond-breakers, as shown in Figure 10-4, which is the recent tendon design form. In this type, bond-breakers (sheathing) are used around the tendons at the beam-ends.

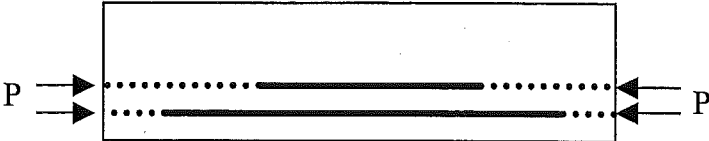


Figure 10-4. PC Girder with Sheathed Tendons

The third model shown in Figure 10-5 is an AASHTO cross-section with draped tendons. In draped girders, end blocks are incorporated to accommodate the anchoring of the tendon on the web.

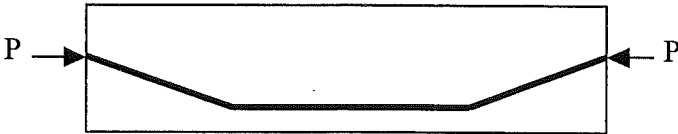


Figure 10-5. PC Girder with Draped Tendons

The design assumptions and the real behavior of the PC girders should be compared to provide more realistic and accurate design procedures. The structural behavior and the stress distribution mechanisms in the girder may be different from what is projected. The main issue here is to improve the assumptions and features to improve design reliability. In order to describe the design approach, a girder with straight tendons will be used as an example. In this case, uniform flexural and axial stresses are created by using straight tendons. The axial stress is regarded as proportional to the applied prestressing load, and inversely proportional to the cross-sectional area of the beam. The nominal stress distribution under prestressing forces is shown in Figure 10-6. The compressive stress considered in the PC girder design is the summation of flexural stresses with axial stresses calculated at the bottom fiber as shown in Equation 10-1. The total axial stress in Equation 10-1 is assumed linear on the beam cross-section and uniform along the beam. This total axial stress is used during design of the PC structures.

In a real girder, the structural behavior is different near the beam-ends from what is considered in the design. The prestressing load is not directly transferred from the tendons to concrete precisely at the girder-end. In prestressed girder, the tendons are eccentrically arranged with respect to the beam centroid. The prestressing load is gradually transferred along the girder at a distance termed as transfer length. As the prestressing force is transferred to the member, the axial load and the flexural stresses gradually develop within the transfer length. During this force transfer, the axial force within the force transfer zone varies as depicted in Figure 10-7.

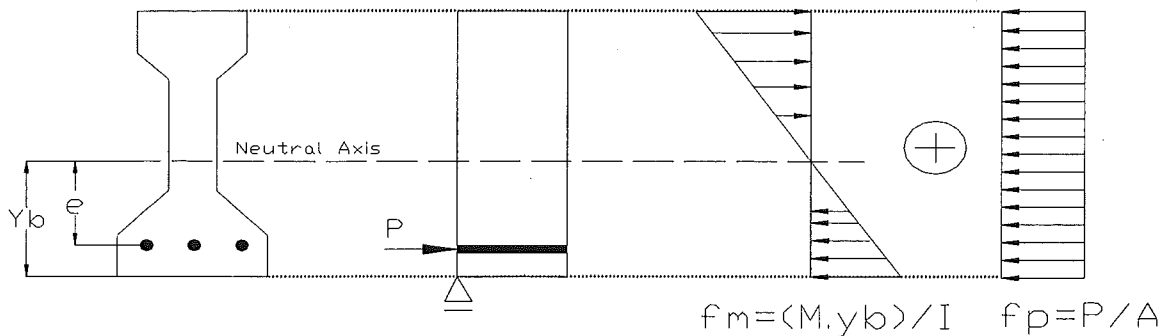


Figure 10-6. Axial Stresses Forming due to Prestressing Load

$$f_b = \frac{M \cdot y_b}{I} + \frac{P}{A}$$

Equation 10-1

where

- A = Cross-sectional area of the girder
- e = The eccentricity of prestressing load measured from neutral axis
- f_b = Total axial stress at the extreme bottom fiber
- f_m = Flexural stress due to eccentric prestressing force
- f_p = Axial stress due to prestressing
- I = Moment inertia of the section
- M = Bending moment due to prestressing load; $M = P \cdot e$
- P = Prestressing force
- y_b = Distance of neutral axis to the extreme bottom fiber

Considering an incremental element within the transfer length, the stress at each side of the element will be unequal (Russel et al, 1997). Thus, shear stress is generated. This change in nominal stresses near beam-end and equilibrium is described on an isolated incremental element as shown in Figure 10-8. Equation 10-2 describes the static equilibrium condition of the incremental element. Beyond the transfer length, the prestressing force remains constant. Therefore, the resultant shear stress shown in Figure 10-8 diminishes. The shear stress can also be explained by the Poisson's effect. By the changing uniaxial stresses, two incremental elements next to each other deform differently due to Poisson's effect. The preceding element lateral deformation is less than the succeeding element within the transfer length zone. Due to this difference in deformations between the elements, shear stresses are generated. Considering the shear stress generation within the transfer length, FE model of the PC I-girder is developed based on the description of force transfer from the tendon to the concrete medium.

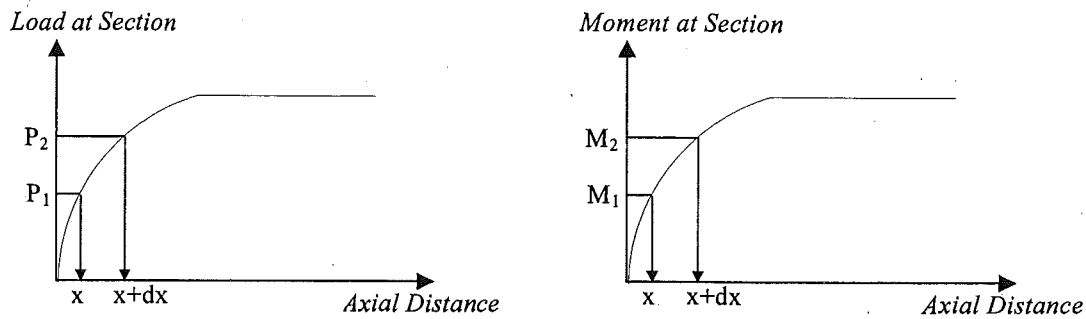


Figure 10-7. Axial Stresses on an Incremental Element

The differences between the approaches in the design and in reality are explained above. It is clearly seen that the design procedure does not address the structural behavior within the transfer length. The significance of the shear stresses generated near the girder-ends will be explained in more detail in the next section titled "Discrete Girder Analysis" on existing girders under prestressing load only so that the analysis may help to judge the accuracy of the design assumptions.

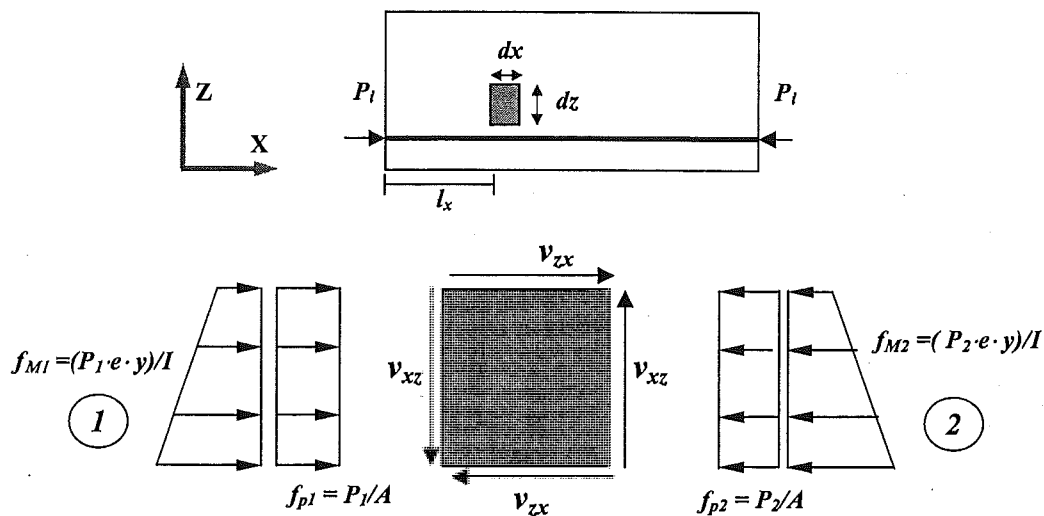


Figure 10-8. Stress Equilibrium of an Infinitesimal Element

$$v = f_{b1} + f_{b2} = \Delta f_m + \Delta f_p$$

$$v = \frac{(M_1 - M_2)y}{I} + \frac{(P_1 - P_2)}{A}$$

$$v = \frac{\Delta M \cdot y}{I} + \frac{\Delta P}{A}$$

Equation 10-2

where

- v = Shear stress
- y = Distance of neutral axis to a fiber on bottom of the section
- f_{b1} = Axial stress at the extreme bottom fiber of the section at side 1
- f_{b2} = Axial stress at the extreme bottom fiber of the section at side 2

10.5 Discrete Girder Analyses

The discrete girder analyses included three PC AASHTO I-beam types as mentioned in the overview. These types are girder with straight tendons, girder with draped tendons, and girder with bond breakers. The models generated for each girder are based on the design drawings. In other words, manufacture related errors are not incorporated.

The concrete properties used during manufacture may vary. These parameters and their significance are out of the scope for this project. However, to incorporate the existing conditions in reality, the concrete quality should be taken as a factor affecting the girder behavior. Therefore, the bond quality effect on the load configuration and transfer length at the beam-end zones are included in the FE analysis. The bond quality of concrete is taken proportional to its modulus of elasticity (Leonhardt, 1964). Here the assumption refers to the bond stiffness, not the bond strength. Assuming strain compatibility between the tendon and the surrounding concrete, the amount of stress developed in concrete will be proportional to the strain. The proportionality constant in this case will be the modulus of elasticity of concrete. The assumed variation is between twice the elasticity modulus as upper bound and one half as lower bound. These bounds are hypothetical, but they will provide an assessment on the sensitivity of the transfer length, and therefore, shear stresses to bond quality.

The load path due to dead and service loads in a girder is important and, therefore, to assess the cracking and the significance of the deterioration. The results of this analysis will help the inspectors to evaluate the safety of the deteriorated girders. Therefore, load path analyses are performed by applying the dead and live loads on a girder to evaluate the vulnerability of a girder with deteriorated ends. In other words, if the load path is clearly described, any girder-end deterioration within the zone of low stress will not necessarily jeopardize girder capacity. However, if deterioration is within high stress zones, girder capacity will be affected. In the load path analyses, one of the girders analyzed under only prestressing load is also analyzed under dead and live loads to document the load path through beam-end onto the support.

10.5.1 Girder with Straight Prestressing Tendons under Prestressing Load

The beam modeled is from a bridge in the Bay Region with inventory ID number S04 of 06111, built in 1968. The bridge description was given in Section 3.3.3. Two standard I-beams according to AASHTO prestressed concrete I-beams standards are used in the bridge. The beam used in the analysis is Type-III, a girder located within the mid-span of the bridge, with a 48 ft length. The material properties for concrete used in the analysis are the modulus of elasticity and Poisson's ratio. The modulus is calculated from design concrete compressive strength of 5,000 psi, using the formulation given in ACI 318-02 as $E_c = 57,000 \cdot \sqrt{f'_c}$, where E_c is modulus of elasticity of concrete and f'_c is compressive strength of concrete. The elasticity modulus of prestressing steel is the only property described in the model. The modulus for the Grade 250 7-wire strand bundle is assumed equal to the steel modulus of 29,000 ksi. It needs to be emphasized that the modulus is in reality the tangent modulus at the initial prestressing force of 24.5 kips. The beam cross-section and tendon geometry are shown in Figure 10-9.

Mark	Type	NUMBER OF 1/2" 7 WIRE STRANDS INDICATED ROW																		Total No	Initial Prestressing Force (Strand) (Lbs)					
		MIDSPAN (Section B-B)						END (View A-A)																		
		BOTTOM						BOTTOM						TOP												
1-I	I	-	6	4	2	-	2	-	-	6	4	2	-	2	-	-	-	-	-	-	-	-	-	-	14	24,200
2-I	I	-	6	4	2	-	2	-	-	6	4	2	-	2	-	-	-	-	-	-	-	-	-	14	24,200	
1-III	III	-	8	4	-	-	-	-	-	8	4	-	-	-	-	-	-	-	-	-	-	-	-	12	24,500	
2-III	III	-	6	4	4	4	-	-	-	6	4	4	4	-	-	-	-	-	-	-	-	-	-	18	24,500	
3-III	III	-	8	4	-	-	-	-	-	8	4	-	-	-	-	-	-	-	-	-	-	-	-	12	24,500	

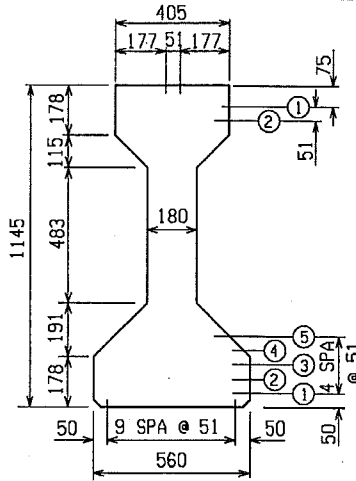


Figure 10-9. Tendon Arrangement and Cross-sectional Geometry of the I-Beam Modeled

Using symmetry, one half of the beam is modeled. Only the prestressing load is taken into account. The self-weight of the beam is not included to evaluate the beam-end stresses under only the prestressing load. In other words, the beam is isolated from other forces just to evaluate the prestressing force impact. The boundary conditions are described as the support at the end zone, roller in longitudinal direction, and the mid-point of the beam, roller in vertical direction, as defined by the symmetry constraints shown in Figure 10-10.

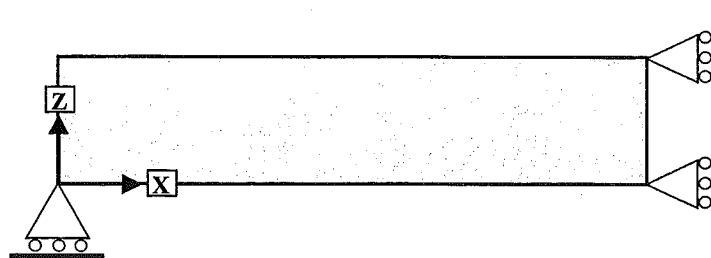


Figure 10-10. Boundary Conditions Described in the FE Model

The FE models are generated by using a finite element pre-processor and post-processor program, HyperMesh, and analyzed by a finite element analyzer program, ABAQUS. The finite element mesh and element selection is formed according to the options and analyzing procedures defined by the programs. The FE model of the girder, shown in Figure 10-11, includes 2185 solid continuum elements with 8 nodes, 342 truss elements with 2 nodes, 342 spring elements with 2 nodes, and 342 kinematic coupling elements with 2 nodes for a total of 24,688 degrees of

freedom. Continuum elements are used to define the concrete medium. The truss elements defining the prestressing tendons are prestressed as an initial condition. The spring members are utilized for the transfer of prestressing force from the truss elements used for tendons to the continuum elements used for concrete girder. The kinematic coupling elements are utilized due to modeling requirements in ABAQUS. They are used as intermediate agents to provide composite action between the spring and truss elements.

The geometry used in the model is identical to that of the real I-beam. The FE mesh is further refined near the beam-end. The length of the finite concrete elements is 4 inches at the beam-end for the first 8 inches, then 6.5 inches for the following 52 inches, and 26 inches for the remaining 234 inches, as shown in Figure 10-11.

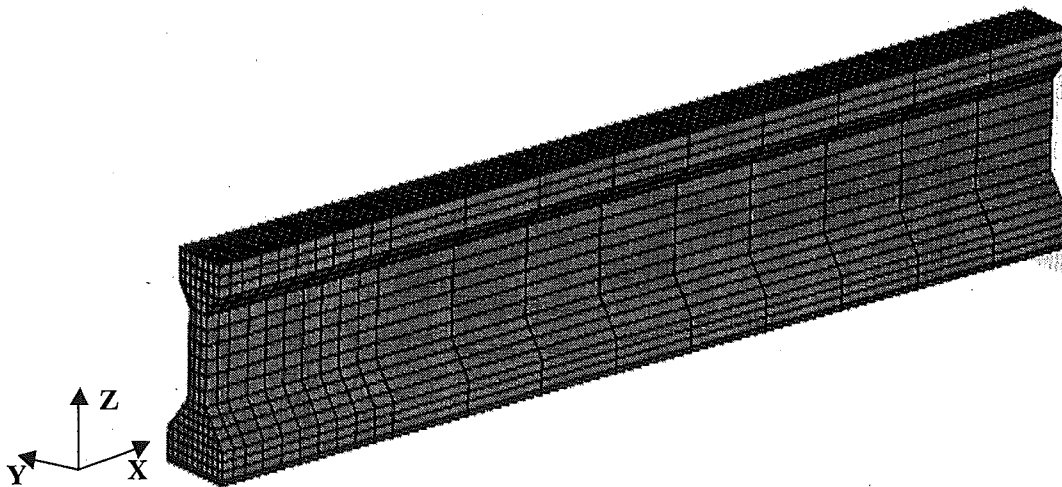


Figure 10-11. The Girder with Straight Tendons

The work performed prior to conducting the analysis dealt with the tuning of bond springs for achieving the theoretical transfer length of 26.7 inches for 7-wire strands with $\frac{1}{2}$ in nominal diameter. The transfer length is calculated by using $l_d = (f_{se}/3) \cdot d_b$, where f_{se} is the effective stress in prestressing steel after losses and d_b is the nominal diameter of the strand (AASHTO, 1998). The tuning of springs stiffness is not within the focus of this report and will not be described here.

The analysis results are presented as contours of various stress components. To help the reader to evaluate the stresses and their variations within the girder-end, a description and coordinate designation of the 3-dimensional state of stress is given in Figure 10-12. On this element, the variation between the axial stresses on each side of the element generates shear stresses. In forming an analogy with the two-dimensional beam model used in design, f_{xx} is the uniaxial, axial and flexural combined, stress, and f_{xz} is the shear stress. The shear stresses at opposite faces are equal i.e. $f_{xz} = f_{zx}$, $f_{xy} = f_{yx}$, and $f_{yz} = f_{zy}$.

First, the analysis results using an average bond quality are described. The axial stress variation near the beam-end is shown in Figure 10-13 and Figure 10-14. As seen in the figures, near the end zone the axial stress gradually redistributes until its contours become uniform at about transfer length distance, between 27.5 and 34 inches from the end. Specifically, Figure 10-14 shows the variation along the beam axis on the x-z plane. It should be noted that the high stress

zone near the tendons at the beam-end gradually redistributes until a uniform stress contour is achieved. In this uniform zone, the maximum compressive stress is around 1,500 psi at the bottom fiber and the stress at the top fiber is tensile at about 100 psi.

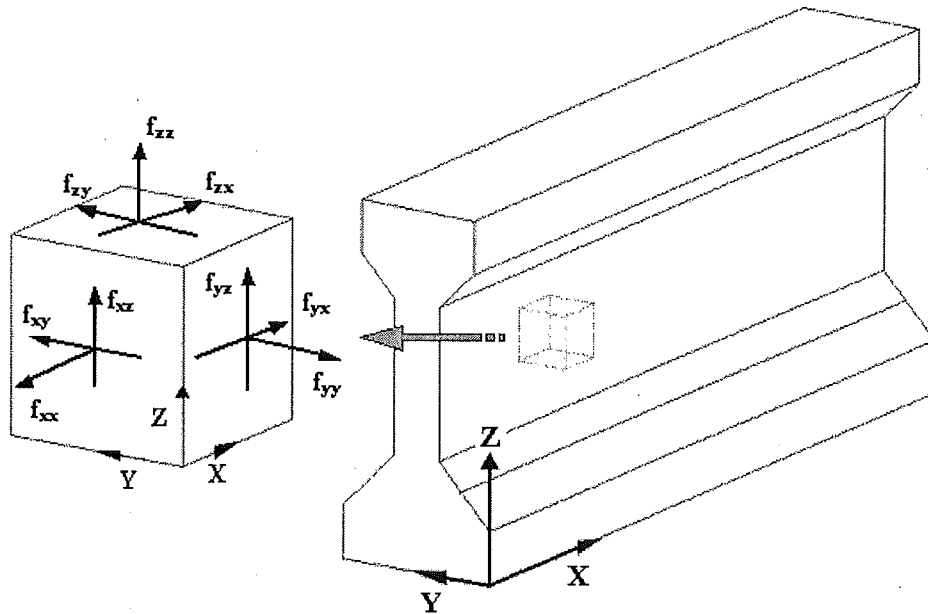


Figure 10-12. Stresses and Coordinate System used in the Model for the Infinitesimal Element

The axial stress distributions in the z and y directions are shown in Figure 10-15-a and Figure 10-15-b, respectively. In Figure 10-15-a and Figure 10-15-b, the zones under tensile stress may initiate cracking. Level of tensile stress that is of significance is only seen in Figure 10-15-a within the web zone, around 390 psi. During field inspection and plant visit, web cracking at the same location was observed (see Figure 10-2-a, -b, -c, and -d).

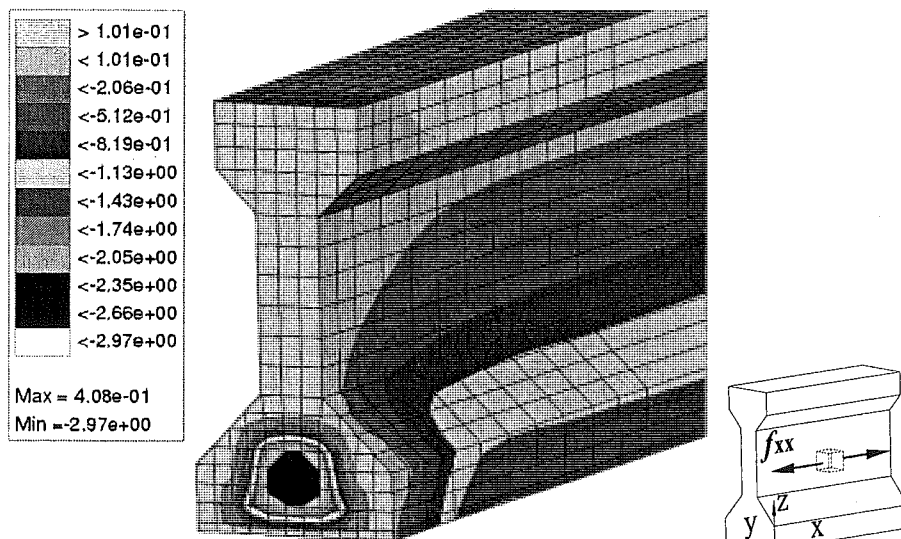


Figure 10-13. Axial Stress near the Beam-end (ksi), in X-Direction

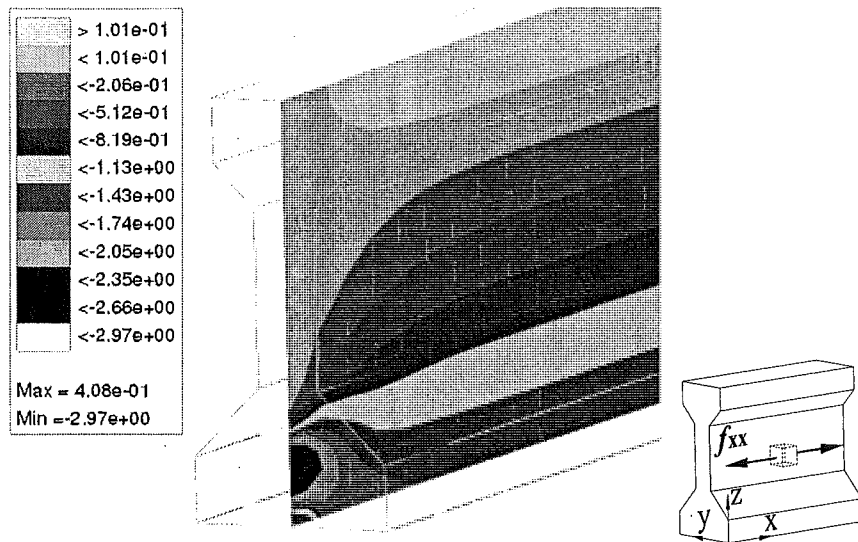


Figure 10-14. Axial Stress (ksi) Trajectory in X-Direction near the Beam-end

The shear stress magnitudes on x-z plane shown in Figure 10-15-c are significant. The maximum values are at the bottom flange, within the proximity of the web. The shear stresses on x-y plane seen in Figure 10-15-d are not significantly lower than the shear stresses on the x-z plane.

The shear stress development on x-z plane is also studied at selected sections along the beam axis as shown in Figure 10-16. In the figure, "Distance Along Z Axis" is along the depth of the beam. Figure 10-16-a to Figure 10-16-i shows the changes in shear stress distribution at sections along the beam starting from the beam-end. The section locations are also defined in the figures by the numerical value of "Distance Along Z Axis." In Figure 10-16, the distance from the beam-end to the location where the shear stress fully diminishes is 47 inches. A closer inspection shows that shear stress is insignificant starting at a distance from the beam-end just beyond 27.5 inches, which designates the point at which the prestressing forces in the tendons are fully developed. It is also important to specify the length at which shear stress remains in excess of allowable. The zones where the shear stress is in excess of $3.5 \cdot \sqrt{f'_c}$ or 247 psi will define the portions of the beam with high cracking potential by ACI (ACI, 2002). However, this does not mean that the zones with high shear stress crack. This information can be useful to define the critical zones. In Figure 10-16, shear stress is in excess of 500 psi on the section 8 inches from beam-end, which is significantly high. In Figure 10-17, the axial stress (flexural stress) variation in the x-direction shows non-uniformity similar to the shear stress distribution seen in Figure 10-16.

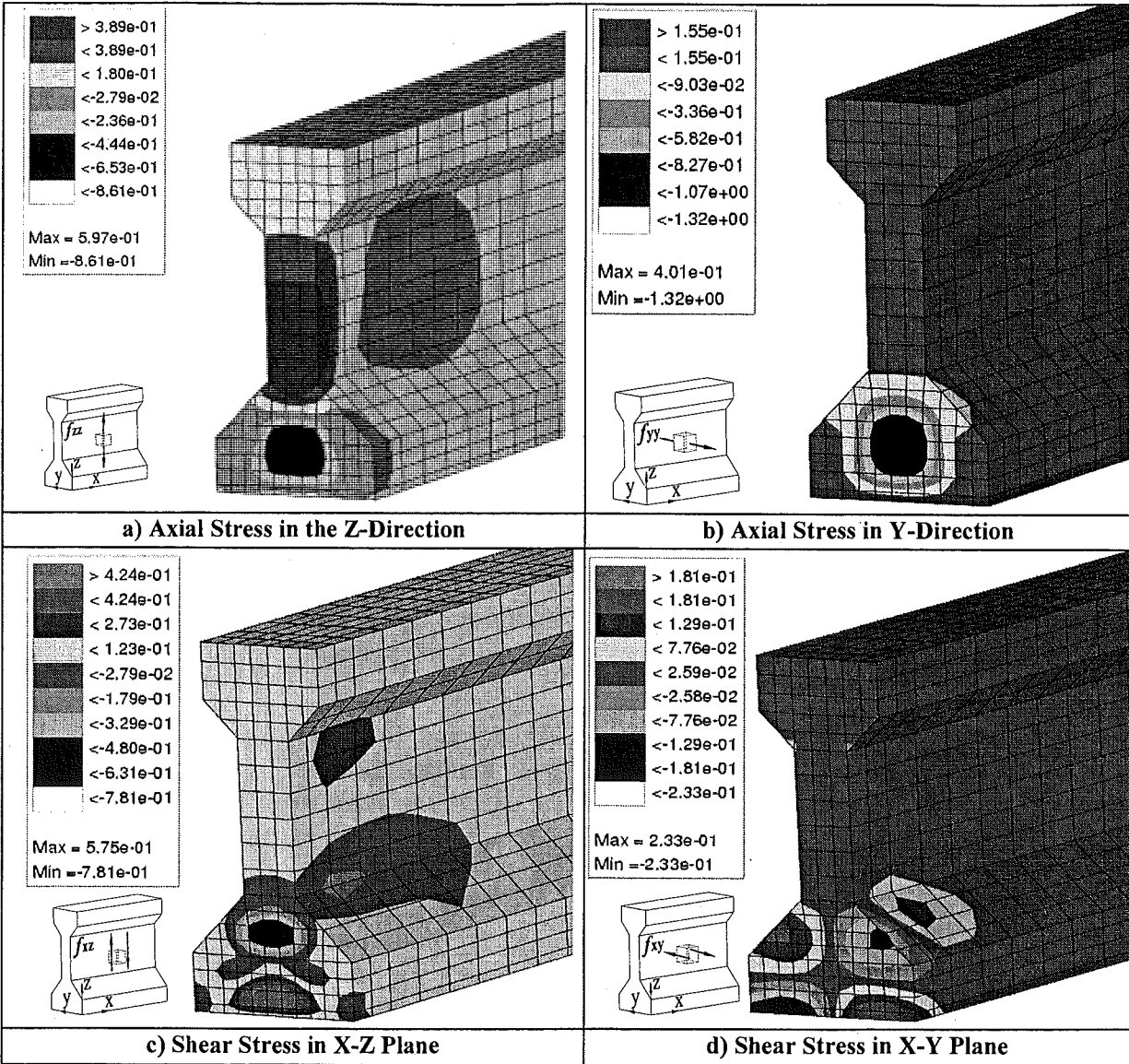


Figure 10-15. Stresses (ksi) Observed near the End of the Girder with Straight Tendons

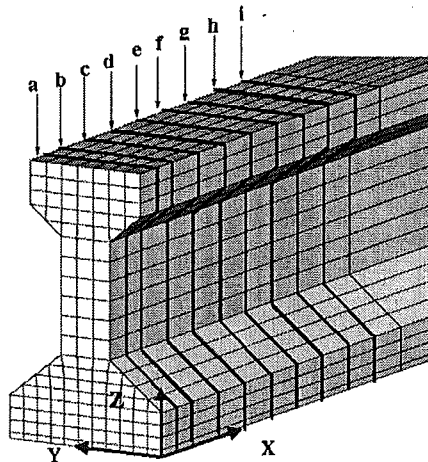
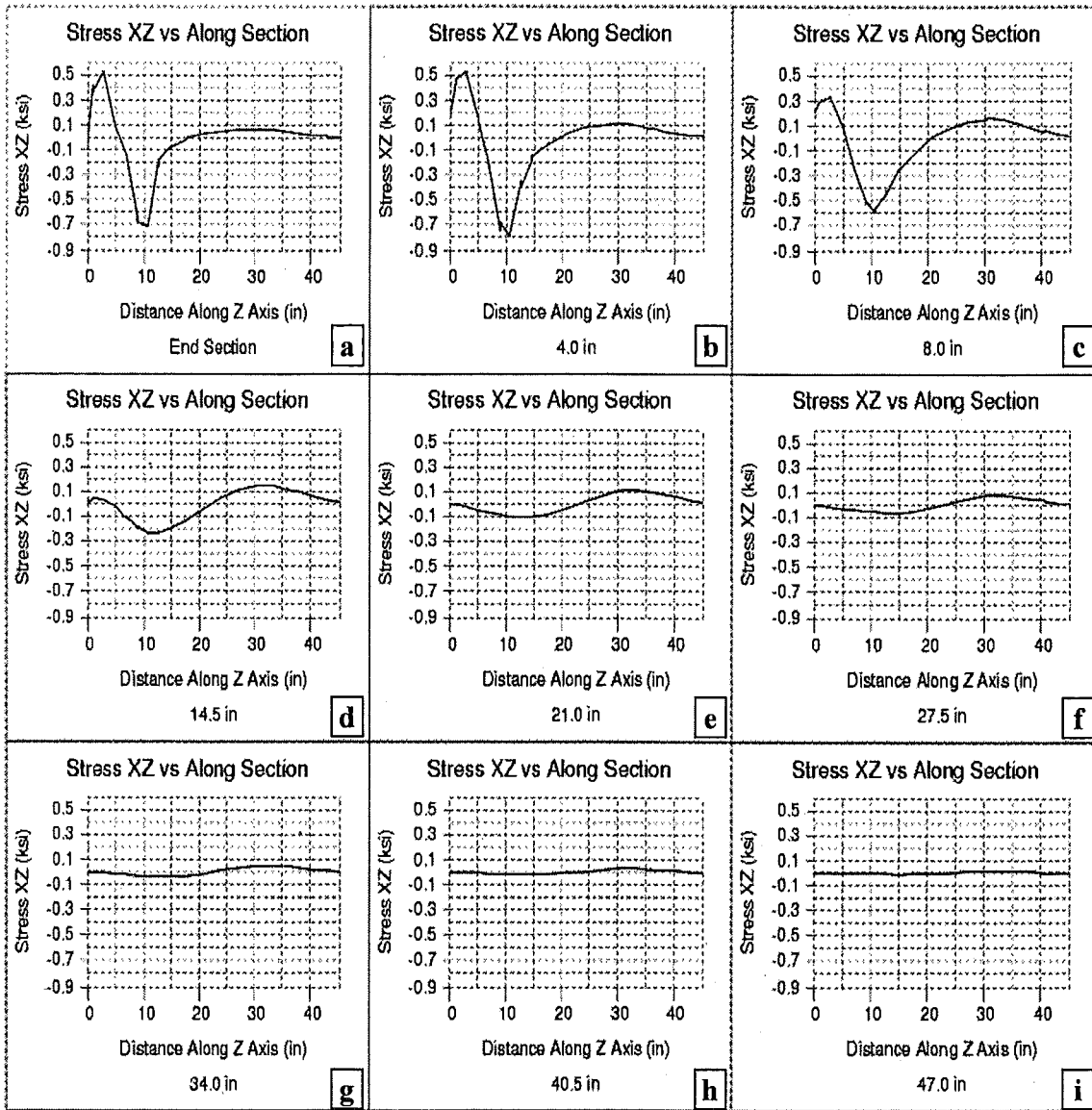


Figure 10-16. Shear Stress Distribution within the Web Projection at Selected Sections near the End Zone under Prestressing Loads

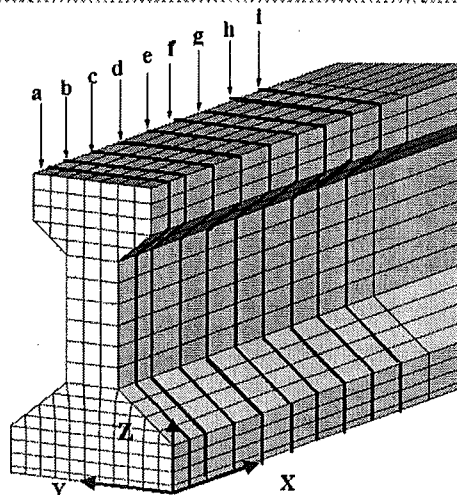
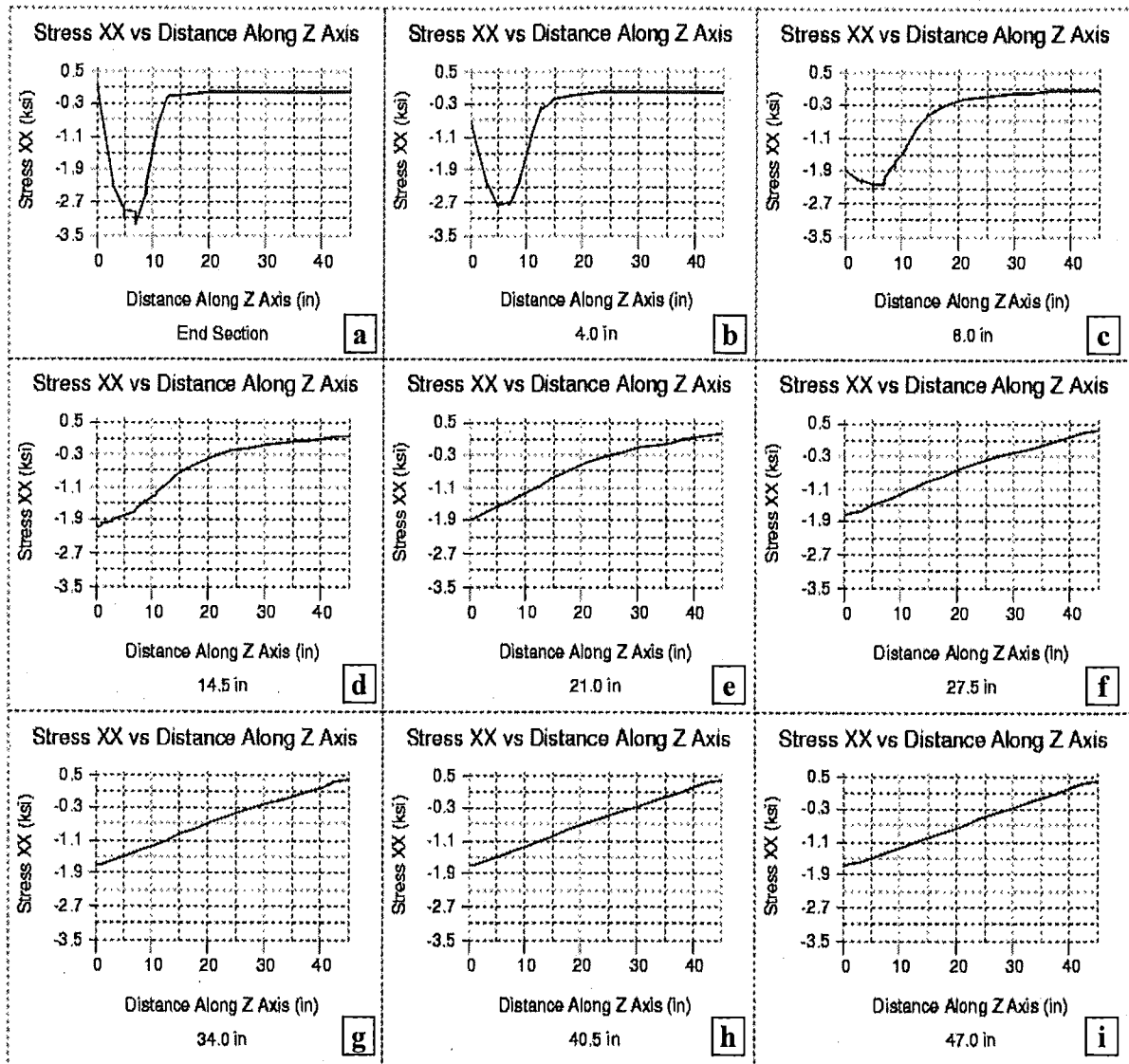


Figure 10-17. Axial Stress Distribution within the Web Projection at Selected Sections near the End Zone under Prestressing Loads

The cracking potential in the end zone is also described by using the principal stress contours. The principal stresses are calculated by rotating the x-y-z coordinates until the shear stress diminishes. In Figure 10-18, the principal stresses on the x-z plane are depicted by rotating the y-z coordinates through an angle " θ " about x-axis. The principal stresses of interest are noted by $f_{\theta 1}$ and $f_{\theta 3}$. $f_{\theta 1}$ and $f_{\theta 3}$ are the maximum and the minimum principal stresses, respectively. The principal stress $f_{\theta 2}$ is not significant for beam elements.

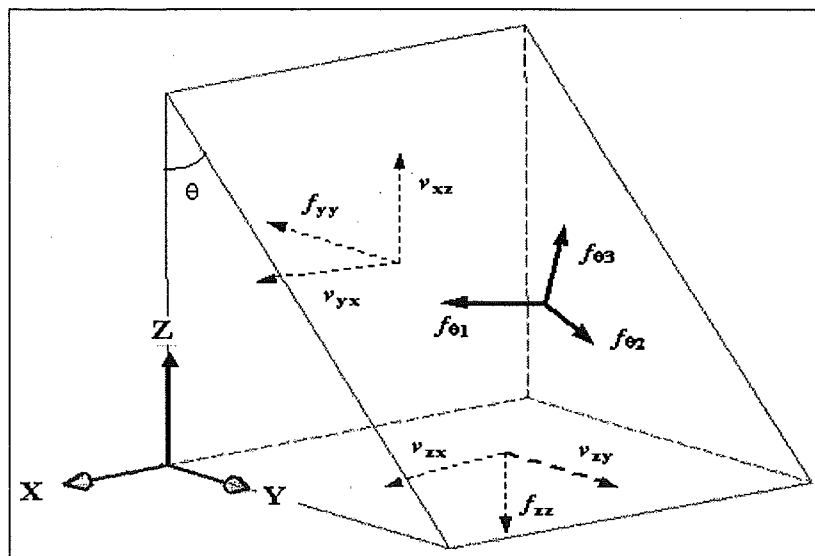


Figure 10-18. Principal Stresses on a Finite Element

The sign convention for the principal stresses is defined such that compressive stress is negative and tensile stress is positive. Principal stress (compressive) contour for $f_{\theta 1}$ is shown in Figure 10-19-a, with a magnitude of reaching a compressive stress of 3000 psi. Principal stress (tensile) $f_{\theta 3}$ shown in Figure 10-19-b is of significance to cracking. The maximum tensile stress magnitude reaches 400 psi near the beam-end on the web. The critical region seen in the principal stress analysis is the web to bottom flange transition area. The region from the bottom flange to the top flange through web, diagonally decreasing towards the end of the transfer length, is under relatively lower stresses (see Figure 10-19-a). The $f_{\theta 3}$ distribution indicates the vulnerability of the mid-web zone to cracking as shown in Figure 10-19-b.

The effects of bond quality on the transfer length and beam-end stresses are analyzed using two limiting values for bond stiffness. For good bond quality, the modulus of elasticity is assumed to be two times the best estimate ($2 \cdot E_c$). For poor bond quality, the modulus of elasticity is taken as half the best estimate ($E_c/2$). The spring stiffness used for modeling the bond between the tendon and concrete is modified to represent these two bounds. In Figure 10-20 and Figure 10-21, the axial and shear stresses for good and poor bond are compared. As the results are investigated, it is seen that the bond stress directly affects the stress intensity within the girder and their magnitude. Bond quality affects the axial and shear stresses near the beam-end as seen in Figure 10-20 and Figure 10-21. The shear and axial stresses increase as the bond quality increases, because the tendon slip decreases.

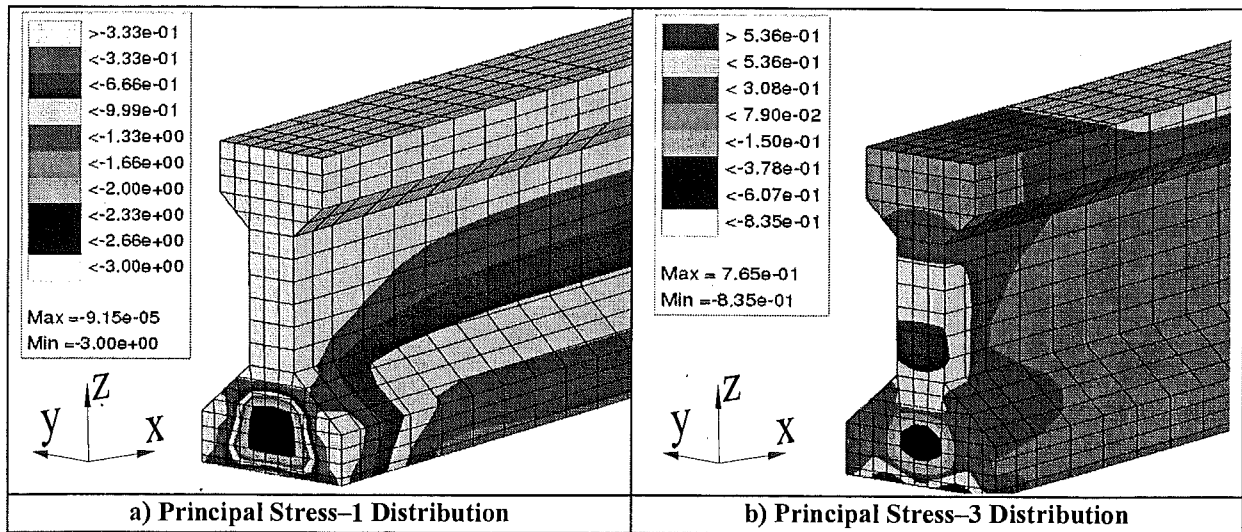


Figure 10-19. Principal Stresses (ksi) near the Girder-end under Prestressing Load

The good bond quality effect on transfer length is not as significant as the effect of poor bond quality. The transfer length in average bond case is around 30 inches; in the bad bond case, it is around 47 inches; and in the good bond case, it is around 27 inches.

The bond quality analyses are performed only on the girder with straight tendons. The main aim is to identify the impact of bond quality on the behavior of the girder. The results obtained are basic and will be the same on the other girders with different geometry and tendon configurations. Therefore, this analysis is not repeated on the other girders with bond-breakers and draped tendons.

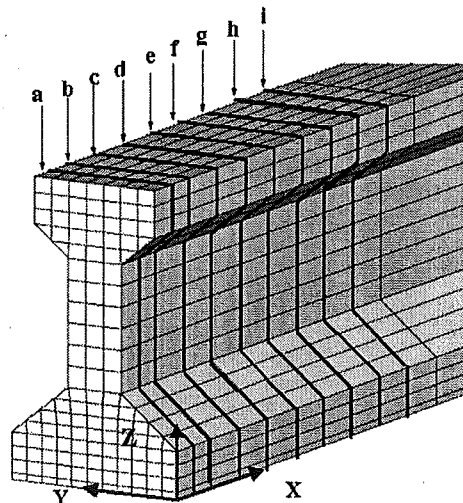
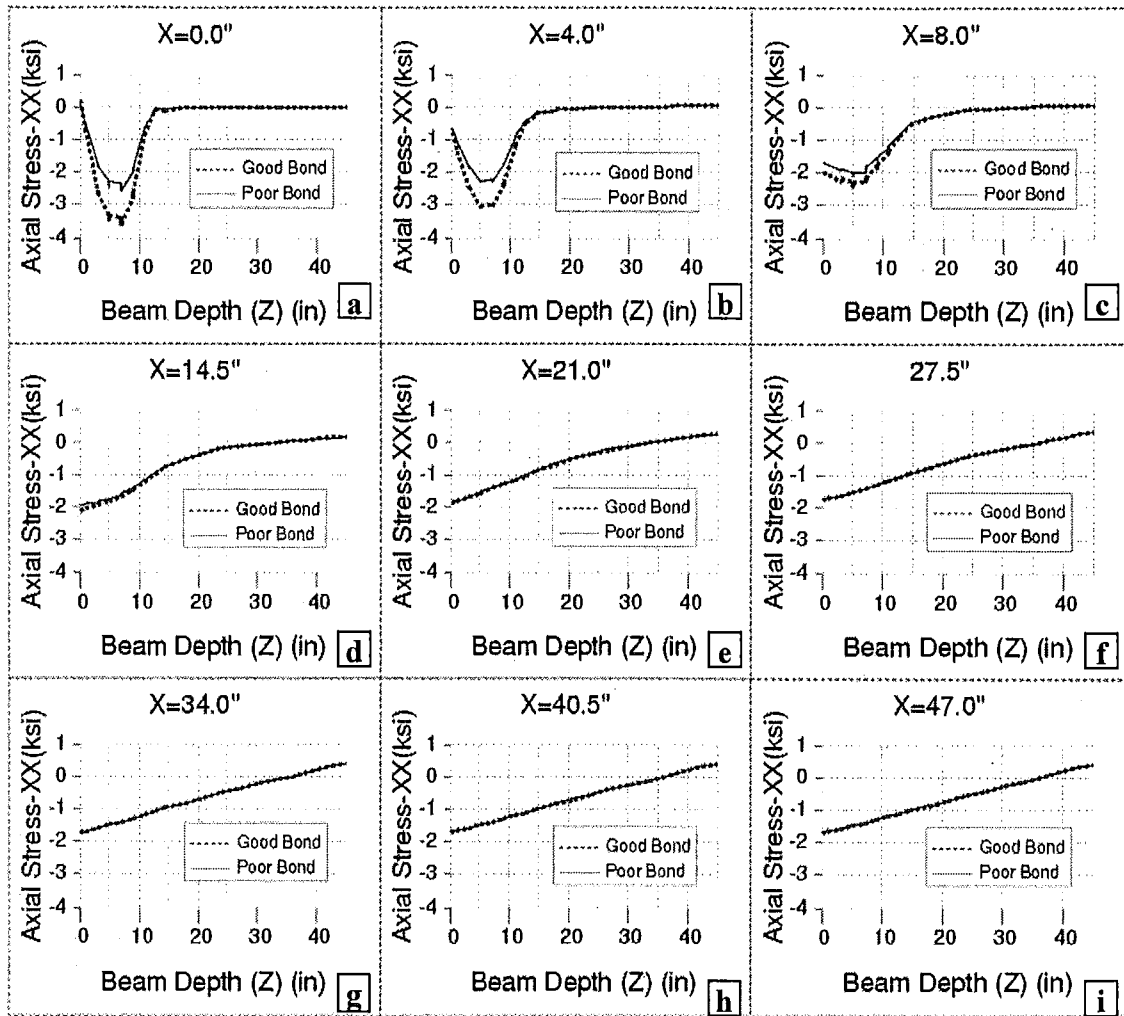


Figure 10-20. Axial Stress Distribution within the Web Projection at Selected Sections near the End Zone under Prestressing Loads with Good and Poor Bond Qualities

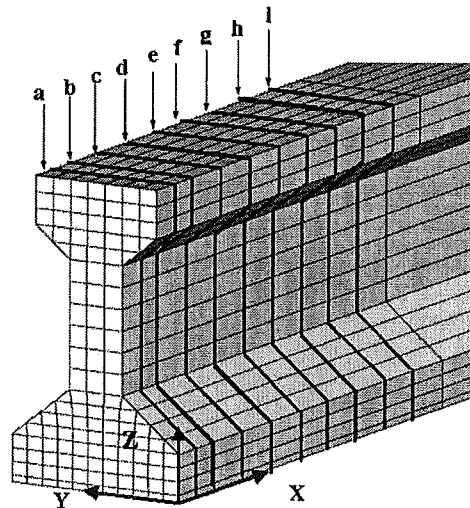
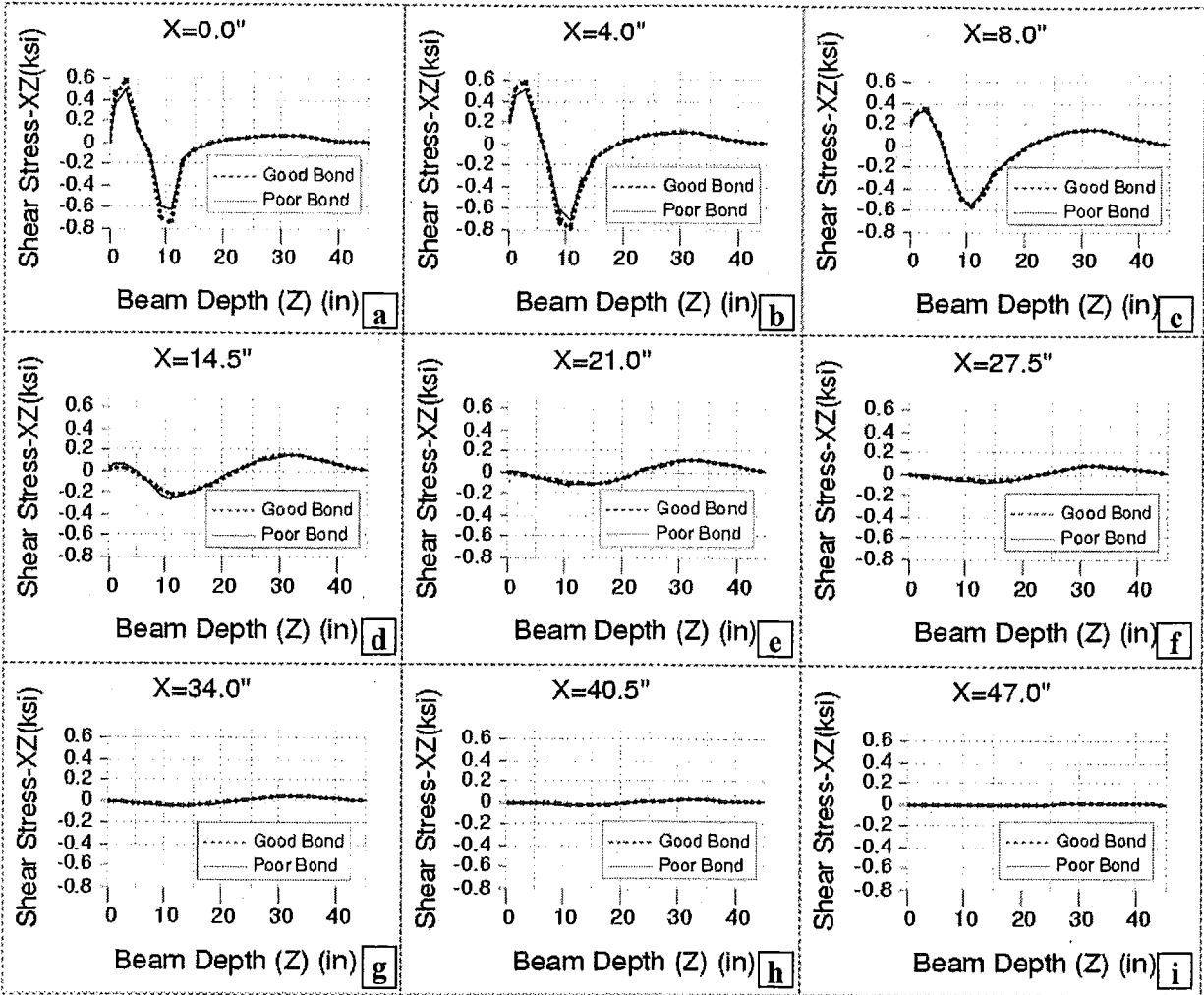


Figure 10-21. Shear Stress Distribution within the Web Projection at Selected Sections near the End Zone under Prestressing Loads with Good and Poor Bond Qualities

10.5.2 Analysis of Prestressed Girders with Bond-Breakers under Prestressing Load

The bond-breakers are employed around the tendons to reduce the concrete stresses near the beam-end. The tendons having bond-breakers are sometimes called sheathed tendons. Some of the strands with bond-breakers are debonded for a length near the beam-ends while the others are retained without bond-breakers. These types of beams were designed more recent than the straight and draped tendons. The year in which these beams are first utilized is seen in Table 10-1 as Michigan 1800 and Wisconsin 70. Using the finite element model (see Figure 10-22), the impact of the bond-breakers is studied. First, the beam is analyzed with straight (uniform) strands and then with bond-breakers. The analyses are compared for stresses and cracking potential, as shown in figures from Figure 10-23 to Figure 10-26.

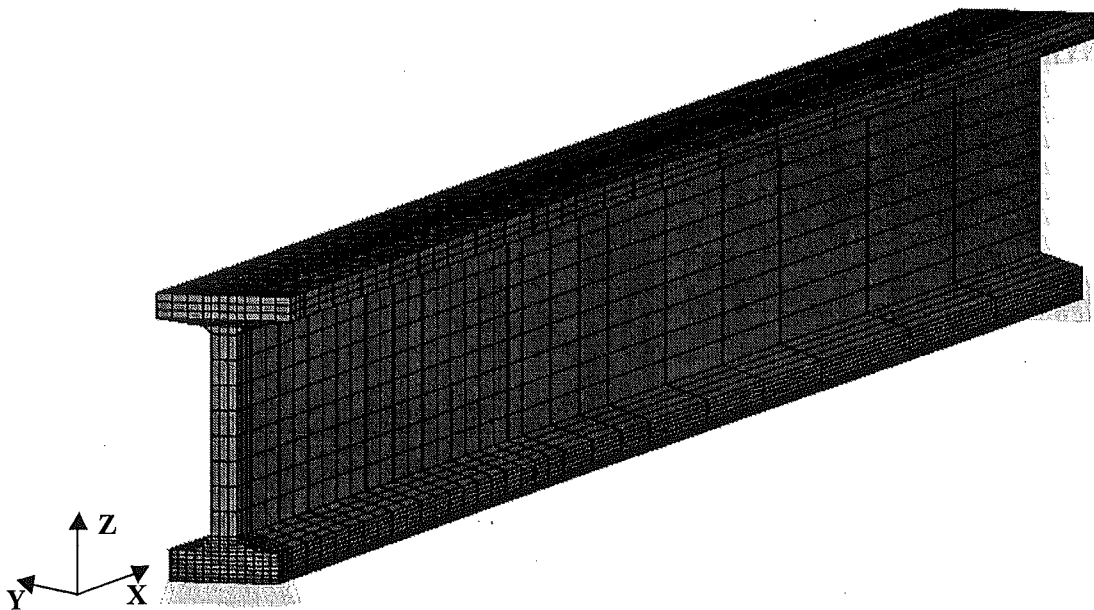


Figure 10-22. General View of the I-Beam with Bond-breakers

The beam modeled is selected from the bridge with the inventory ID of S05 of 53034, a three-span bridge, with skew of $14^{\circ} 30'$. The beam length is 111.5 feet. The total number of the strands is 34 with $\frac{1}{2}$ -inch nominal diameter. The strands are 7-wire low-relaxation steel having 270 ksi strength. Ten of these strands are sheathed for 8 feet, and another ten for 15 feet. The beam cross-sectional geometry is Wisconsin 70 with a height of 70 inches, and flange thickness is 6 inches at the top flange and 7.5 inches at the bottom flange. The initial prestressing force in each tendon is 31 kips. The design compressive strength for concrete is 5,000 psi.

In girders without bond-breakers, axial stress achieves a uniform distribution after prestressing transfer is complete as shown in Figure 10-23. However, in the case of girders with bond-breakers at locations where the strands are released, changes in axial stresses are observed as shown in Figure 10-27. The axial stress magnitude, which is not shown here, in the beam without bond-breakers (7.4 ksi maximum) is higher than in the beam with bond-breakers (5.35 ksi maximum). The shear stress distributions in x-z plane are similar for beams with and without bond-breakers. One minor difference is the presence of shear stress near the tendons' release

points. The shear stress magnitude, however, is approximately 30% lower in the girder with bond-breakers. The maximum shear stress on the web in the beam without bond-breakers is around 1.5 ksi, while in the beam with bond-breakers it's around 1.0 ksi (see Figure 10-24-a and Figure 10-26-a).

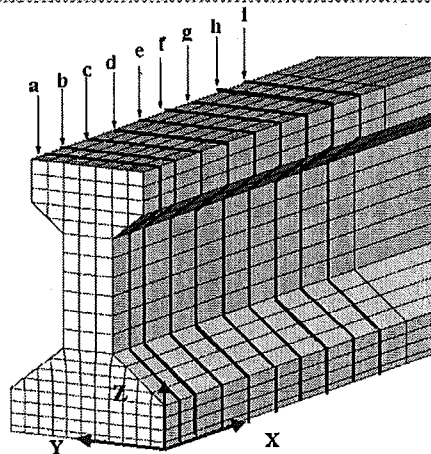
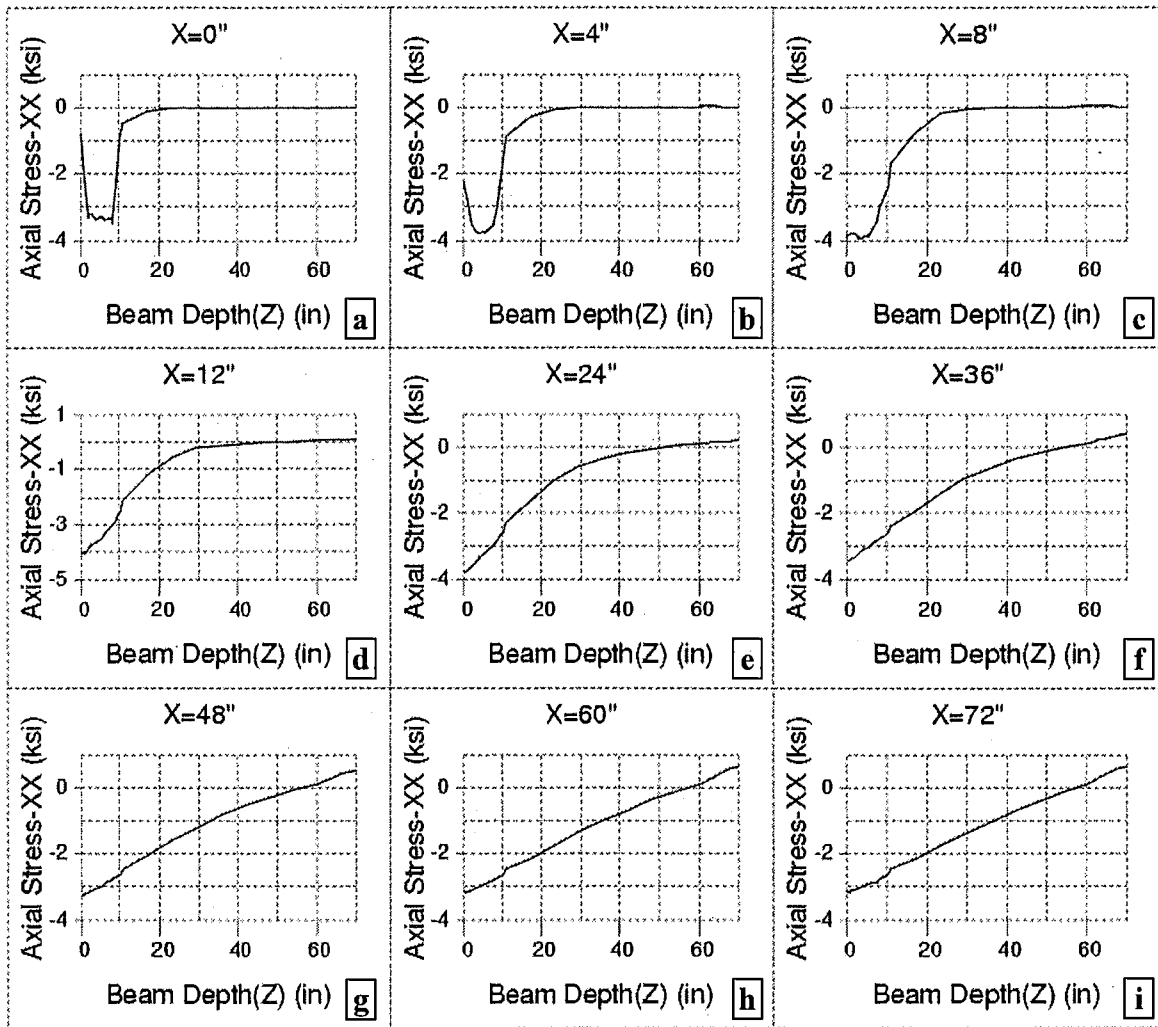


Figure 10-23. Axial Stress Distribution within the Web Projection at Selected Sections near the End Zone under Prestressing Loads on the Girder without Bond-Breakers

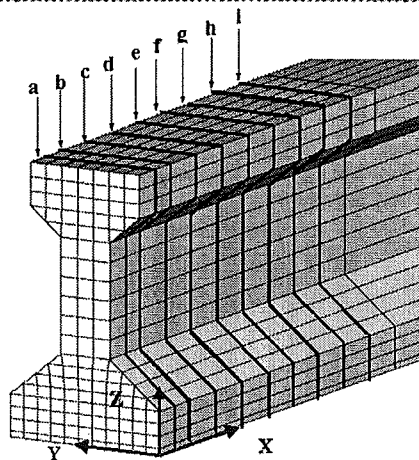
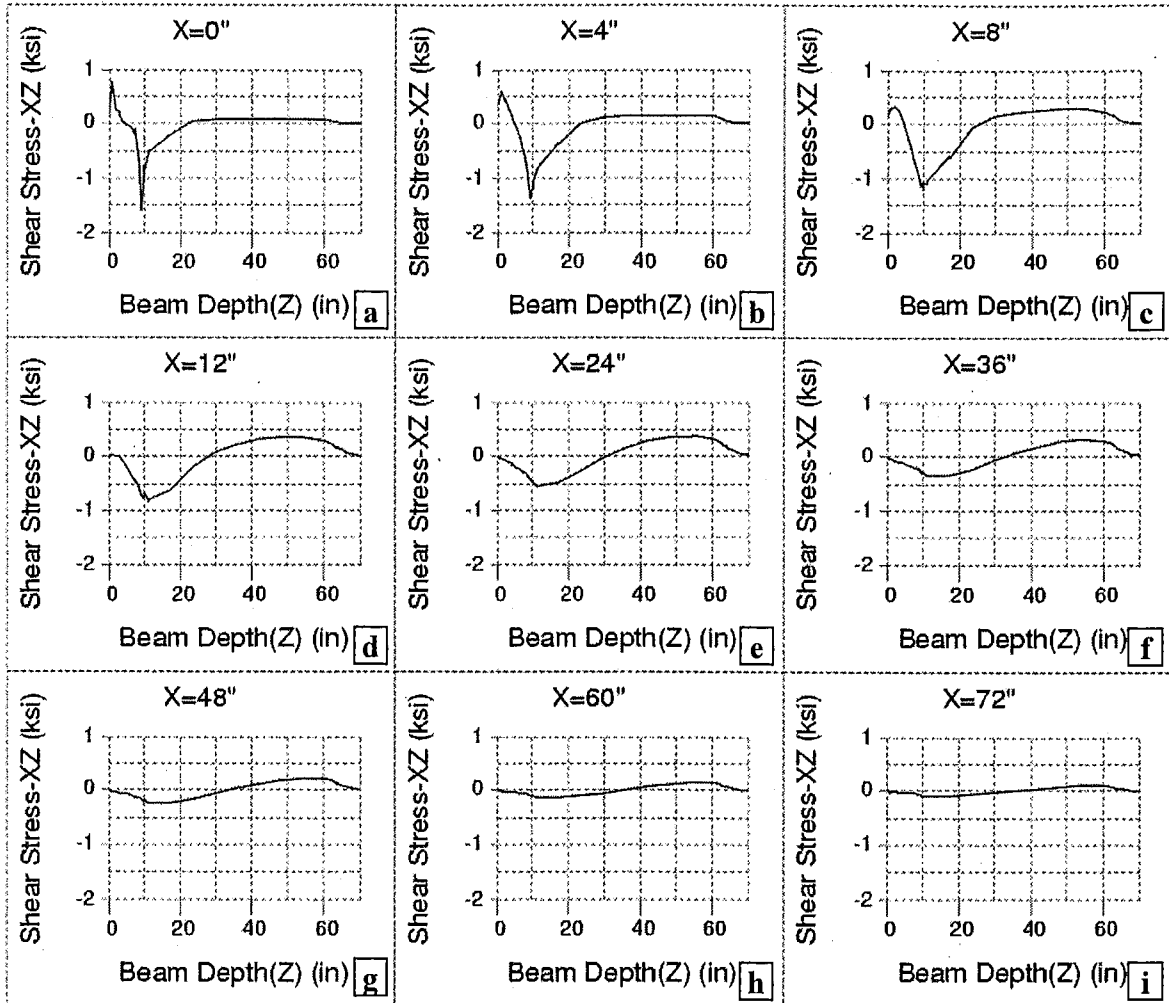


Figure 10-24. Shear Stress Distribution within the Web Projection at Selected Sections near the End Zone under Prestressing Loads on the Girder without Bond-Breakers

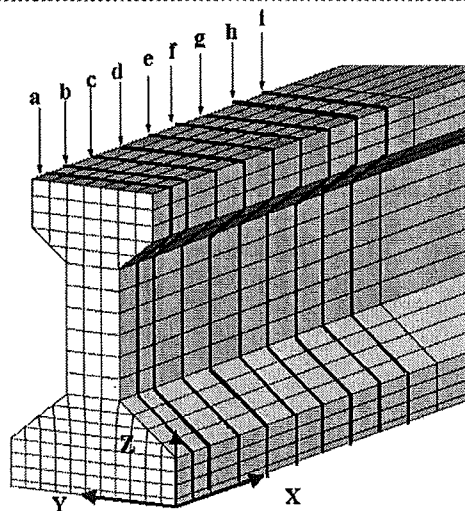
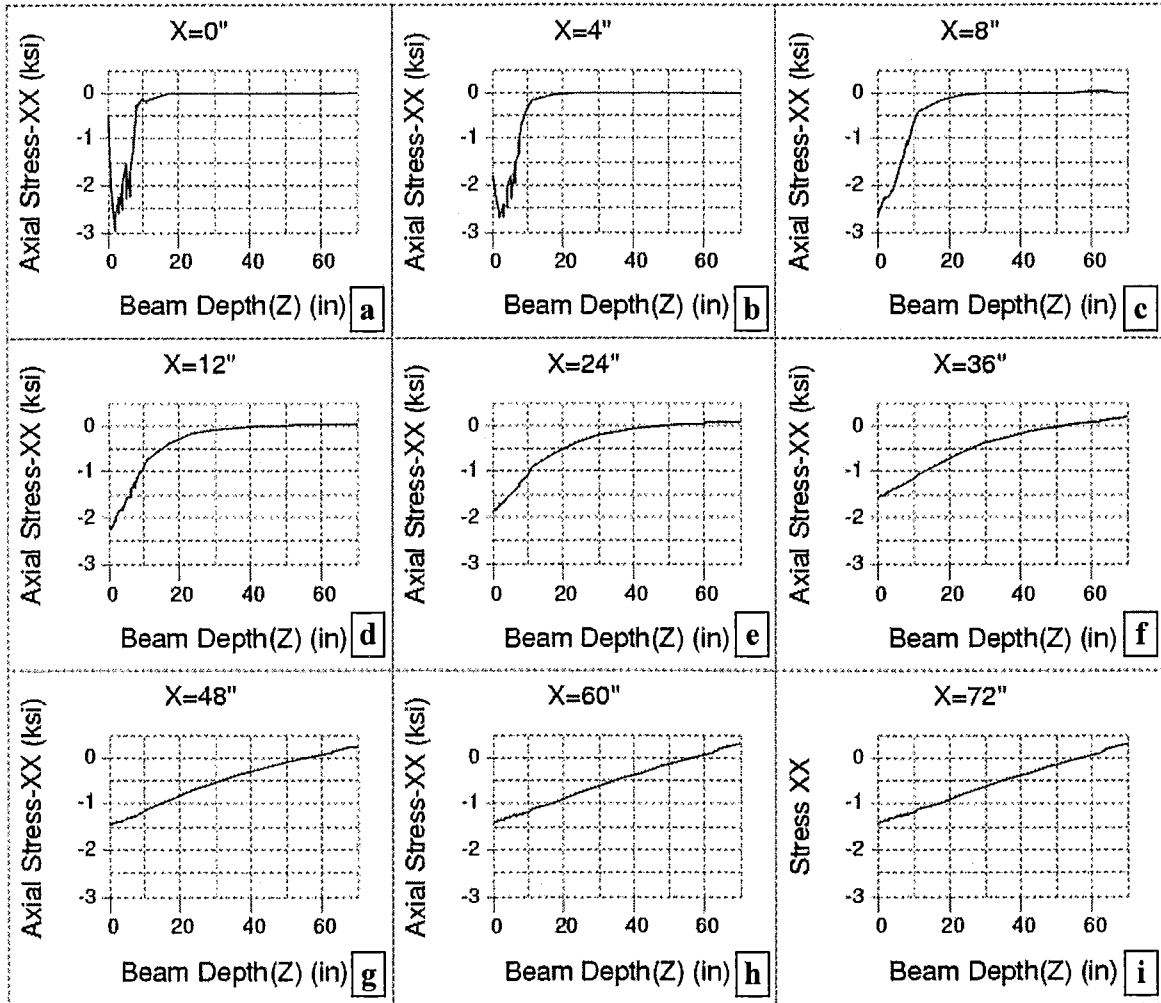


Figure 10-25. Axial Stress Distribution within the Web Projection at Selected Sections near the End Zone under Prestressing Loads on the Girder with Bond-Breakers

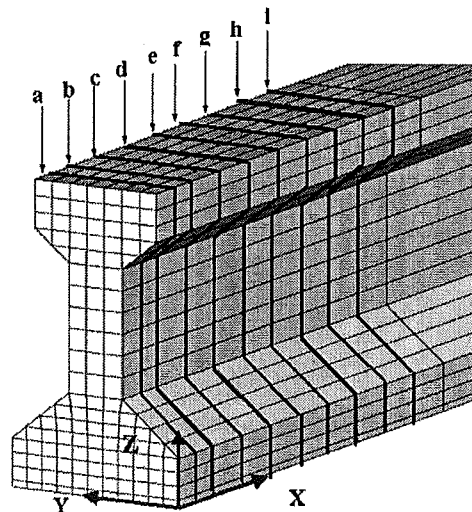
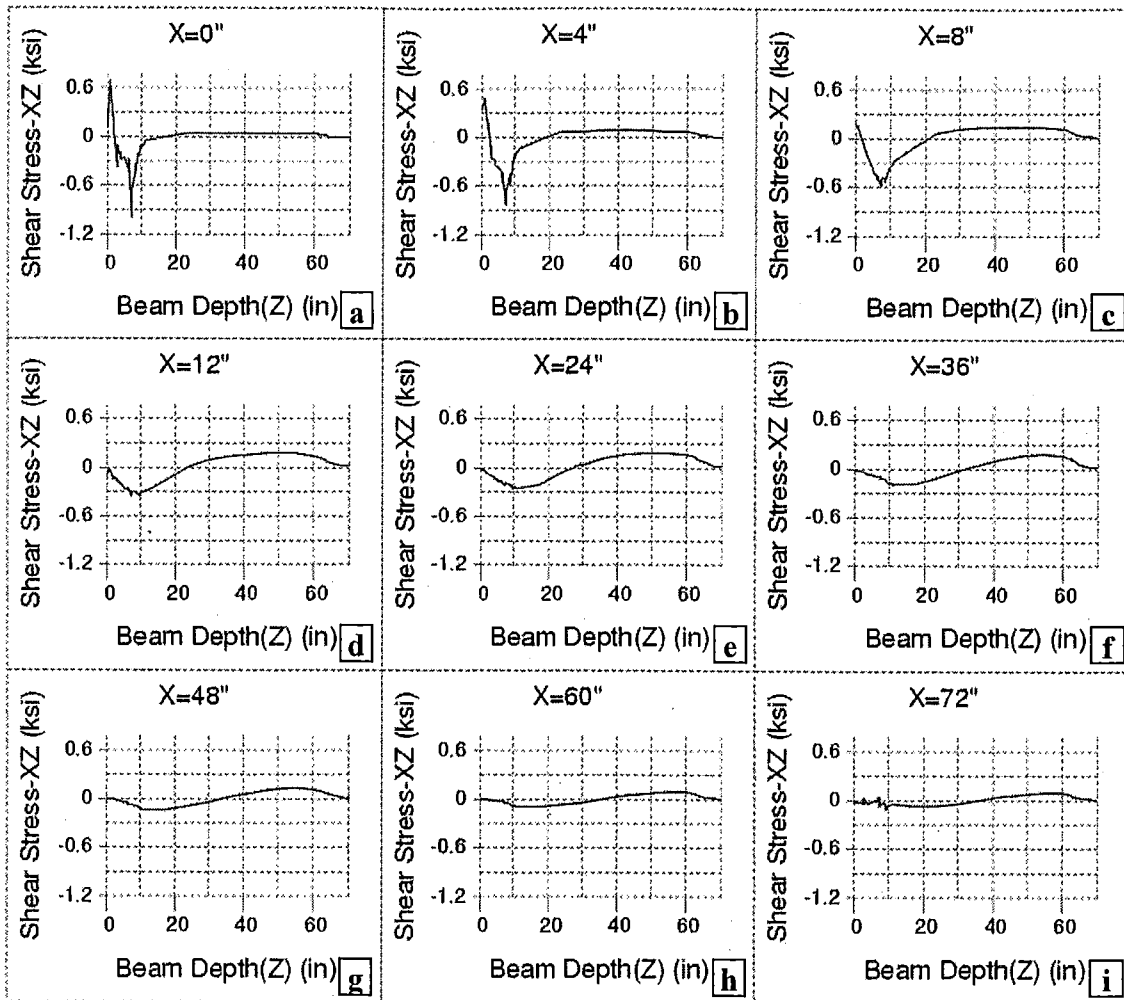


Figure 10-26. Shear Stress Distribution within the Web Projection at Selected Sections near the End Zone under Prestressing Loads on the Girder with Bond-Breakers

Axial and shear stress distribution at sections around the debonding locations are shown in Figure 10-27 and Figure 10-28. Small deviations are observed in both axial and shear stresses on

the girder within 24 inches, where debonding ends. The maximum shear stress is calculated as around 500 psi at the first release point as shown in Figure 10-28-a. Deviation of the axial stress between Figure 10-27-b and Figure 10-27-c is not significant.

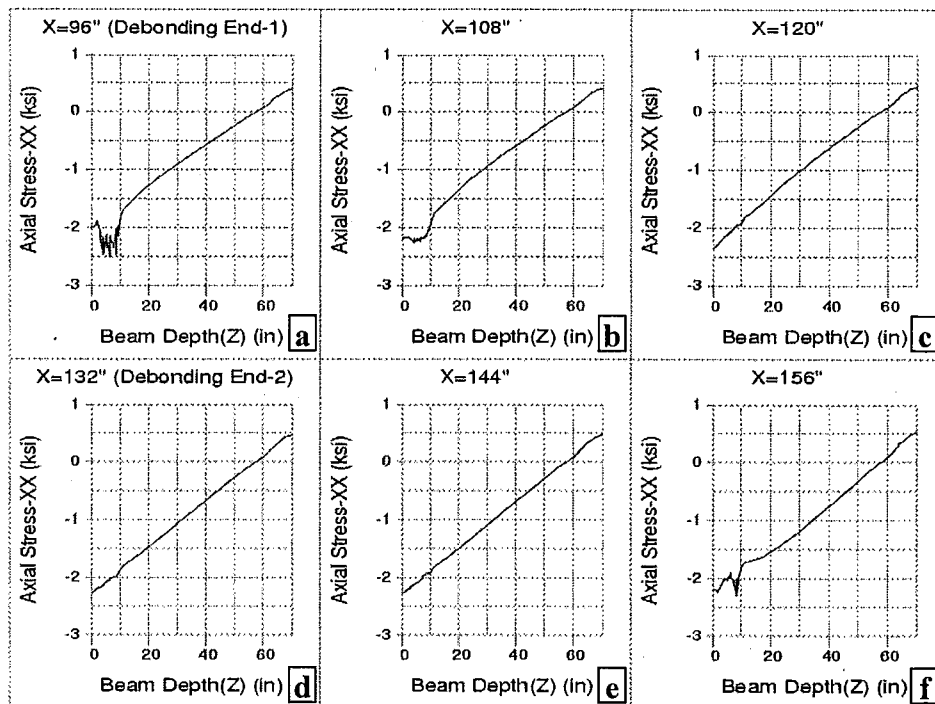


Figure 10-27. Axial Stress Distribution within the Web Projection at Selected Sections near the Release Points on the Girder with Bond-Breakers under Prestressing Loads

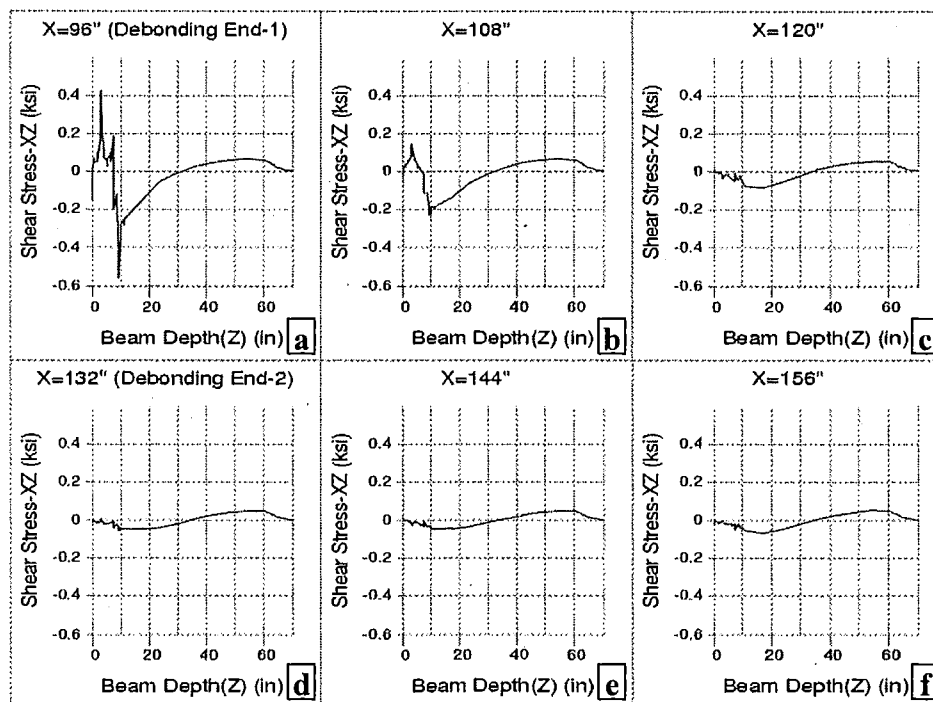


Figure 10-28. Shear Stress Distribution within the Web Projection at Selected Sections near the Release Points on the Girder with Bond-Breakers under Prestressing Loads

The shear stress cracking pattern may be described by the principal stresses. The maximum and minimum principal stresses for the beam with bond breakers are shown in Figure 29-a and -b. The maximum principle stress is 3.6 ksi around the tendons and the ends of debonding as shown in Figure 29-a. This stress is compressive and well below the compressive strength of concrete. The minimum principle stress, shown in Figure 29-b, is around 1.2 ksi. This tensile stress may be the main reason for the shear cracking. Because the stress value found exceeds the tensile strength of concrete, which is 424 psi. As it is seen in Figure 29-b, the web zone is prone to cracking due to excessive tensile stress.

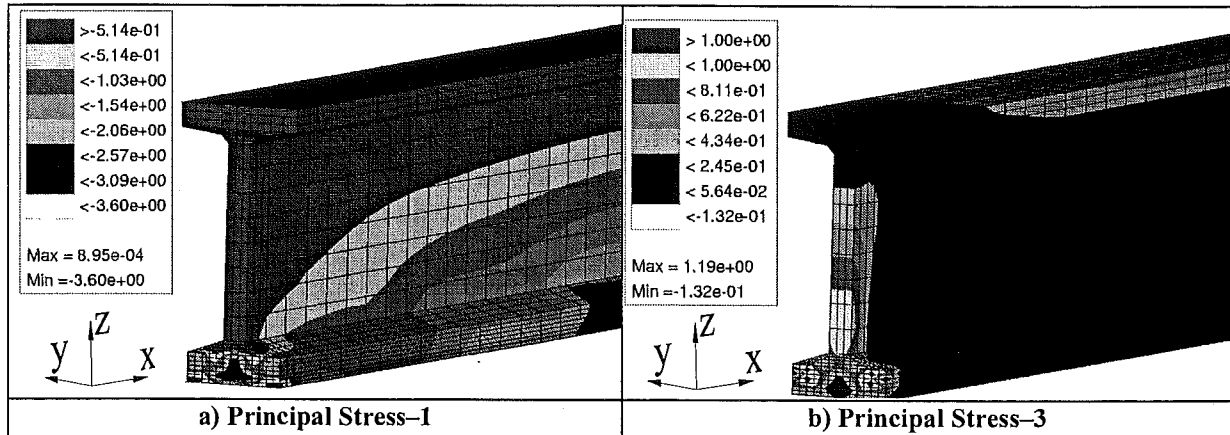


Figure 29. Principal Stresses (ksi) near the Beam-end under Prestressing Load for the Beam with Bond-breakers

10.5.3 Analysis of Girders with Draped Tendons under Prestressing Load

The third type of girder analyzed under prestressing load is the girder with draped tendons. In draping, the tendons are anchored at about the one-third points of the beam and pulled towards the top flange of the beam. In this girder type, end blocks are incorporated in order to accommodate the anchoring of the tendons near the girder-ends. Draped tendons with end blocks are commonly seen in earlier bridges, and they appear to be rare in recent bridges. Because there are many bridges built with draped beams suffering from end distress, it is important to analyze and discuss the effects of draping and the effect of the end block on stresses near the beam-ends.

The draped beam model is selected from the bridge with inventory ID S06 of 41027, with a length of 65 feet and 6 inches. The total number of strands used is 36, 28 strands are kept straight and 8 strands are raised near the beam-ends. The nominal diameter of the 7-wire strands is 7/16 inches. Initial prestressing load is 19.05 kips on each tendon, which has an ultimate strength (f_{pu}) of 250 ksi. The concrete design compressive strength is defined as 5,000 psi.

As described earlier in the straight tendon case, the change in the effective prestressing load transferred to the beam generates the change in axial stress distribution along the beam's longitudinal axis that in turn generates the shear stresses. In the beams with draped tendons, there are three parameters affecting change in the axial stress distribution. These are prestressing

force transfer between the tendon and concrete, angle of inclination of the draped prestressing tendons, and the change in the cross-sectional area due to the transition to the end block.

The FE model and mesh for the girder with draped strands shown in Figure 10-30 is significantly different than the other two tendon arrangements analyzed earlier. In this mesh, some of the elements are inclined in order to accommodate the inclined tendon and the end-block, where the web is gradually make thicker towards the beam-end.

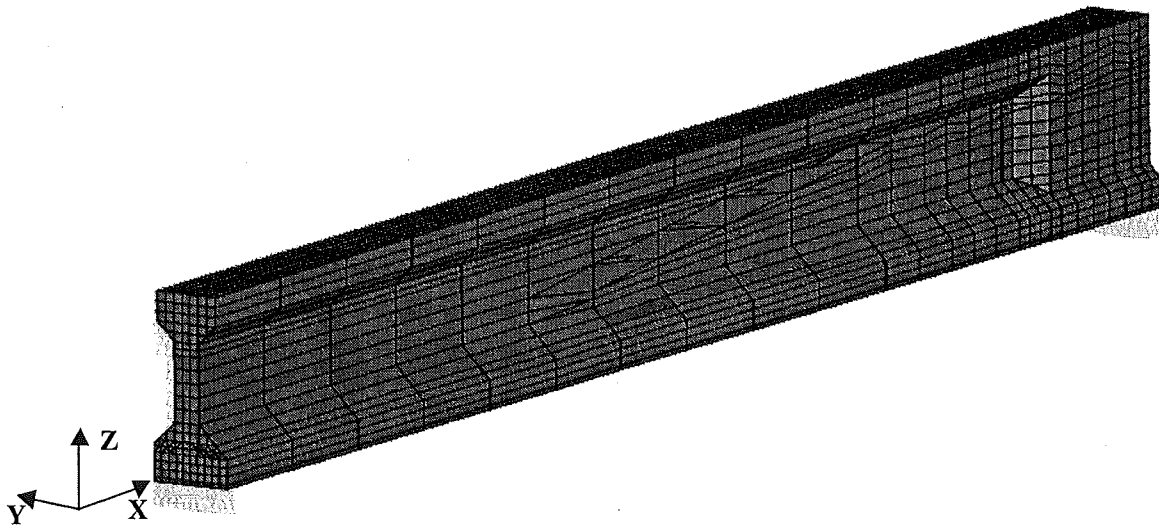


Figure 10-30. One Half of a Beam with Draped Tendons and End Block

The axial stress distribution in x-axis is shown in Figure 10-31 and the shear stress distribution on the x-z plane is shown in Figure 10-32. As seen in Figure 10-32, the change in effective prestressing force within the transfer length results in shear stresses generated near the top flange within the end block and near the zone where the end block is gradually discontinued. The shears stress near the girder-end exceeding 600 psi shows the vulnerability of these girders to cracking. The shear strength of the concrete is around 247 psi, according to AASHTO (AASHTO, 1998)

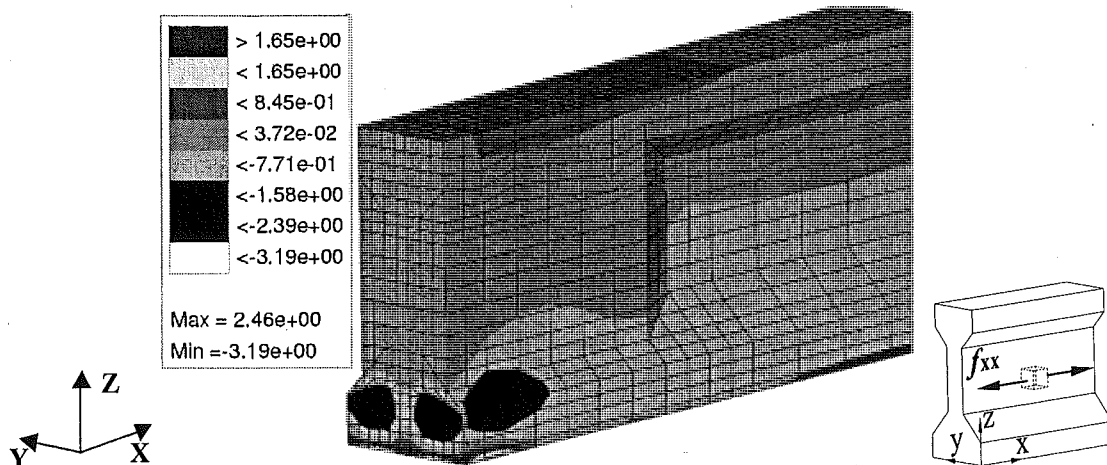


Figure 10-31. Axial Stresses (ksi) in Beam Model with Draped Tendons

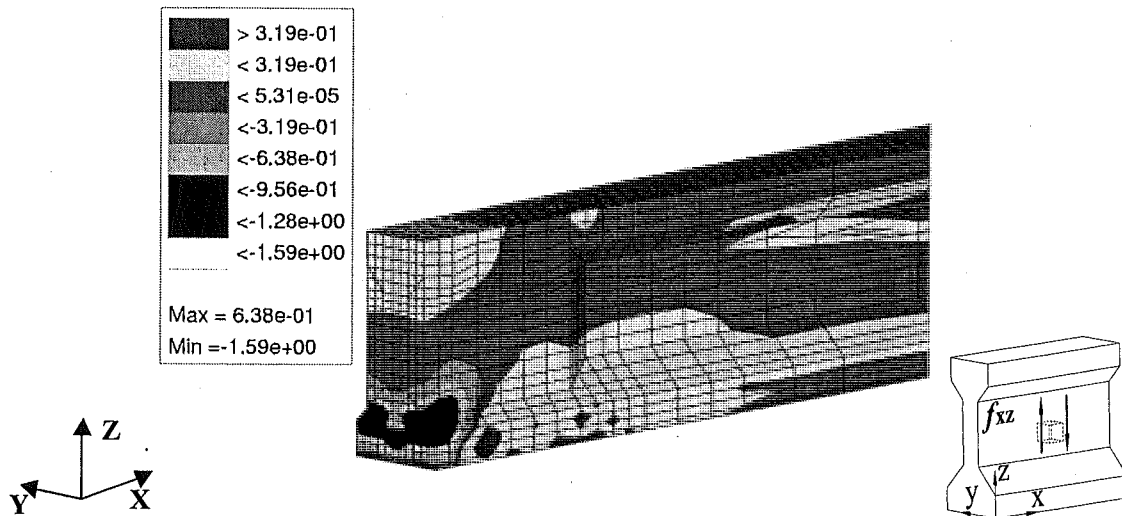


Figure 10-32. Shear Stresses (ksi) in Beam Model with Draped Tendons on X-Z Plane

10.5.4 Load Path Analysis

Load path analysis is performed to establish the portions of the beam-end that are within the load path under the combined action of dead, service, and prestressing loads. The purpose is to provide a means of evaluating the beam-end deterioration impact to its “load transfer” capacity. In other words, the beam-end evaluation is based on whether the zones with section loss interfere with the load path.

The bridge inspection revealed that significant numbers of elastomeric bearing pads appear to have lost their deformability. Similar conditions are observed from other inspections stated in the literature (Yazdani et al, 2000). The main reasons are stated as cold temperatures and aging. The analysis is performed under dead and live loads to establish the load path within the beam-end zone, including non-functional elastomeric bearing pads to simulate the realistic constraints at the girder-end. The non-functional bearings are modeled by modifying girder support restraints to adapt for this condition.

The diaphragms are employed to control the relative movement between the girders, and to help in maintaining the load transfer from the deck to the girders. In other words, diaphragm stiffness properties and location control the live load distribution to individual girders. In this case, the diaphragms are not included in the analysis model, and it is assumed that the girder load distribution factors given by AASHTO are applicable. Further information on the diaphragms is provided in the full bridge modeling section of this report.

The load path analysis is performed on a single girder, utilizing the same model developed in “Girder with Straight Prestressing Tendons under Prestressing Load” analyses (see section 10.5.1). The effects imposed on the girders by the diaphragms and the decks are not incorporated here.

The deck, the wearing surface, the barriers, and the girder are included in the dead load estimation. With a concrete unit weight of 0.150 k/ft^3 the dead load estimated for a girder is

0.583 k/ft. The deck dead load with an effective width of 45.5 inches and 8 inches of thickness is 0.379 k/ft. For the haunch with 1-inch thickness, the dead load is 0.017 k/ft. The barriers with an area of 2.61 ft² and 0.131 k/ft weight are described as superimposed dead load. The wearing surface with 2.5 inches of thickness adds 0.204 k/ft to superimposed dead load. AASHTO HS20-44 truck load (AASHTO, 1998) is used for the live load and applied at a position to generate the maximum flexural stress at the mid-span. The truck load used is for a gross truck weight of 72,000 lb, which is an approximated load amount for simulating the largest stress. For live load effect on a single girder, the distribution factors as given in the AASHTO codes are used. The girder spacing is 91 inches on center. Therefore, the live load distribution factor is calculated as 1.379 by using the formula given in AASHTO (AASHTO, 1998) as $DF=S/5.5$, where DF is the distribution factor and S is the girder spacing. The dead, superimposed dead, loads are distributed longitudinally uniform over the top surface. The live loads are distributed transversely uniform at the wheel locations at the top surface of the beam.

Influence of the bearing on the load path is an important parameter contributing to the stresses at the beam-end. The elastomeric bearing pad sits under a steel bearing plate. The concrete beam and the bearing plate are assumed in composite behavior, when the elastomeric bearing pads are deformable. However, when the elastomeric pad becomes non-functional, as shown in Figure 10-33-a, differential deformations between the bearing plate and the girder are observed. As the beam deforms under bending, the bearing without any deformability rocks on the pier cap. The effective support area is thus reduced. The exaggerated deformation is shown in Figure 10-33-b. Therefore, these differential deformations make the girder vulnerable to cracking, as shown in Figure 10-33-c.

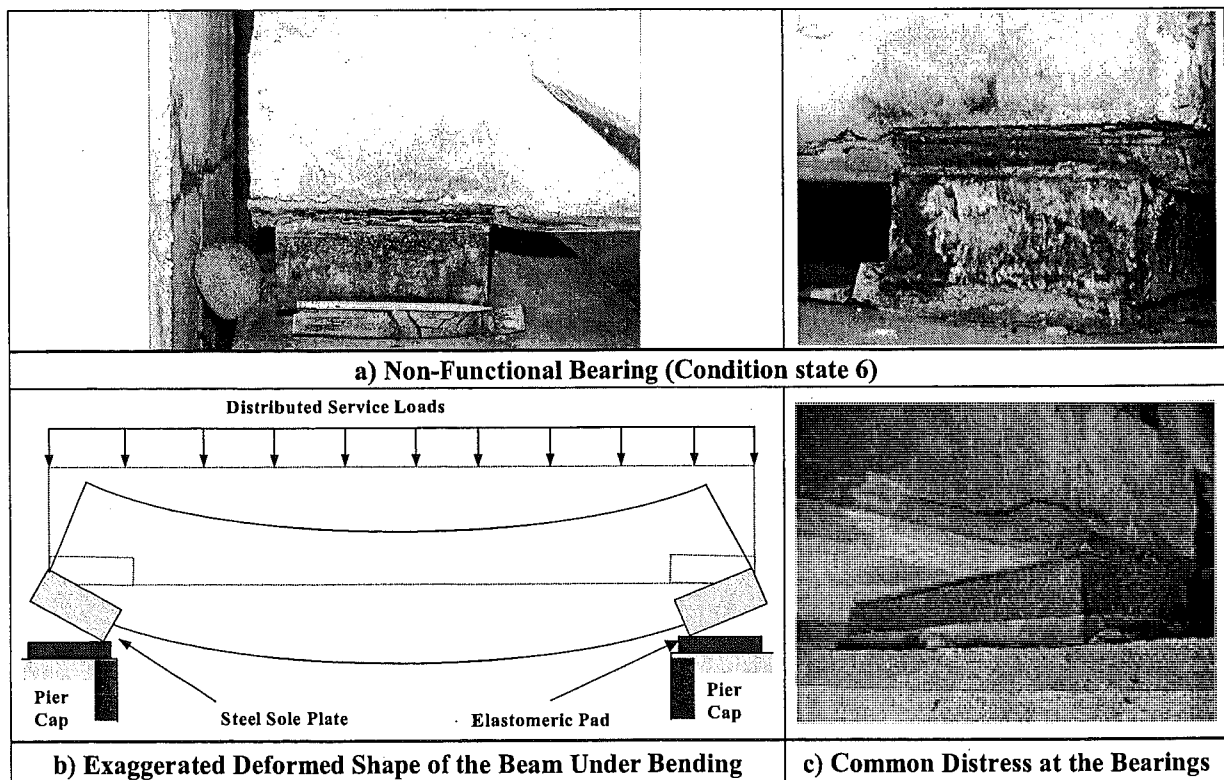


Figure 10-33. a) Condition of the Elastomeric Bearing Pads; b) the Exaggerated Deformed Shape of a Girder under Flexural Bending; c) Common Distress Observed at the Bearings

The beam model under dead load is shown in Figure 10-34-a with the modified support to simulate the rocking of the bearing plate over the non-functional bearing under bending. The beam under dead load is also analyzed for truck load that is live load (see Figure 10-34-b).

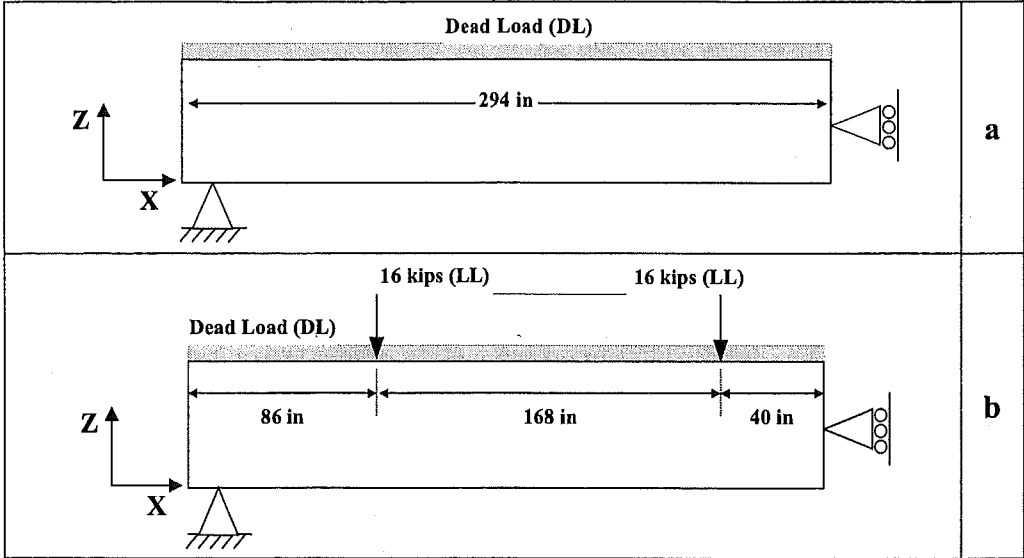


Figure 10-34. a) Beam FE Model and Loading under Dead Load; b) Live Load Distribution on the Girder

Figure 10-35 shows the axial stress distribution under prestressing and dead loads. It is seen that the tensile stresses are increased at the top flange due to reduction in support area. Negative moment is seen at the top of the support because the beam-end now hangs over the support as a cantilever beam. However, the maximum tensile stress, calculated as 290 psi, is less than the concrete tensile strength, which is 424 psi according to AASHTO given as $6 \cdot \sqrt{f'_c}$. Another important result is the stress pattern that describes the load path. The zone on the girder with the stress value of around 740 psi and above compressive stress defines the load path under dead load only. When the live load is included, a similar stress pattern and load path is observed near the end zone. In this case, the load path is defined by the zones of compressive stress of 760 psi and greater (see Figure 10-36). Tensile stresses develop at the beam-end under live load. The accuracy of the stress value is questionable because the deck contribution to load capacity of the beam is not considered in the analytical model.

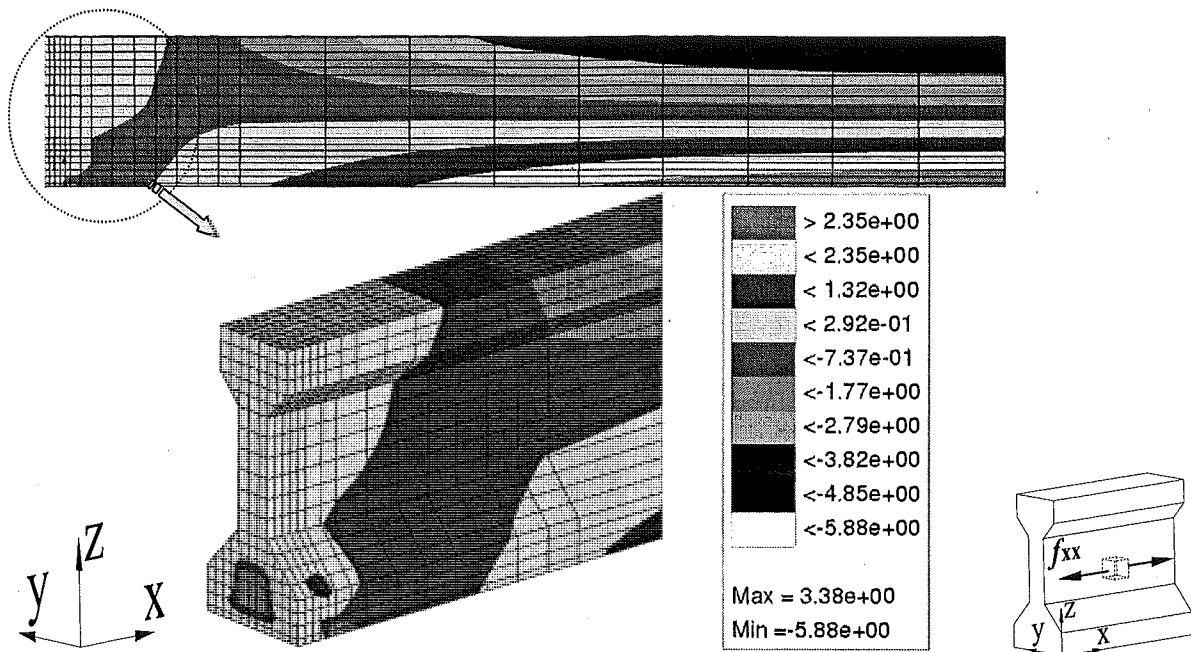


Figure 10-35. Axial Stress (ksi) in the Beam under Prestressing and Dead Load

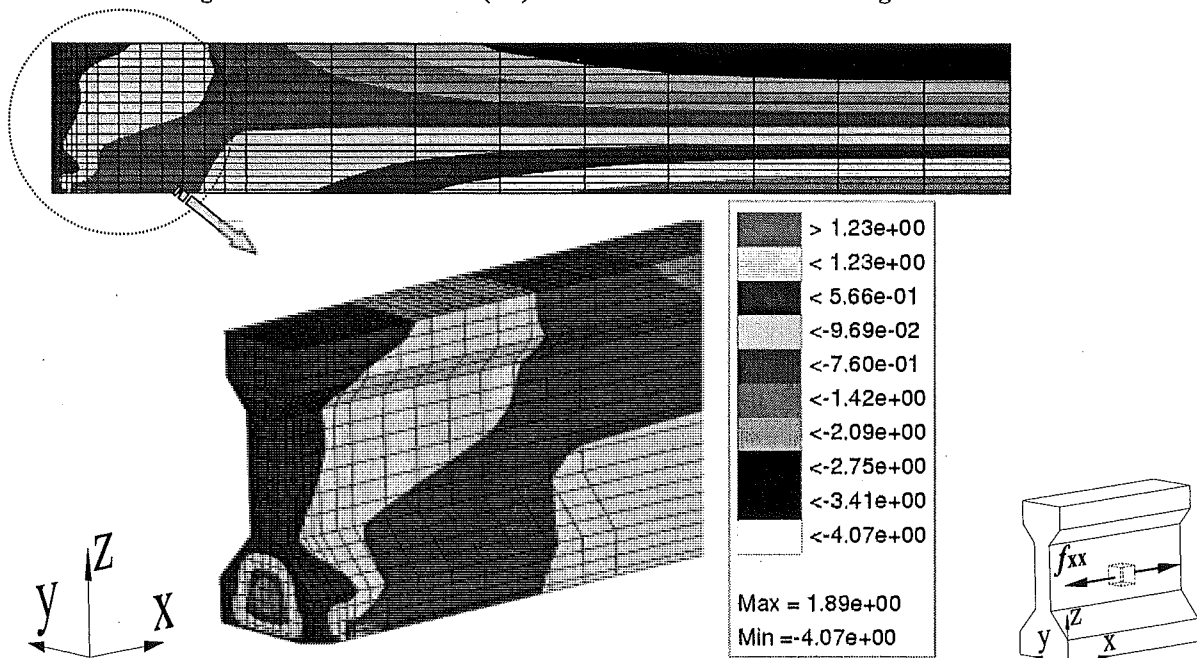


Figure 10-36. Axial Stress (ksi) in the Beam under Prestressing, Dead, and Live Loads

The shear stress distributions shown in Figure 10-37 under dead load and Figure 10-38 under dead and live loads are useful to document stress state near the beam-end. These figures are provided for documentation purposes, and evaluations will not be provided.

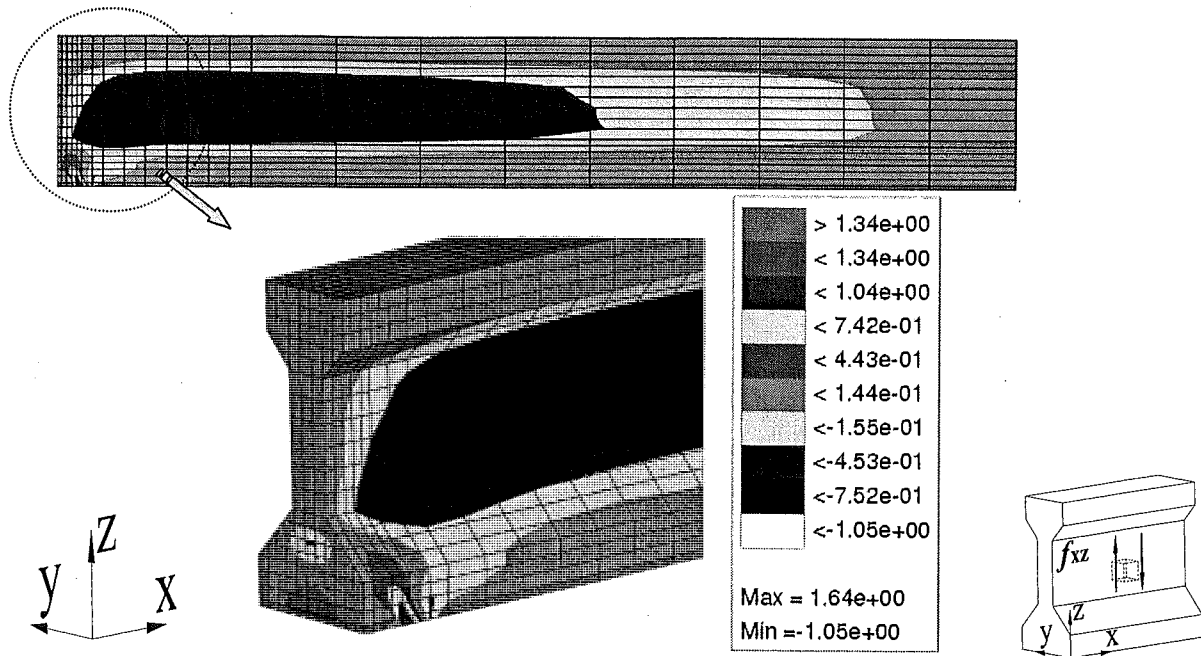


Figure 10-37. Shear Stress (ksi) under Prestressing and Dead Loads

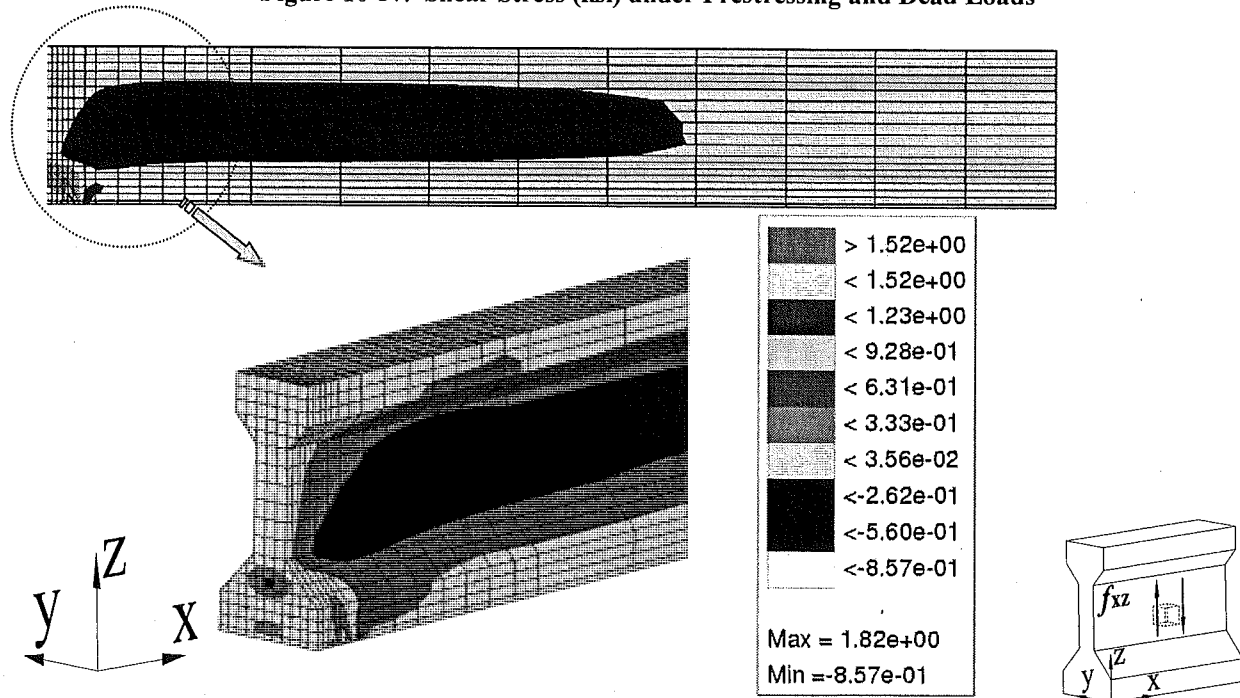


Figure 10-38. Shear Stress under Prestressing (ksi), Dead, and Live Loads

The axial and shear stress comparisons under dead and live loads at selected sections near the beam-end are shown in Figure 10-39 and Figure 10-40. The impact of the non-functional elastomeric bearing is also depicted in the figures. As the support area is reduced due to rocking of the bearing plate, consequently the stress intensities are increased. The dead and live loads give similar stress distributions around the support. The beam-end portion near the support under shear stress intensities exceeding 1.2 ksi is vulnerable to cracking as seen in Figure 10-40-f.

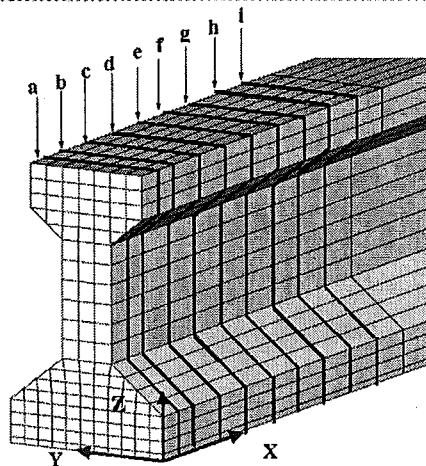
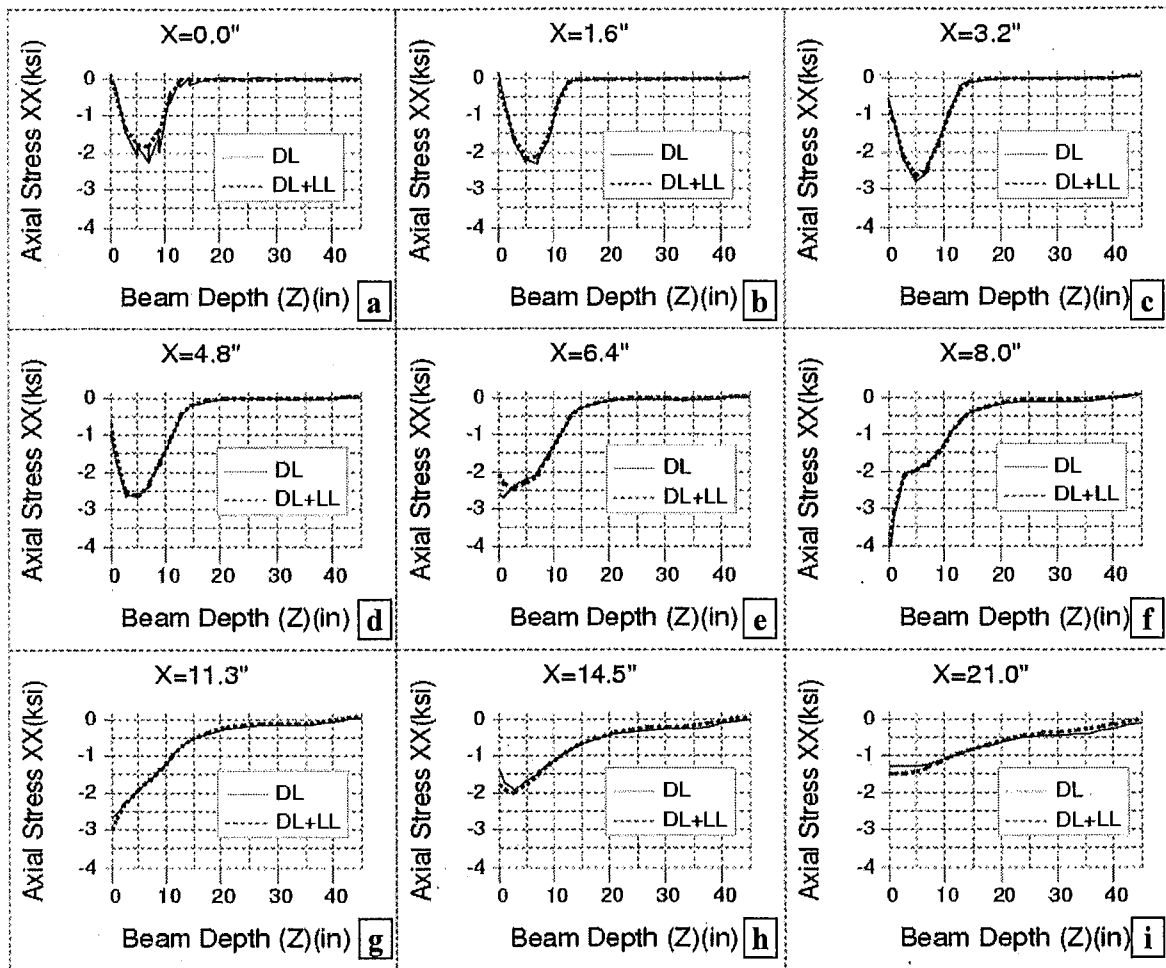


Figure 10-39. Axial Stress Distribution within the Web Projection at Selected Sections near the End Zone under Prestressing, Dead, and Live Loads

The principal stresses generated near the beam-end due to non-functional elastomeric bearing pads are shown in Figure 10-41-a and Figure 10-41-b. As shown in the figures, the stress intensity at the bottom flange is high. In particular, the principal stress intensity around the bearing is significant. The maximum compressive stresses observed under dead and live loads

are 7.84 ksi and 8.09 ksi, respectively. Considering the compressive strength of the concrete described, 5 ksi, principal stress, $f_{\theta 1}$, is significant and higher than the compressive strength of concrete.

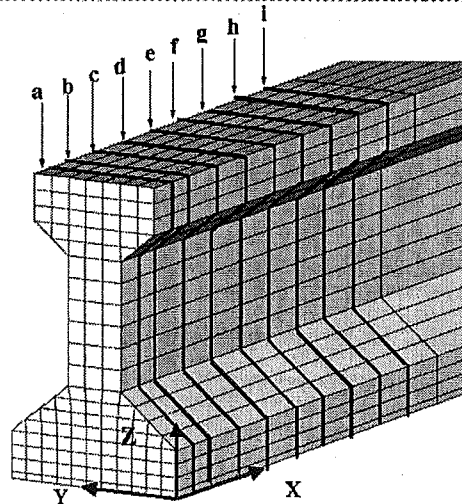
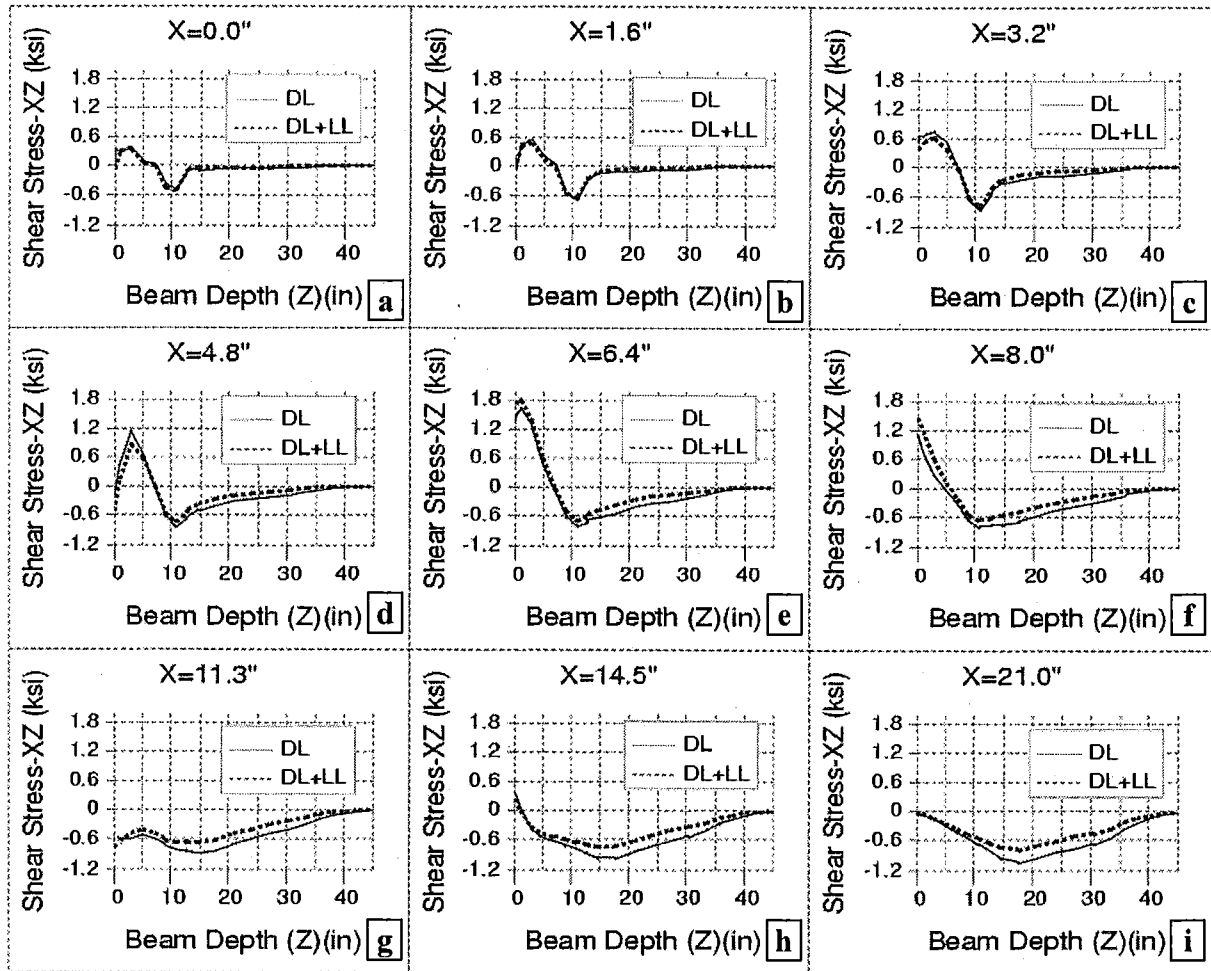


Figure 10-40. Shear Stress Distribution within the Web Projection at Selected Sections near the End Zone under Prestressing, Dead, and Live Loads

The load path in the girder is also investigated to identify the critical zones at the girder-ends. Von Misses stresses in Figure 10-42-a and Figure 10-42-b are utilized for describing the load path near the beam-end. The zones of the beam-end that is within stress contour of 1,920 psi under dead load and 2,400 psi under live load are defined as the load path and shown in Figure 10-42-c and Figure 10-42-d, respectively. The concrete zone shown in Figure 10-42-c defines the load path near the beam-end with non-functional bearing. Any deterioration that intrudes into the load path increases the vulnerability of the beam-end and its load carrying capacity. The beam-end condition may be assessed according to the intrusion of deterioration into the load path. Any kind of deterioration, such as delamination and spall that are not within this diagonal region or reaching the load path, can be repaired using the repair techniques described for condition states of "10" and "11" as given in Table 12-2 in Chapter 12 of this report.

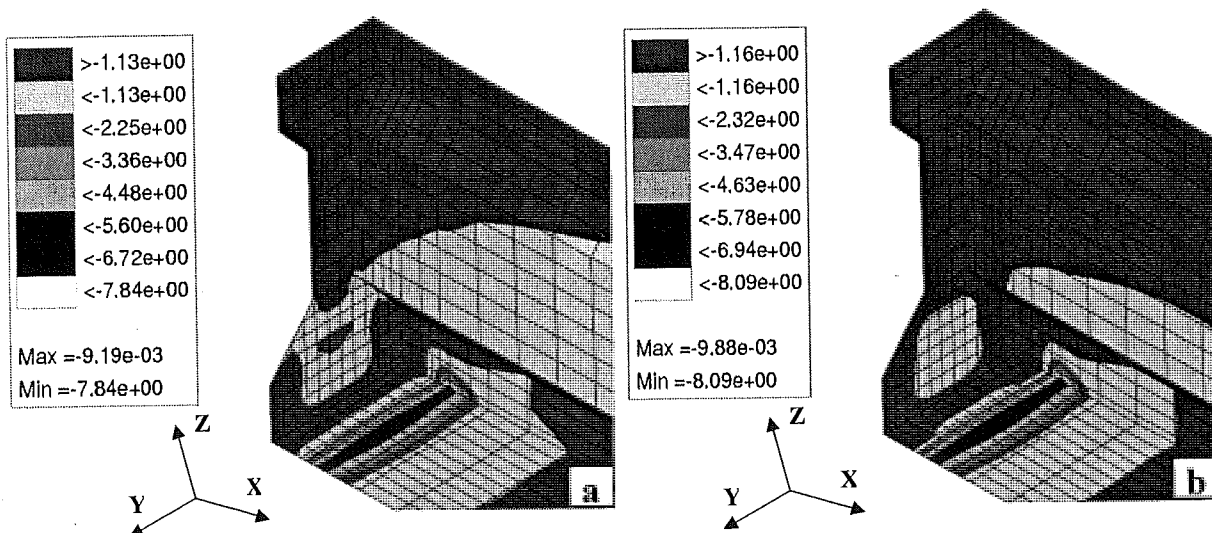


Figure 10-41. Principal Stress (Compressive), a) Under Dead Load (ksi); b) Under Dead and Live Loads (ksi)

The non-critical zones shown in Figure 10-42-c are removed for Figure 10-42-d, to generate a template for the inspectors to assess the significance of the deterioration at the beam-ends. Any deterioration on the regions shown in Figure 10-42-d is considered at risk.

The analysis results are shown only at the beam-end, specifically, for describing the load path. In this analysis the deck is not included as part of the load transfer medium. The model should include the deck for more realistic assessment of the load path.

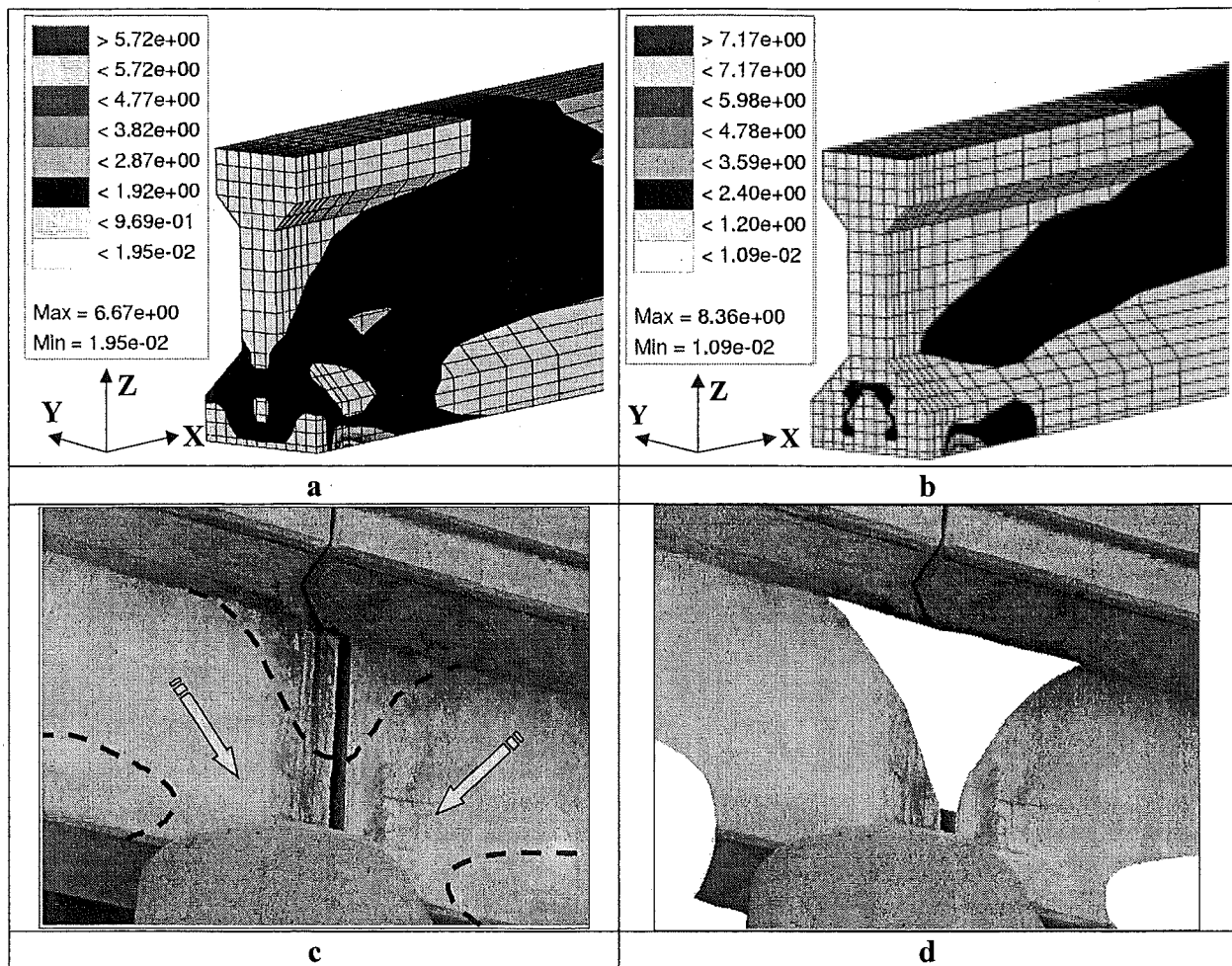


Figure 10-42. a) Von Mises Stress for Dead Load (ksi); b) Von Mises Stress for Dead and Live Loads (ksi); c) Load Path on a Girder; d) Critical Regions on Load Path

10.5.5 Shear Reinforcement Effects on Crack Reduction near Beam-end

The beam-end cracking due to combined high shear and flexural stresses near the beam-end can be controlled by providing confinement reinforcement. The confinement reinforcement primarily confines the zones of high axial stress with closed loops. As seen in Figure 10-43, triaxial stress application remarkably increases the strength of the concrete members. Elements under uniaxial loading show lateral deformation due to Poisson's effect. The lateral reinforcement generates passive pressure around the concrete inside the reinforcement by preventing the lateral deformations (Ersoy, 1997). Therefore, core concrete is loaded triaxial instead of uniaxial. Spiral and square hoop lateral confinements are shown in Figure 10-44. The reinforcement geometry and amount used influences the confining pressure supplied. The volume ratio of transverse steel to the volume of concrete member, the strength of the steel used, and reinforcement spacing is directly proportional to the confining pressure and therefore to the concrete strength (Park and Paulay, 1975). Spiral confinement is relatively more effective,

providing higher confinement. As it is seen in Figure 10-44, the section under lateral stress is larger inside the closed loop reinforcement.

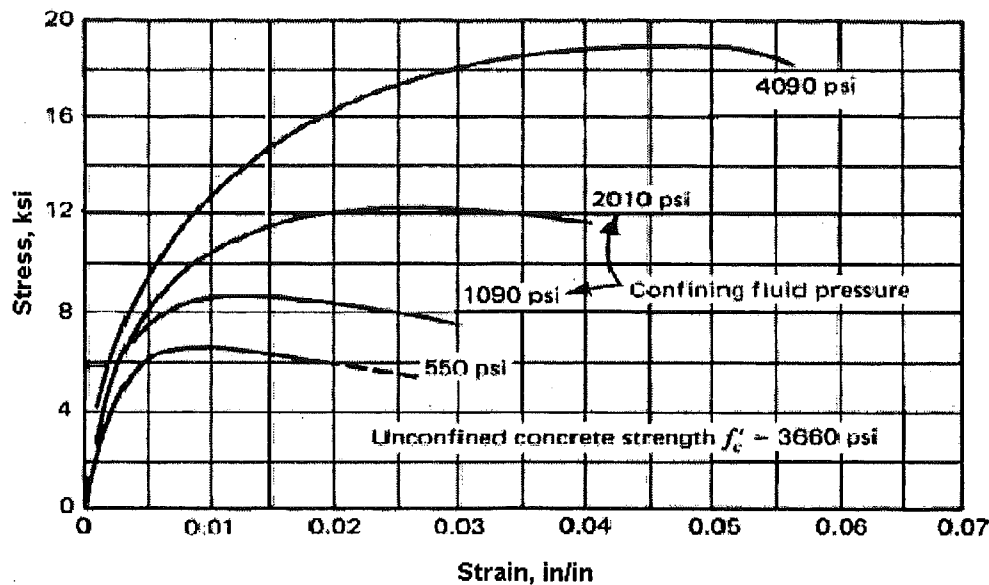


Figure 10-43. Axial Stress-Strain Curves from Triaxial Compression Tests on Concrete Cylinders (Park and Paulay, 1975)

Lateral confinement increases the member strength and provides greater shear capacity. For end stresses within transfer length due to prestressing transfer, if adequate reinforcement is supplied, the shear capacity of the member is improved and the crack width and length is reduced (Sozen, 1965 and Sozen, 1967).

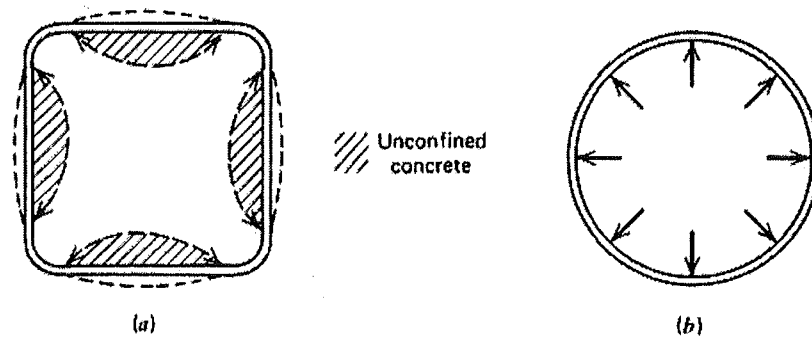


Figure 10-44. Confinement by a) Square Hoops and b) Spiral Hoops (Park and Paulay, 1975)

In the literature and the standards, member-end confinement is recommended as a remedy for bursting cracking. Vertical (lateral) reinforcement recommended for end stresses at transfer by PCI (PCI, 1999) is given in Equation 10-3. Further, the prestressing load effect creates temporary stresses at the time of transfer, and this reinforcement should not be in addition to shear and torsion reinforcement. Although the area needed can be estimated by the equation, the spacing and stirrup geometry is not described.

$$A_{vt} = \frac{0.021 P_0 h}{f_s l_t}$$

Equation 10-3

Where

- A_{vt} = Area of stirrups required at the end of a girder uniformly distributed over a length $h/5$ from the end.
- f_s = Design stress in stirrups
- h = Depth of the member
- l_t = Strand transfer length
- P_i = Initial prestressing force
- P_0 = Prestress force at transfer ($0.9 \cdot P_i$)

Figure 10-45 shows the shear reinforcement used near the end zone of the girder. The shear capacity of Type III girders calculated accordingly is much higher than the maximum shear stress estimated in the discrete girder model. The shear reinforcement recommended by PCI (PCI, 1999) for the PC members under service loading and reinforcement stated in Equation 10-3 by PCI (PCI, 1999) for end zone is calculated. This formulation is not given in AASHTO. It is seen from the design drawings that the shear reinforcement supplied in existing beams is often more than required (see Figure 10-45). However, the shear reinforcements are not closed and they cannot provide the lateral confinement as described earlier. However, these stirrups will increase the shear capacity of the member and perhaps can reduce the crack width and propagation to some extent. The spacing for shear reinforcement specified in the design is 3 inches, which creates significant congestion.

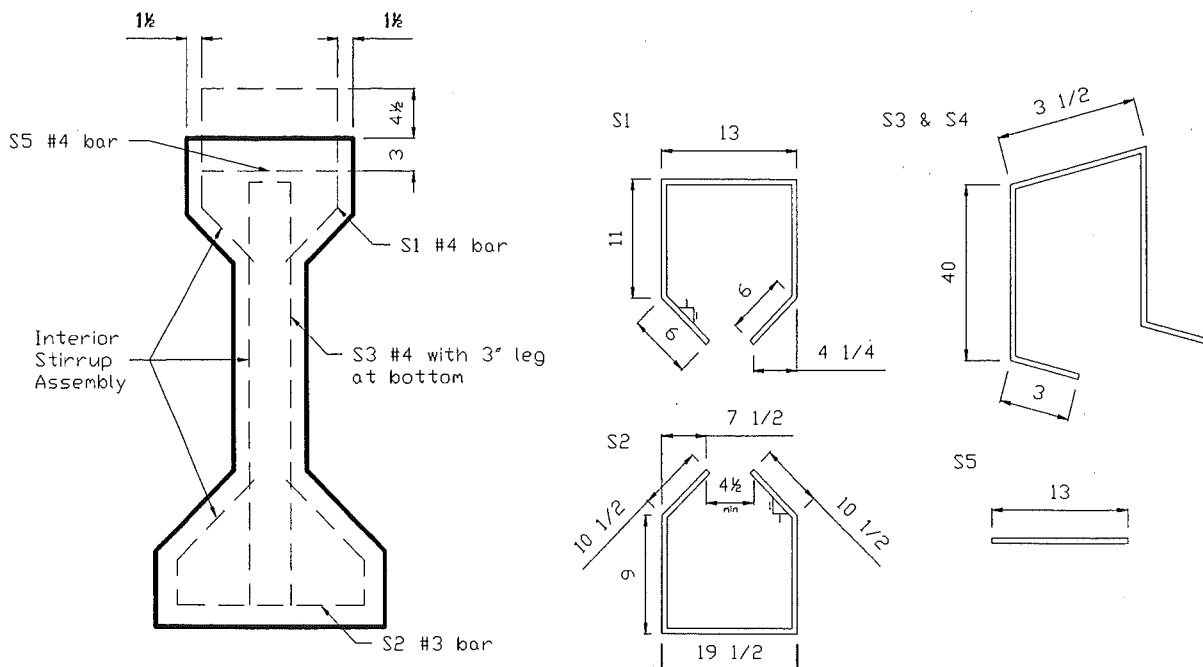


Figure 10-45. Shear Reinforcement used in the Girder Described in the Analytical Model (MDOT PC I-Beam Details)

MDOT Bridge Design Guides (MDOT, 2001) shows that confinement reinforcement is used in newly manufactured girders as seen in Figure 10-46-a, -b, and -c. From these drawings, it is observed that closed hoops are utilized as the shear reinforcement replacing the open hoops used in earlier designs. The purpose for the crack prevention and crack width reduction is noticed from these closed hoop confinement. In the field inspection, it is seen that the girders manufactured according to new shear reinforcement details also show of initial bursting cracking (see Figure 10-46-d). The reason may be concluded that the confinement reinforcement may not be sufficient to eliminate or reduce the width of initial cracks. Earlier studies state that the cracking is due to the transverse stresses in I-girders within the anchorage zone (Sozen, 1965 and Sozen, 1967). Sozen indicates that the reinforcement provided does not prevent cracking. The reinforcement provided becomes effective after the cracking takes place and therefore, confinement reinforcement may only reduce the width and length of cracks. The adequacy of the reinforcement should be studied in detail to assess the confinement effects. The reinforcement analysis is not provided here. The subject may be included as a further research project.

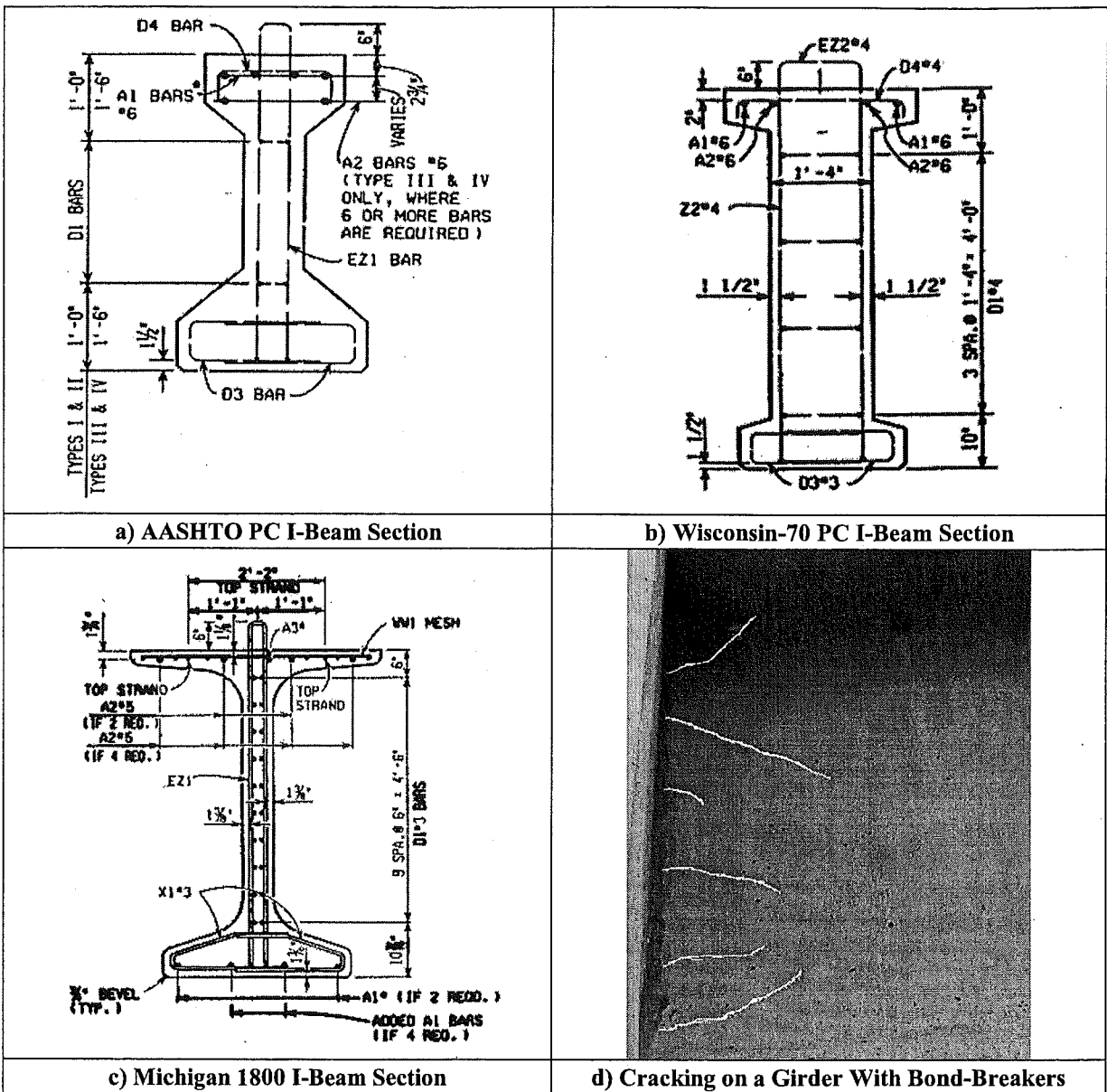


Figure 10-46. Shear Reinforcement used in Newly Manufactured Girders and Web Cracking Observed during Field Inspection on a PC I-Beam with Bond-Breakers

10.6 Modeling and Analysis of a Full Bridge

10.6.1 Overview and the Finite Element Model of a Prestressed Concrete I-Beam Bridge

Concrete diaphragms utilized in the PC I-beam bridges have a typical thickness of 8 inches. The concrete diaphragms have some disadvantages as far as the girder-end inspectability, maintenance performance, and the durability of the girders are concerned. The concrete diaphragms are placed between the girders in such a way that the beam-ends are not visible for the inspectors. The quality of the inspection will be impacted if the beam-ends are difficult to inspect. The beam-ends blocked with concrete diaphragms are also cumbersome to examine for cracking and deterioration.

Another disadvantage of concrete diaphragm is their influence on beam-end maintenance and durability. Concrete diaphragms make the beam-ends inaccessible so that maintenance cannot be performed. Small, inaccessible openings formed by the diaphragms around the beam-end cannot ventilate, hence, moisture accumulates. In some bridges, these also become bird-nesting areas, also affecting durability. Consequently, alternative diaphragm geometries and materials should be explored to replace the standard concrete diaphragms.

The analytical modeling is performed on the bridge with inventory ID S04 of 06111, also described in the discrete girder analysis. The three-span bridge has exterior spans of 31 feet 3 inches in length and a mid-span of 49 feet in length. The bridge deck has a uniform width of 43 feet 2 inches with two lanes. The minimum deck thickness is 8 inches. The drawing in Figure 10-47 shows the general view of the bridge.

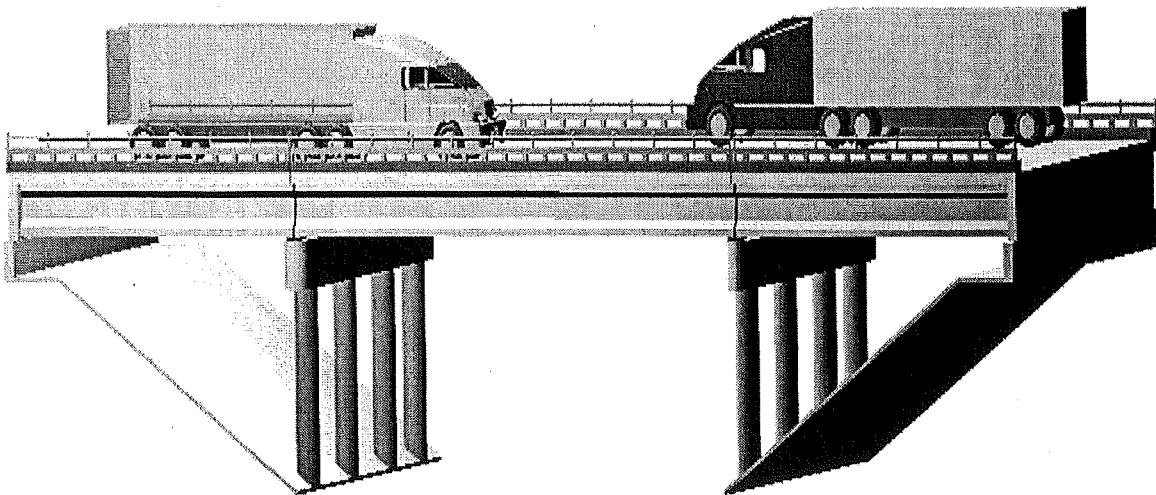


Figure 10-47. Drawing of the PC I-Beam Bridge Modeled

In bridge design, the purpose of diaphragms is to provide the girder with lateral support, and help with live load distribution. The diaphragm types provide different girder constraints due to the differences in cross-sectional geometries and material properties. The diaphragm is modeled with a spring group, each spring representing the shear, bending, and torsional properties. Different diaphragm types seen in the bridge are analyzed independently to calculate their stiffnesses that are incorporated in the model.

The diaphragm types employed between Type-III girders are Type-A on the pier cap as end-diaphragms and Type-G at mid-span as intermediate diaphragms. Between Type-I and Type-III girders, Type-J diaphragms are used. Type-B diaphragms are incorporated between two Type-I girders. All diaphragm types observed on PC I-beam bridges are shown in Appendix-I. Diaphragm and beam arrangement is shown in Figure 10-48. The representation of the girders and diaphragms in the FE model is shown in Figure 10-49. In the figure, the supports are at beam-ends, and the diaphragms are connected to the beams near the beam-end and geometrically aligned with the centerline of the physical diaphragms.

In addition to concrete diaphragms, steel X-bracings are also utilized as diaphragms in the U.S. for reducing the effects of lateral-impact loads from high load hits (HLH). Iowa State University (<http://www.ctre.iastate.edu>) is carrying out a project on steel-bracing diaphragms for the Iowa Department of Transportation in order to reduce the HLH effects. During HLH with the use of concrete diaphragms, the interior beams are also subjected to significant loads in addition to fascia beams. The approach is to protect the interior beams from the impact loads. Additionally, with steel diaphragms, beams and especially with open beam-ends, better ventilation is developed and conditions are less favorable for bird nesting. It is the consensus of concrete durability researches that, if animal intrusions and moisture effects are minimized, durability improves. In this project, steel diaphragms are being compared and their features are being compared to concrete counterparts for structural effectiveness. It is proposed that the intermediate steel bracing will provide the same efficiency as concrete diaphragms. The general appearance of the X-bracing is shown in Figure 10-50.

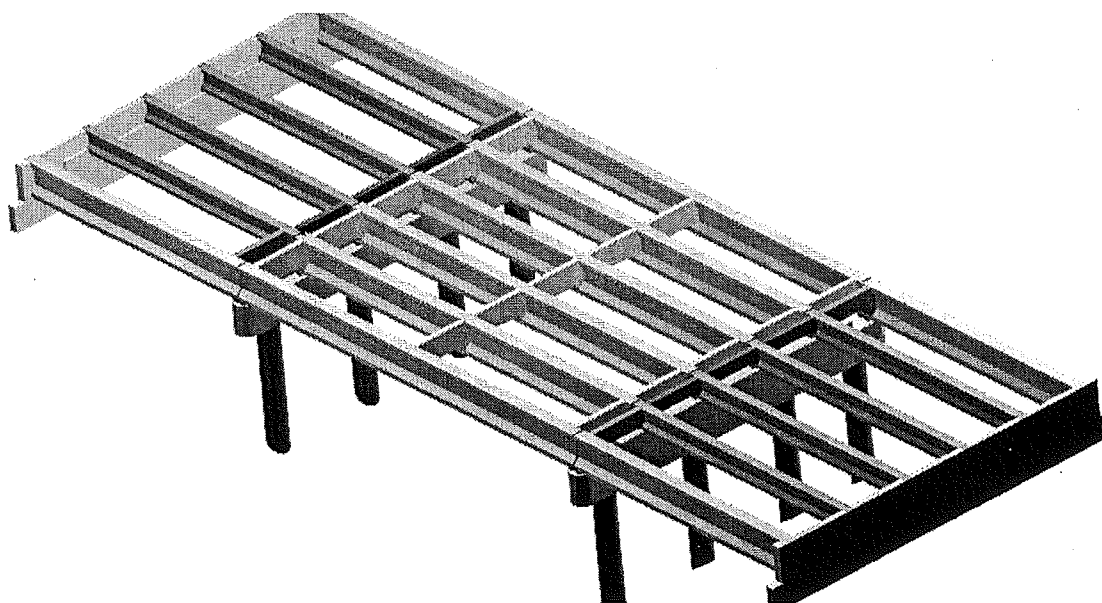


Figure 10-48. General View of the Diaphragm Arrangement in Early PC I-Beam Bridges

The beams are designed as simply supported, and bending moments are assumed to vanish at the supports. However, under service loads due to constraining effects of the diaphragms, bending stresses may generate near the beam-ends. The effect of diaphragm restraint to the beam under bending and torsion is investigated using the FE model.

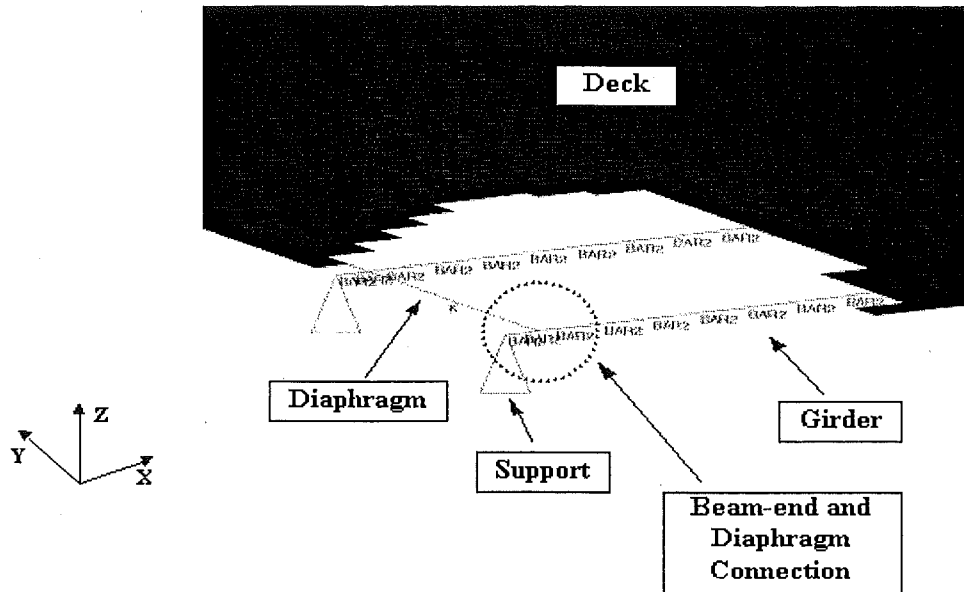


Figure 10-49. Diaphragms, Deck, and Beams in the Model

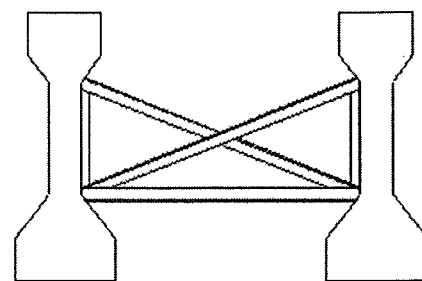


Figure 10-50. Steel Diaphragms between the Beams and the Cross-Section

The behavior of the bridge under temperature effects is also studied to evaluate the impact of non-functional elastomeric bearings. The bearings are assumed as roller supports in design, allowing the beam to bend and move in the axial direction (Yazdani et al, 2000). Deteriorated bearings restrain the beam in the axial direction, creating additional stresses near the beam-end. This restrains the elongation or shortening under temperature effects. Using the FE model, the

behavior of the bridge is investigated with pinned supports in order to simulate the deteriorated bearing condition under differential thermal loads.

The primary assumptions utilized in developing the FE analyses model are:

1. Ideal composite action between diaphragms, deck, and beams is assumed.
2. Secondary stresses due to deformation are ignored.
3. The members are described in their original condition.
4. The analyses are performed in the elastic region, and the material behavior is defined as elastic.

The bridge is modeled in three-dimensional domain using line elements; therefore, the cross-sections of structural members are simplified accordingly. The diaphragms are incorporated as springs, the beams as two dimensional bar elements, and the deck as thin shell. The bridge is modeled with the diaphragm restraining the beam in three directions: shear, bending, and torsion. For shear action axial (K_V), for bending (K_M) and torsion (K_T) rotational springs are employed (see Figure 10-51). The supports and bearings are placed at beam-ends as rollers in longitudinal and transverse directions, but restrained in the vertical direction.

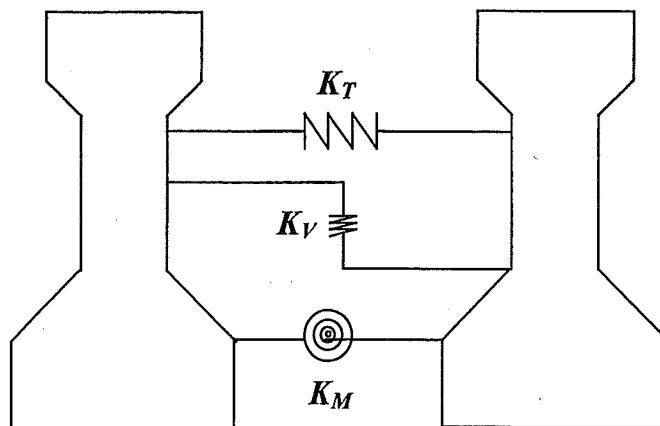


Figure 10-51. The Spring Representation of the Diaphragms

The diaphragm and the deck are sometimes monolithic, and in composite action. In this case, the spring stiffnesses for the diaphragms include the deck. The recommended effective width values are 48 inches by AASHTO and 64 inches by ACI. However, the length of deck on one side of the diaphragm is 10 inches. In that case, it is not possible to consider the diaphragms with the recommended effective width values. The cross-section of the diaphragm is estimated by adding an effective deck width of 10 inches on each side of the diaphragm. The spring stiffnesses representing the various diaphragm configurations are shown in Table 10-2.

The steel bracing can only develop shear stiffness. The shear stiffnesses of bracing with different geometries are given in Table 10-3. The main parameters considered in the stiffness calculations are the cross-section area (A), the modulus of elasticity of the bracing member, the girder spacing (S), and the angle of member inclination with the horizontal axis.

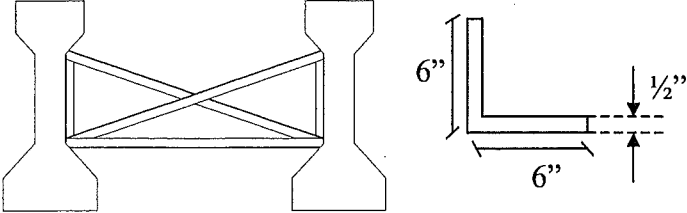
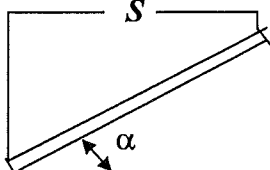
10.6.2 Finite Element Analyses Results of a Prestressed Concrete I-Beam Bridge

10.6.2.1 *The Finite Element Analyses of the Bridge under Dead Loads*

To document the influence of the diaphragms, the bridge is analyzed with and without the diaphragms. The first analysis is performed under dead load including the deck, the barriers, and the beams. In Figure 10-52 and Figure 10-53, bending moments on the interior beams and exterior beams are compared with and without diaphragms. The differences in bending moments are not significant. Effectively, the diaphragms increase the bending moment of the interior beams while reducing the bending moment of the exterior beams. Diaphragm effects are more pronounced when shear diagrams of the interior and the exterior girders are compared in Figure 10-54 and Figure 10-55. Additionally, torsion diagrams of interior and exterior girders are shown in Figure 10-56 and Figure 10-57.

In conclusion, the diaphragms' structural role in the bridge is to provide load distribution between the girders. The diaphragms increase bending moment, shear force, and torsional moment on the exterior girders while decreasing the load effects on the interior girder, thus equalizing the contribution of interior and exterior girders. The increase in shear forces reaching around 2 kips is significant in terms of increasing the cracking potential near the end of the exterior girder with diaphragms as shown in Figure 10-54 and Figure 10-55.

Table 10-3. Spring Stiffnesses to Represent Steel Diaphragms

Spring Stiffness for the Steel Diaphragms	Shear Stiffness (kips/in)
	$(K_V = 2A \cdot E / S \cdot \cos^2 \alpha)$ 
Between two Type III	3,680
Between Type III and Type I	3,630
Between two Type I	3,880

Bending Moments on Interior Beam With and Without Diaphragms

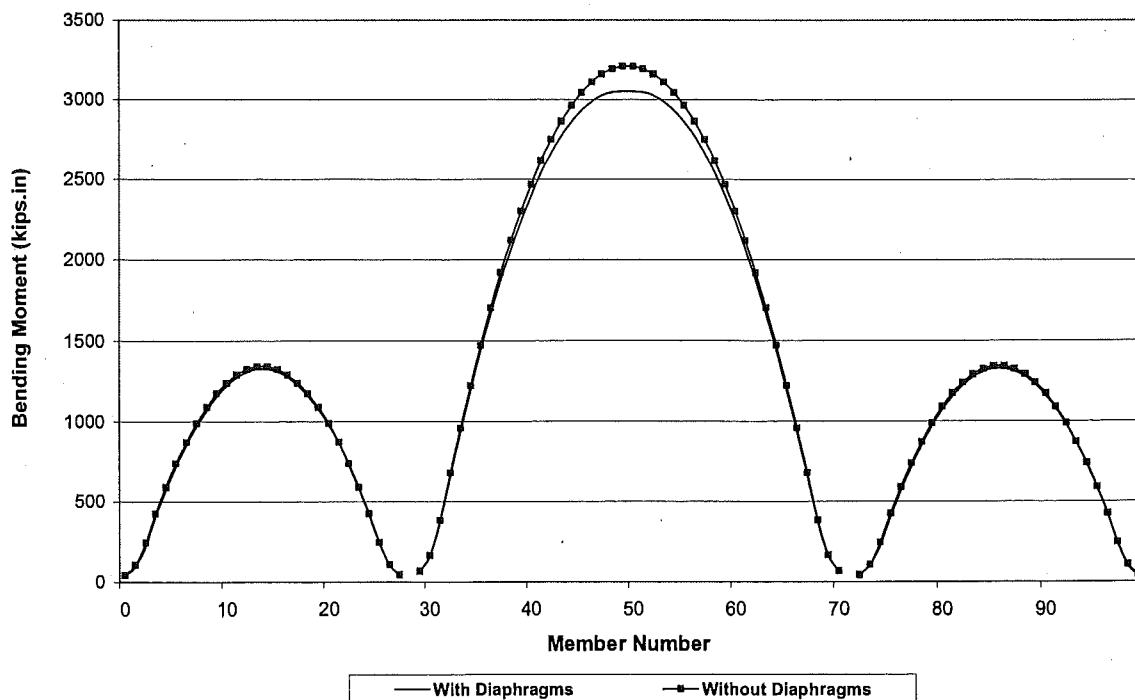


Figure 10-52. Bending Moment Diagram on the Interior Beams with and without Diaphragms

Bending Moments on Exterior Beam With and Without Diaphragms

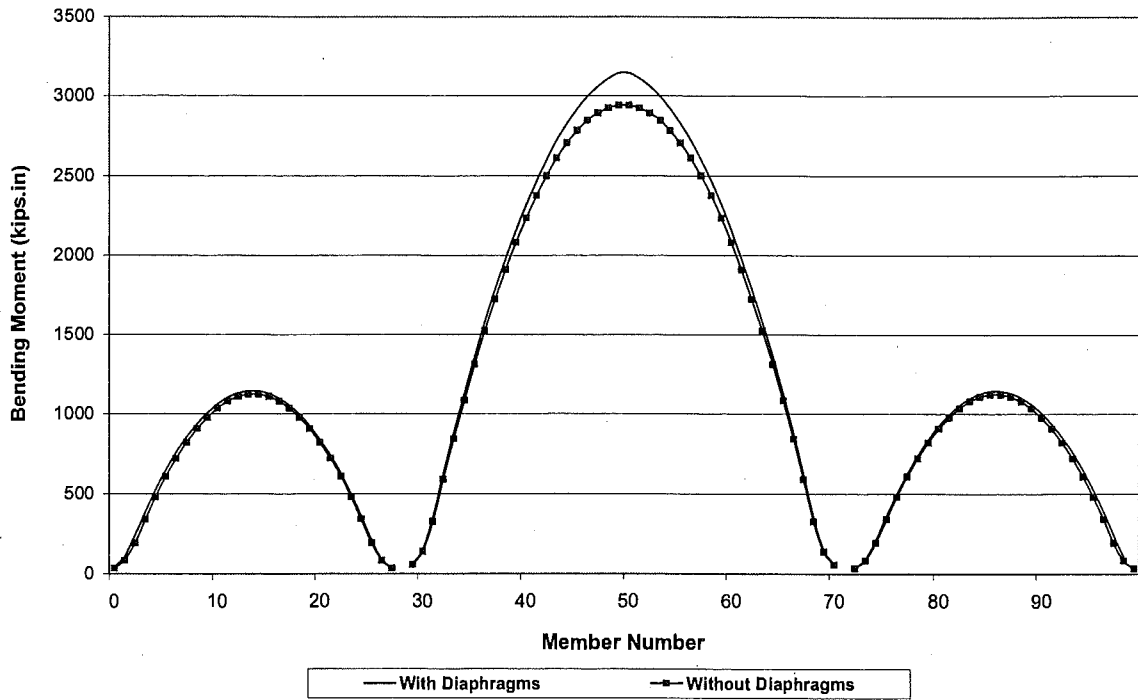


Figure 10-53. Bending Moment Diagram of the Exterior Beams with and without Diaphragms

Shear Force on Interior Beam With and Without Diaphragms

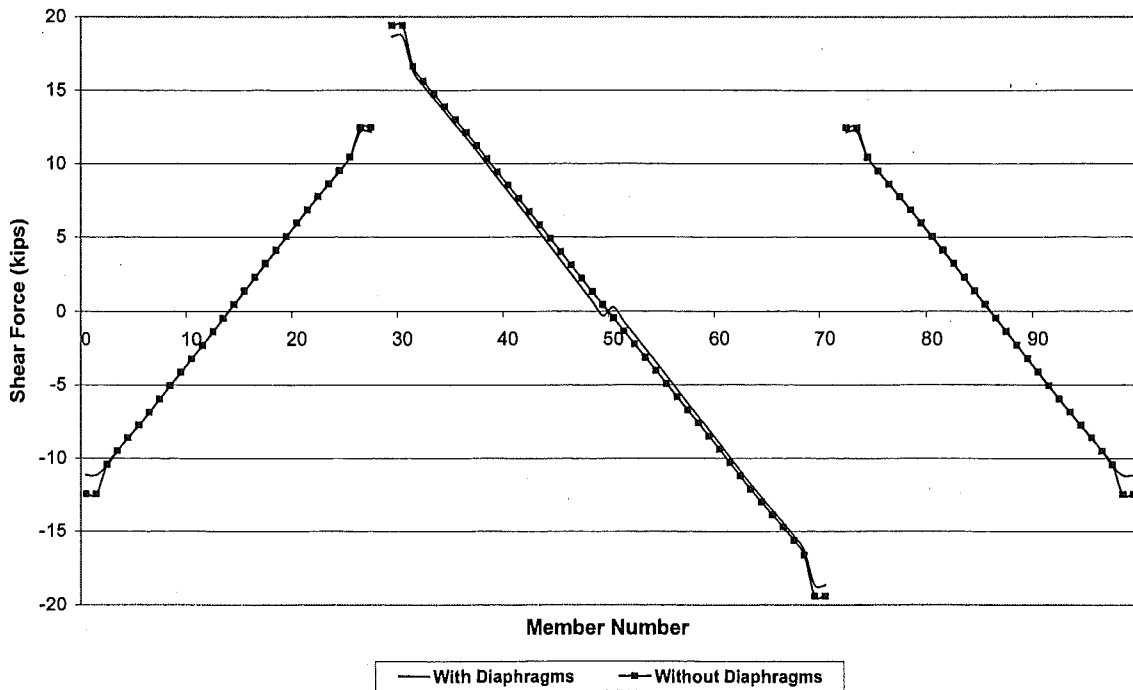


Figure 10-54. Shear Force Diagram of the Interior Beams with and without Diaphragms

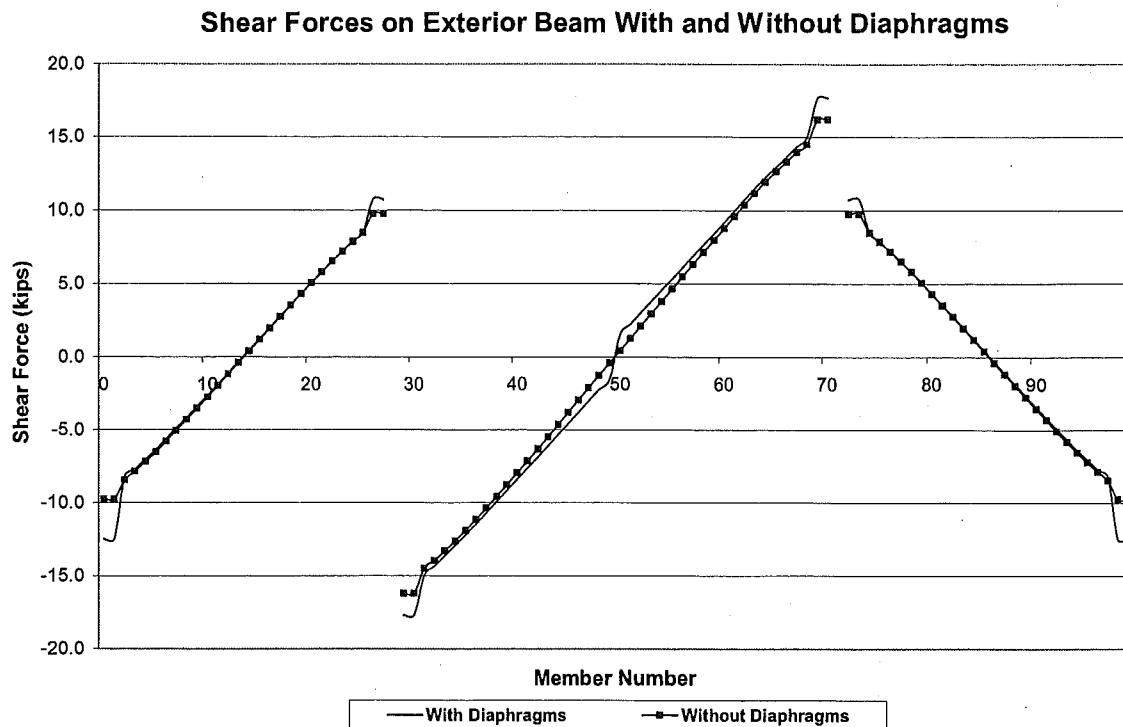


Figure 10-55. Shear Force Diagram of the Exterior Beams with and without Diaphragms

Torsion diagrams shown in Figure 10-56 of the interior girder and in Figure 10-57 of the exterior girder also demonstrate the diaphragm impact on the girders. The torsion observed on the interior girder is lower than on the exterior girder. The load is distributed symmetrically around the interior beam; consequently, torsion magnitudes are lower than those on the exterior beam. The shapes of the torsion diagrams are significantly different on girders with and without diaphragms. However, the magnitude of this difference is not significant.

Torsion on Interior Beam With and Without Diaphragms

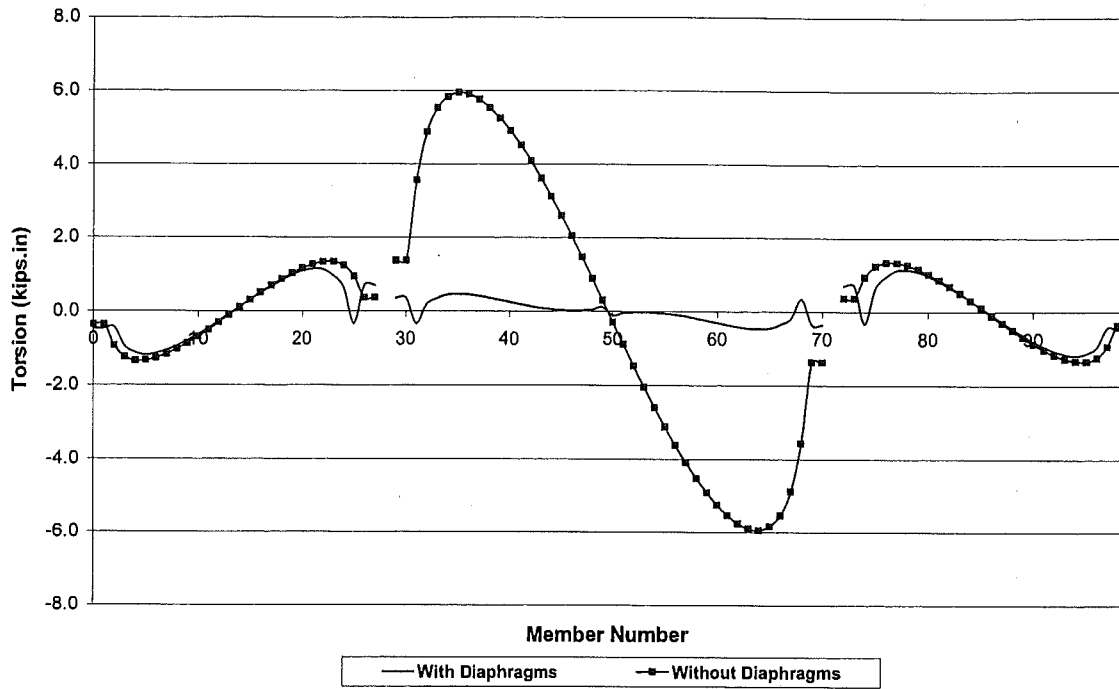


Figure 10-56. Torsion Diagram of the Interior Beams with and without Diaphragms

Torsion in Exterior Beam With and Without Diaphragms

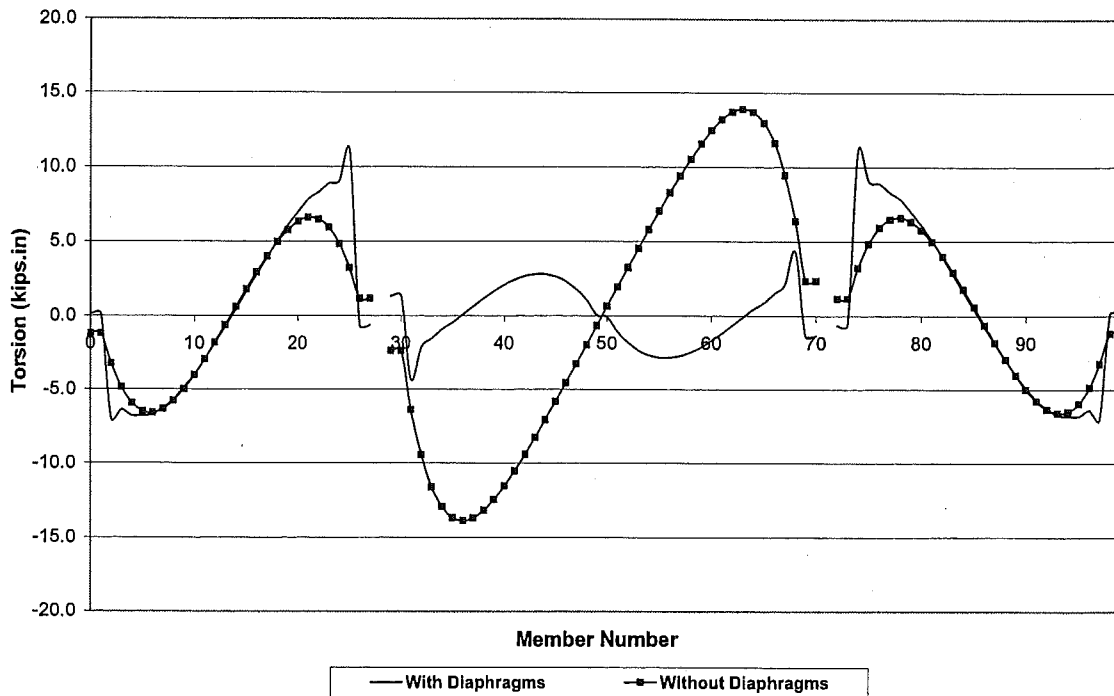


Figure 10-57. Torsion Diagram of the Exterior Beams with and without Diaphragms

10.6.2.2 The Finite Element Analyses of the Bridge under Dead and Live Loads

To evaluate the impact of the diaphragms on the exterior and the interior beams under live load, the bridge is analyzed with truck load in addition to dead load. The primary purpose is to evaluate the diaphragm effect on the girder load distribution. Later this analysis is compared to the girder load distribution when steel bracings are utilized instead of the concrete diaphragms. As live load, two trucks are placed on the bridge for maximum moment at the mid-span. The axle spacing used in bridge design is 14 feet according to AASHTO. However, in order not to change the mesh geometry of the deck and the girders, the axle spacing is altered to 13 feet 7 inches and 14 feet 4 inches to fit to the existing finite element mesh. The general orientation of the trucks on the FE model is shown in Figure 10-58 through Figure 10-60. Both trucks are located within a width of two lanes. The lateral spacing between the trucks is taken as 4 feet, as shown in Figure 10-59.

The analyses results are shown in Figure 10-61 through Figure 10-69. In these figures, the origin designated as "Member Number" axes is the beam-end on the abutment. The last point on the "Member Number" axes is the beam-end at the pier.

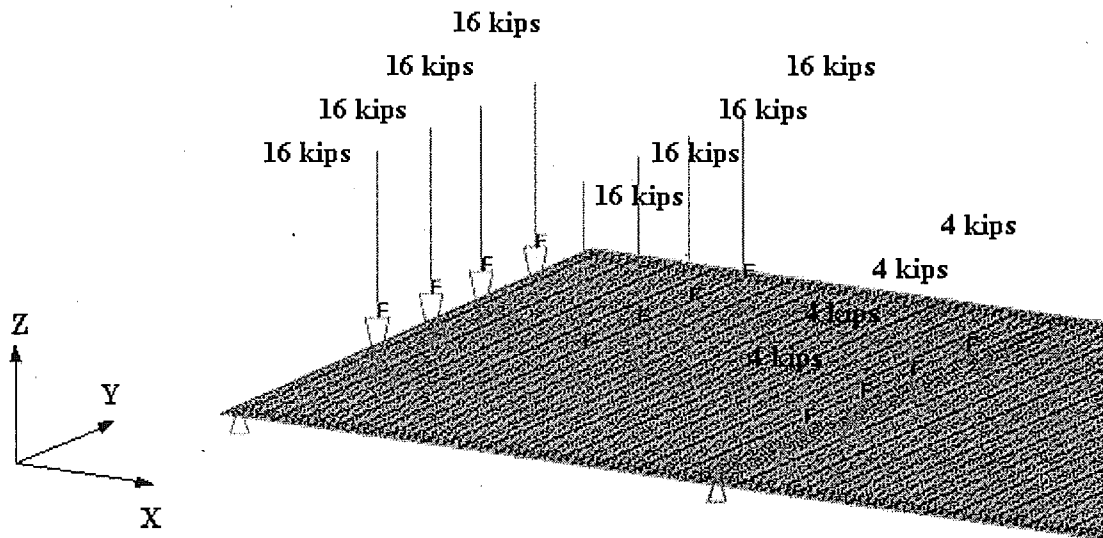


Figure 10-58. General View of Truck Load Distribution

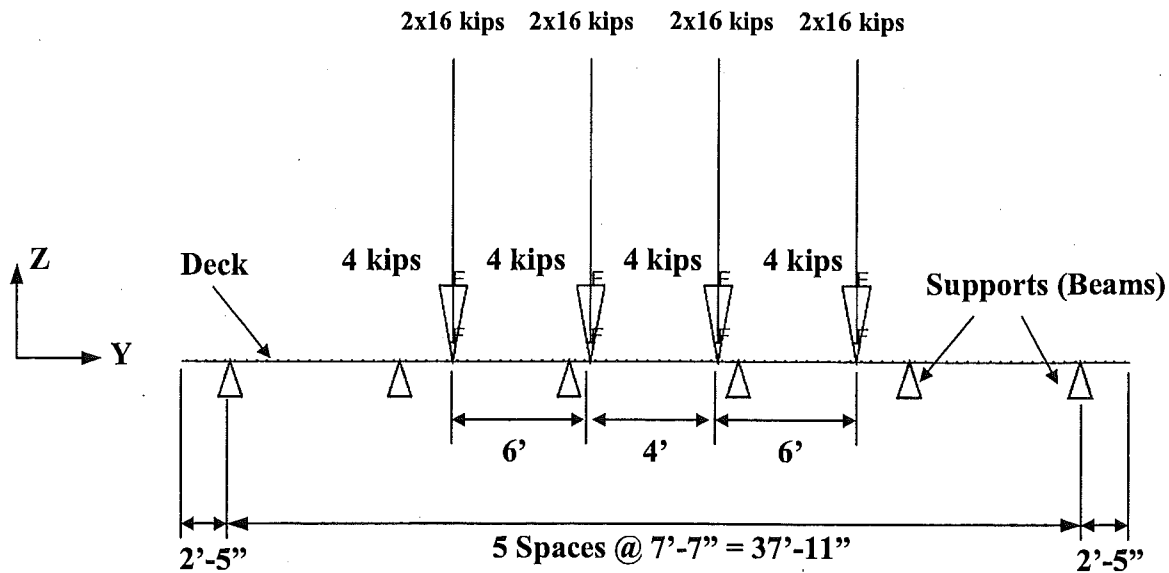


Figure 10-59. Transversal View of the Truck Load Distribution

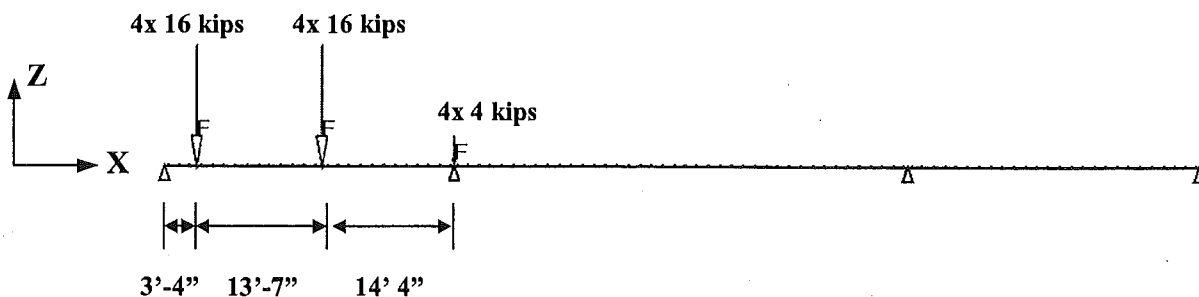


Figure 10-60. Longitudinal View of the Truck Load Distribution

The shear force diagram on one exterior and one interior beam on one of the exterior spans is shown in Figure 10-61. Shear force distribution on girders is affected by the truck axle locations. However, a dramatic difference is seen when the shear distributions on interior and exterior girders are compared. On both interior and exterior beams, the diaphragm effects on shear force are seen near the beam-ends. As seen in Figure 10-61, the diaphragms redistribute the shear force near the beam-ends by distributing the load. Consequently, the diaphragms increase the shear force on exterior girders, especially around 20 kips near the abutment where a Type A diaphragm is located. Another essential outcome of the analysis is the structural behavior difference observed at two ends of the girders due to differences in diaphragms with different shear stiffnesses. The diaphragms at the abutment are stiffer than the ones near the piers. Consequently, the diaphragm effect on the beam-end stresses is proportional to the diaphragm shear stiffness.

The bending moment diagrams for exterior and interior girders are shown in Figure 10-62. The diaphragm effect on moment transfer is negligible near the beam-ends.

The diaphragms influence the torsional moments near the beam-ends. The torsion diagrams for interior and exterior girders are shown in Figure 10-63. Increasing bending stiffness of the diaphragm reduces the torsional stresses near beam-ends. This is seen in Figure 10-63 when

torsion on interior and exterior girders is compared at both beam-ends. The torsion on girders is equal at the abutment end and diverges at the pier end. The load is distributed symmetrically around the interior beam; consequently, torsion magnitudes are lower than those on the exterior beam, as shown in Figure 10-63.

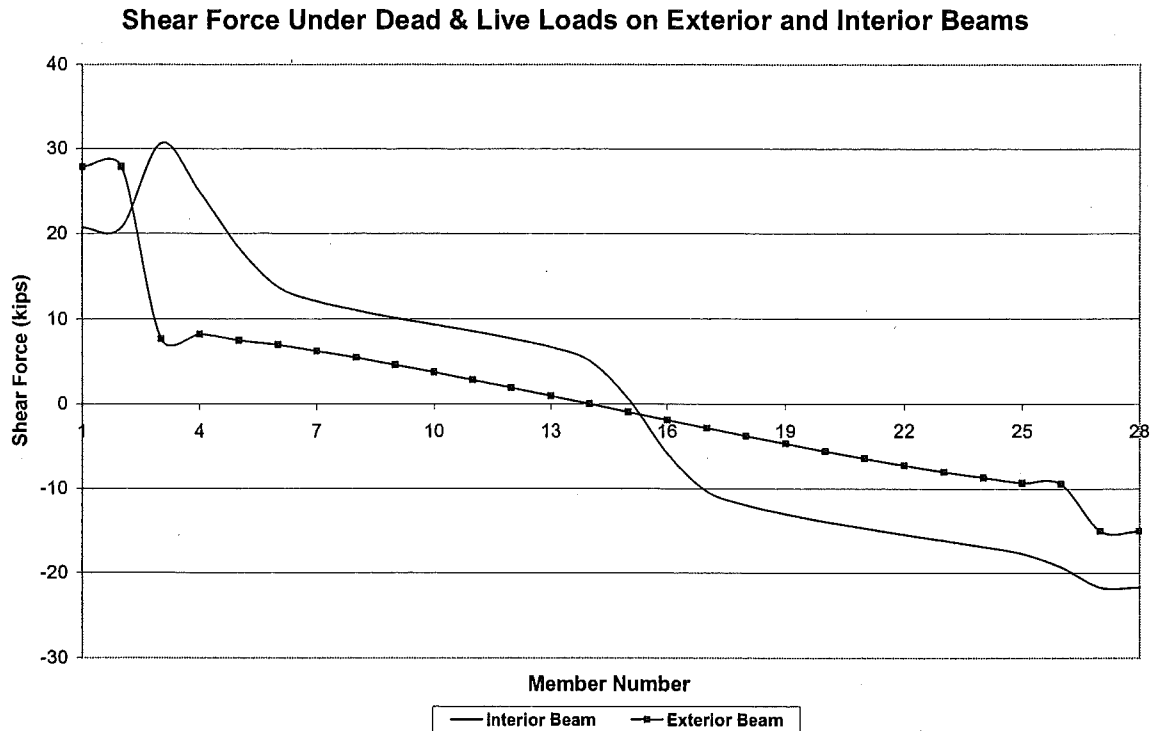


Figure 10-61. Starting from Abutment, Shear Force under Dead and Live Loads on Exterior and Interior Beams

The load distribution factor for the live load according to AASHTO is compared to the live load analysis. Distribution factor by AASHTO is calculated from the formula $DF = S/5.5$ for a PC I-beam bridge, where DF is the distribution factor, S is the girder spacing in feet, and 5.5 is a constant. Center to center girder spacing is 91 inches (7 feet 7 inches) giving a distribution factor of 1.38. From the shear diagram in Figure 10-61 for the interior beam, the distribution factor is calculated as approximately 0.50 for the beam-end at the abutment, and approximately 0.85 for the beam-end at the pier. These distribution factors correspond to a distribution factor of $S/15.2$ at the abutment end and $S/9.1$ at the pier end. The diaphragm stiffnesses at each beam-end are different; thus, corresponding distribution factors also differ. The distribution factor formulations for the interior girder is not comparable to the factors used in design. However, it demonstrates the diaphragm stiffness influence on the load distribution to the girders. In addition, a constant distribution factor is not realistic for obtaining the girder moments and shears.

Bending Moment Under Dead & Live Loads on Exterior and Interior Beams

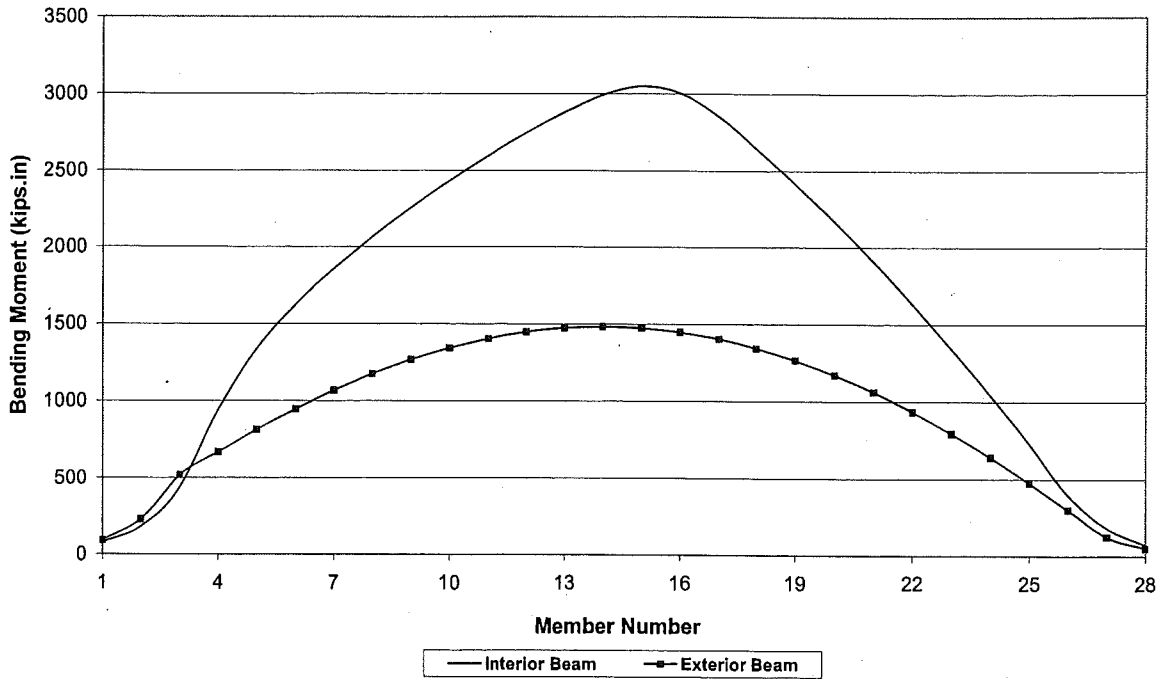


Figure 10-62. Starting from Abutment, Bending Moment under Dead and Live Loads on Exterior and Interior Beams

Torsion Under Dead & Live Loads on Exterior and Interior Beams

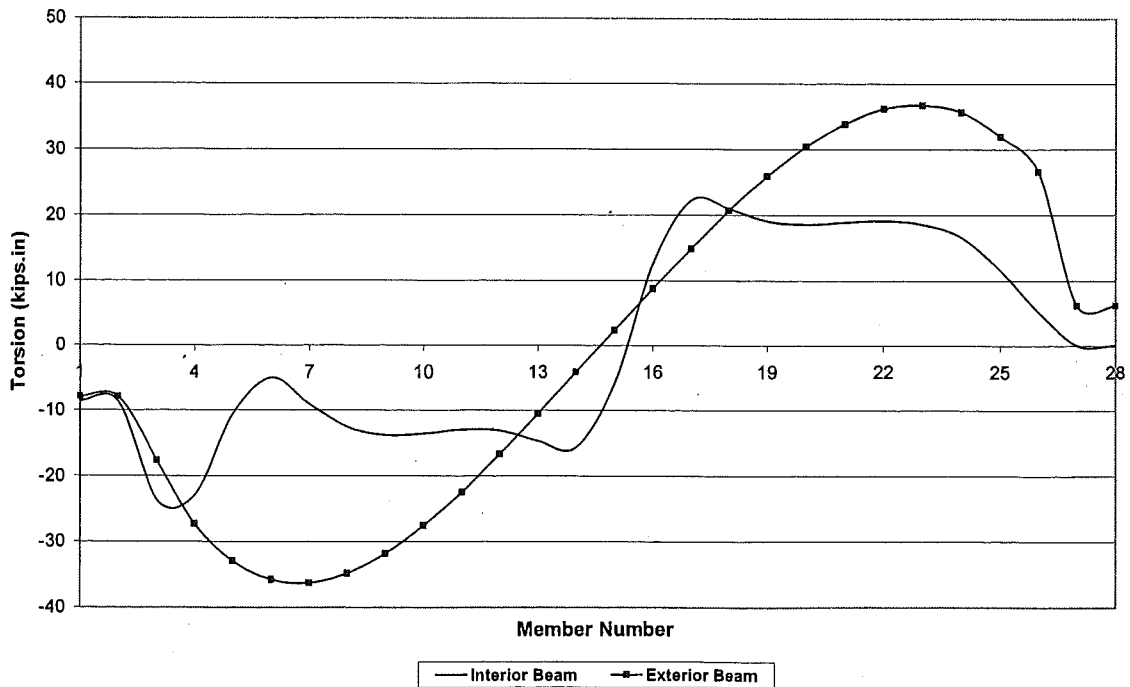


Figure 10-63. Starting from Abutment, Torsion under Dead and Live Loads on Interior and Exterior Beams

Bending Moment on Exterior Beam Under Dead & Live Loads with Concrete & Steel Diaphragms

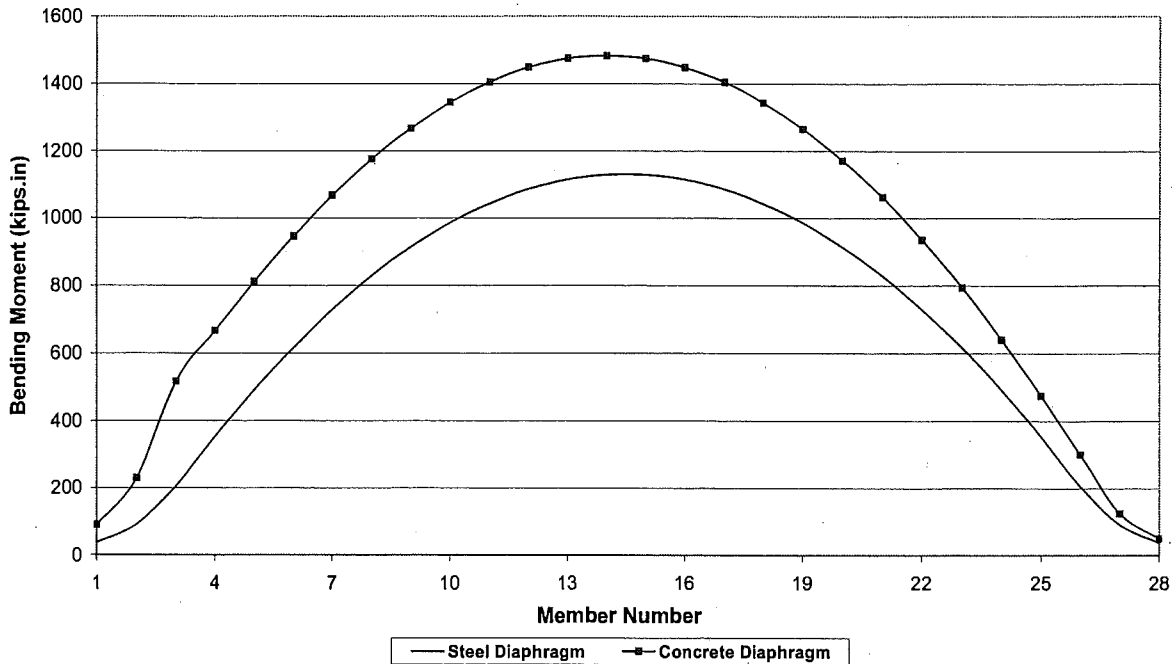


Figure 10-64. Starting from Abutment, Bending Moment on Exterior Beam under Dead and Live Loads with Concrete and Steel Diaphragms

10.6.2.3 *The Finite Element Analyses of the Bridge with Steel Bracings*

In order to evaluate the steel bracing as diaphragms, the bridge is further analyzed under dead and live loads after modifying the diaphragm stiffnesses. Bending and torsional stiffnesses of the steel bracings are zero, while its shear stiffness is higher than the concrete diaphragms (see Table 10-3). The bending moment diagrams for exterior and interior girders are shown in Figure 10-64 and Figure 10-65, respectively. These figures compare the influences of steel and concrete diaphragms on the girders. The material and the geometry influence on the bending moment magnitudes are negligible near the beam-ends. In other words, steel bracings do not change the bending moments at the beam-ends.

Bending Moment on Interior Beam Under Dead & Live Loads with Concrete & Steel Diaphragms

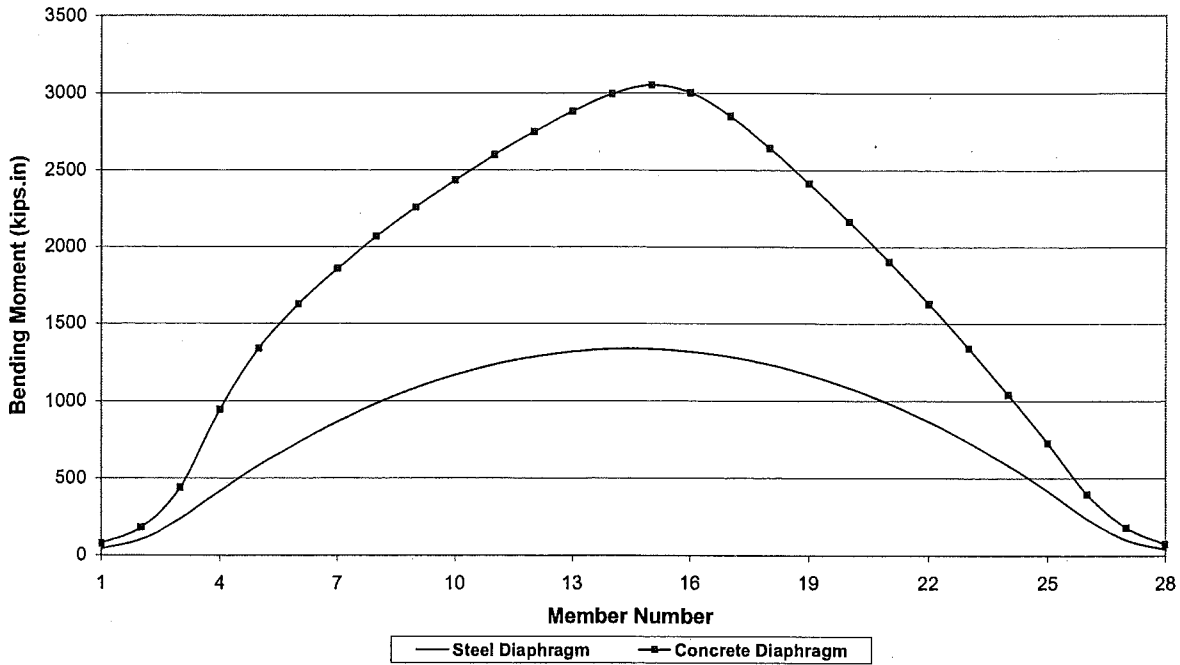


Figure 10-65. Starting from Abutment, Bending Moment on Interior Beam under Dead and Live Loads with Concrete and Steel Diaphragms

The torsion diagrams on exterior and interior girders are shown in Figure 10-66 and Figure 10-67, respectively. The figures show that the torsion on the girders with steel bracings is remarkably less than on the girders with concrete diaphragms. The magnitudes of torsion on both girders are not high; around 10 kips-in near the beam-end and 38 kips-in within the span on the girder with concrete diaphragms. The torsion on the girder vanishes when steel bracings are utilized as diaphragms. As observed in analyses results presented earlier, the diaphragm stiffness controls the load distribution near the beam-ends.

Torsion on Exterior Beam Under Dead & Live Loads with Concrete & Steel Diaphragms

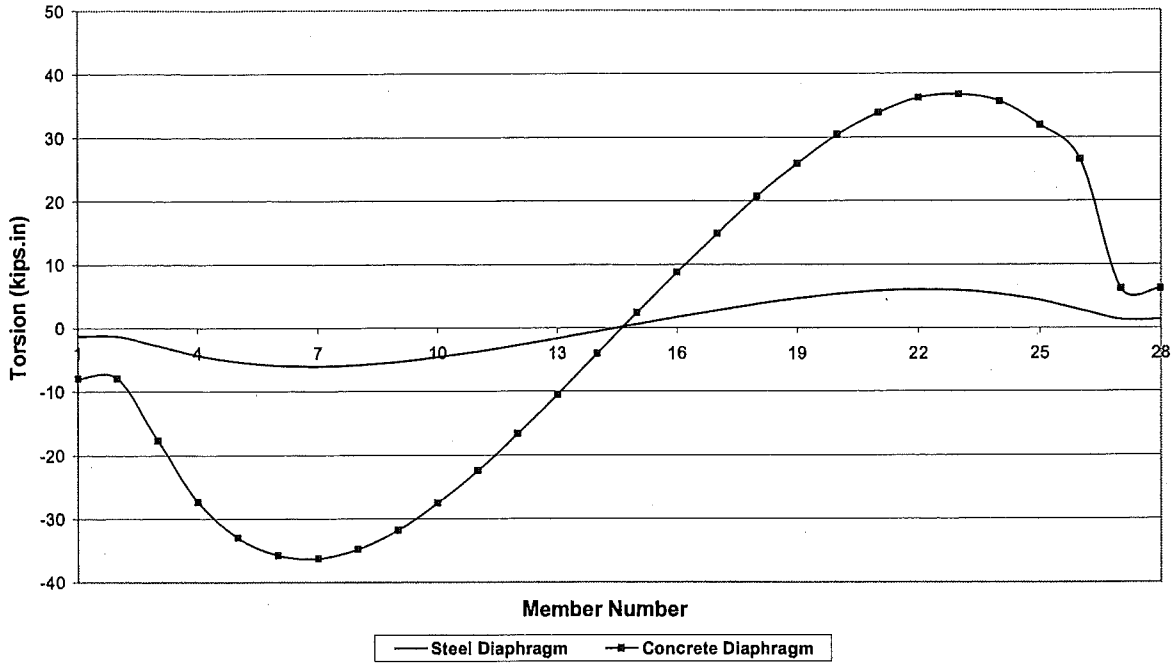


Figure 10-66. Starting from Abutment, Torsion on Exterior Beam under Dead and Live Loads with Concrete and Steel Diaphragms

Torsion on Interior Beam Under Dead & Live Loads with Concrete & Steel Diaphragms

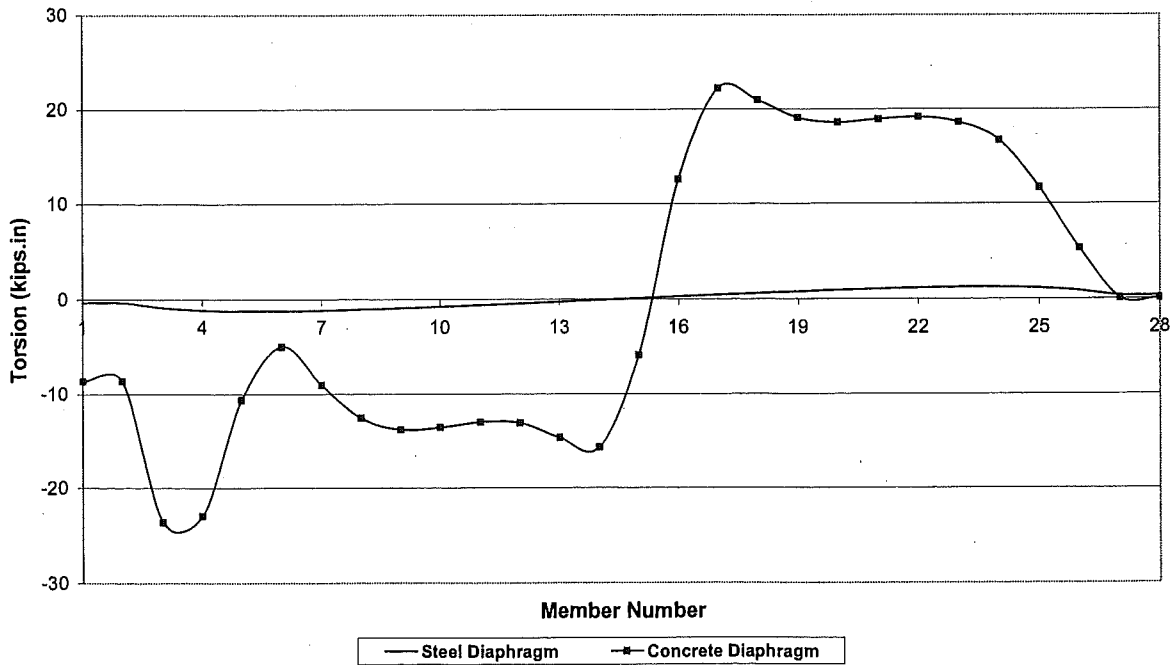


Figure 10-67. Starting from Abutment, Torsion on Interior Beam under Dead and Live Loads with Concrete and Steel Diaphragms

The shear force diagrams shown in Figure 10-68 on the exterior girder and in Figure 10-69 on the interior girder are used for comparing the steel bracings with concrete diaphragms. As seen in the figures, the beams have equal shears at the abutment and pier ends when steel diaphragms are used. The differential restraining effects of the diaphragms at the abutment and pier ends influence the internal force distribution when concrete diaphragms are used.

Use of steel diaphragms provides a uniform shear distribution among the girders as shown in Figure 10-68 and Figure 10-69. It should also be noted that lower values of shear force are calculated at the beam-ends when laterally supported with steel diaphragms. This will also positively impact by reducing the beam-end cracking potential.

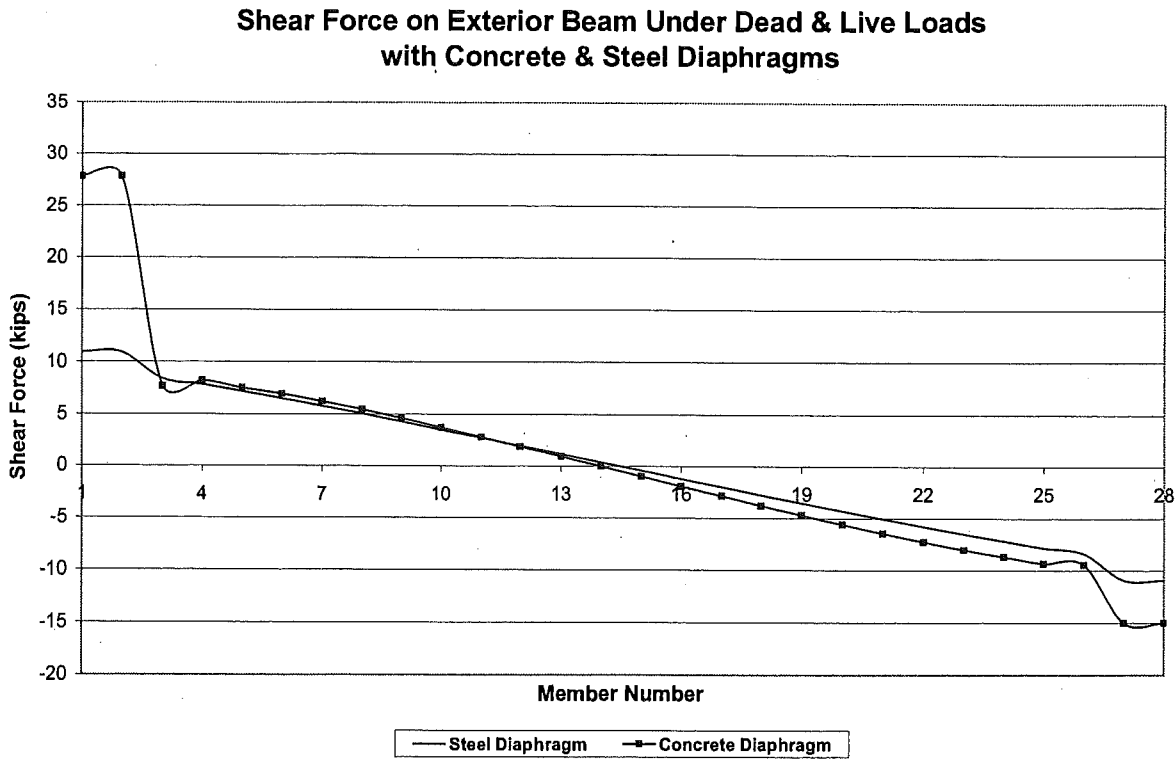


Figure 10-68. Starting from Abutment, Shear Force on Exterior Beam under Dead and Live Loads with Concrete and Steel Diaphragms

Shear Force on Interior Beam Under Dead & Live Loads with Concrete & Steel Diaphragms

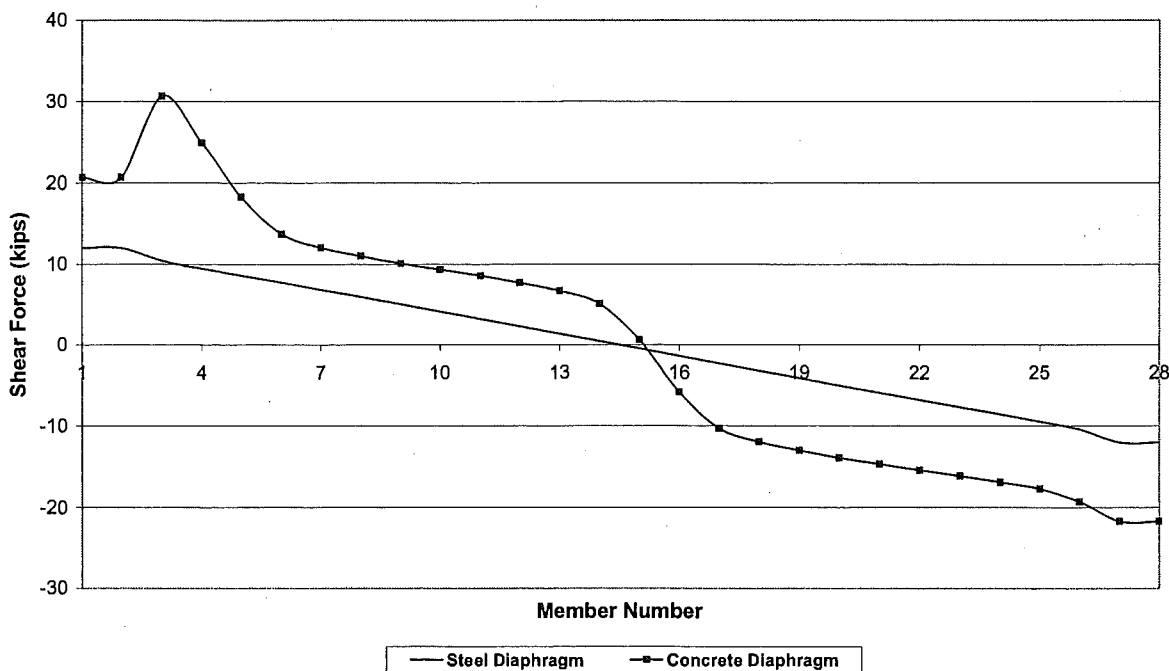


Figure 10-69. Starting from Abutment, Shear Force on Interior Beam under Dead and Live Loads with Concrete and Steel Diaphragms

The bridge model with concrete diaphragms is also analyzed under differential temperature effects. The hypothesis was that the differential temperature between the deck and the girder along on fascia beam would generate measurable stresses on the girders within the proximity of the diaphragms. These thermal stresses would be generated, because the diaphragms constraint the deformation of the girders. In the bridge model, non-functional bearings are also incorporated assuming that this will amplify the thermal effects. However, upon the analyses the stresses due to thermal effects are calculated to be insignificant. For this reason, the analysis results are not included here.

10.7 Summary

The finite element analyses are performed to evaluate the stresses near the beam-end, and to understand the structural behavior of a PC I-beam bridge. The analyses are performed for discrete I-beam analyses and complete bridge analyses under various load conditions.

A PC I-beam is modeled, and the distress in the transfer length region is investigated. The stresses near the beam-end and its impact on the cracking pattern are studied. Three types of I-beams with different tendon geometries are examined and compared (beams with straight tendons, with bond-breakers, and with draped tendons). The I-beams with straight tendons are also analyzed under varying bond quality between the tendon and concrete for the purposes of

evaluating the effects on stresses generating near the beam-end. The beams are representative of those used in existing bridges in Michigan.

The shear stresses observed in the prestressing load transfer region and this stress formation are compared for the three tendon configurations. Significance of high stress concentration near the beam-end is also evaluated. Overall, the analysis shows that the beams with draped tendons are more vulnerable to cracking due to end-block use and the tendon angle. The beams with bond-breakers are the least vulnerable to end cracking. The impact of the bond quality of concrete on the load transfer length and the stress pattern near the beam-end showed that good quality bond reduces the transfer length, and with poor bond quality, the elastic loss and shear stresses are increased.

The beam with straight tendons is further analyzed under service loads, to estimate the bearing effect and the load path near the beam-end. Significantly high stresses are calculated near the supports when the elastomeric bearing pads are non-functional.

A PC I-beam bridge is modeled and analyzed to evaluate the impact of the diaphragm and the deck on the beam-end stresses. The load distribution among the girders is also studied when the bridge is under combined dead and live loads. The analyses showed that the restraining effect of the diaphragms on the beam-ends is significant, which increased the shear and torsional stresses. The increase in stress is directly proportional to the stiffness of the employed diaphragms, which also can be different at each end of the beam. The steel bracing use as a lateral support is compared to the concrete diaphragms. The shear restraining effect of the steel bracing is more significant, but a more uniform shear force distribution among girders is obtained.

Finally, differential thermal effects are analyzed combined with the non-functional elastomeric bearing pads, and the effects on the beam-end stresses are found to be insignificant.

The analyses results are summarized first for the single girder analysis. The PC I-beam and load transfer induced stresses at PC I-beam ends are presented. The analytical modeling included three girder types and three bond qualities. The stresses were calculated for the load effects during manufacturing and under service loads. The shear and axial stresses near the beam-ends are presented in Table 10-4 and Table 10-5. The results in the tables clearly demonstrate that beam-end cracking is to be expected.

Full bridge is modeled and analyzed under dead load, live load, and thermal effects. Composite action between bridge members and the impact of diaphragm rigidity on beam-end forces are investigated.

The forces near the beam-ends from the full bridge analysis are shown in Table 10-6. The table is organized according to loads, diaphragm types, and force locations. The results are grouped under locations along the beam defined as outside the diaphragm (OD) and inside the diaphragm (ID) to show the diaphragm influence on the beam-end forces. The analyses results are presented only for the first span and the middle span. The beam-end forces are also shown in Table 10-6 for the exterior (fascia) and the interior girder.

Table 10-4. Stresses in Girders under Prestressing Load Only

Girder Type Tendons		Maximum Shear Stress (ksi)	Axial Stress (ksi)	
			Compression	Tension
Straight (Uniform) Tendon		0.8	3.0	0.4
Draped Tendon		1.5	3.2	$>f_{ct}$
Bond-breakers	With Bond-breakers	3.0	5.4	$>f_{ct}$ (424 psi)
	Without Bond-breakers	4.0	$\gg f_c'$ (5,000 psi)	$>f_{ct}$ (424 psi)

Table 10-5. Bearing Analysis on the Beam with Uniform Tendons

Loading Case	Maximum Shear Stress (ksi)	Axial Stress (ksi)	
		Compression	Tension
Under Prestressing Load	0.8	3.0	0.4
Under Dead Load	2.0	$\gg f_c'$ (5,000 psi)	$>f_{ct}$ (424 psi)
Under Live Load	3.4	5.2	$>f_{ct}$ (424 psi)

The major conclusions derived from the analytical study are as follows:

1. High shear stress intensity is calculated near the beam-ends upon tendon release.
2. High tensile stresses are formed at the web near the beam-end upon tendon release.
3. High shear and tensile stresses will initiate cracks on the web and near the web transition to the bottom flange upon tendon release.
4. The shear reinforcement provided in the girders will not prevent end bursting and shear cracking. Shear confinement only controls the width and progression of the cracks. For the durability beam-ends should be protected by external means such as coating and sealants.
5. End blocks and draping employed in draped beams increase the cracking vulnerability near the beam-ends by amplifying the shear stresses.
6. Bond-breakers decrease the shear stresses within transfer length induced by prestressing load transfer. Thus, they reduce shear stress intensity and cracking potential.
7. The bearing condition directly affects the load path and stress pattern near the beam-ends with non-functional bearings; the support area reduction by rocking of the bearing plate generates high stresses near the support.
8. Replacement of non-functional bearings should be included in the preventive maintenance program.
9. In full bridge analysis for girder design, the boundary conditions must include the restraining effect of the diaphragms on the beam-ends.
10. The steel bracing will be an effective replacement for concrete diaphragms.

11.0 Performance Evaluation of Partial Depth Repair Materials (Task 11)

11.1 Introduction

Corrosion induced deterioration has been identified through field investigations as the major cause of beam end distress for I-beams in Michigan bridges. The resulting forms of distress include concrete spalling, delamination, cracking, and corrosion of reinforcement. The loss of concrete permits accelerated deterioration of reinforcing and prestressing steels, allows detensioning of prestressing steel, and increases the stress demand (bearing, shear, flexural) on the remaining section (see Photo 11-1).

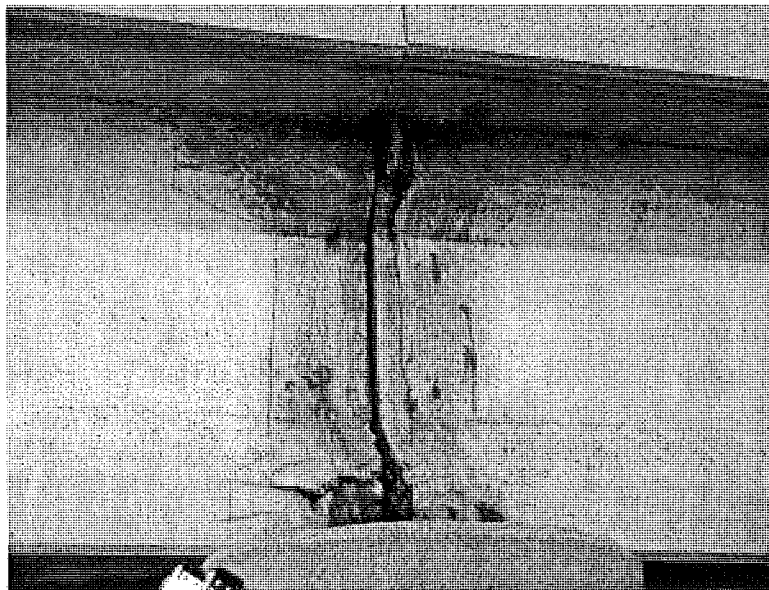


Photo 11-1. Typical beam-end deterioration

While complete replacement of the superstructure beam is an option, it is costly. If certain conditions are met, a more attractive alternative is to repair the deteriorated beam-end. At a minimum, a properly functioning repair can restore cover to reinforcing and prestressing steels and re-establish the original intended cross section of the concrete.

Briefly summarizing Chapter 2, several techniques exist for preventative maintenance and repair of concrete. These techniques may be subjectively categorized for low, moderate and high